

THESIS FOR THE DEGREE OF DOCTOR OF PHILOSOPHY

IN

SOLID AND STRUCTURAL MECHANICS

**On improvement of cast iron brake discs  
for heavy vehicles**

Laboratory experiments, material modelling  
and fatigue life assessment

GAËL LE GIGAN

Department of Applied Mechanics  
CHALMERS UNIVERSITY OF TECHNOLOGY  
Gothenburg, Sweden, 2015

On improvement of cast iron brake discs for heavy vehicles

Laboratory experiments, material modelling and fatigue life assessment

GAËL LE GIGAN

ISBN 978-91-7597-289-3

© GAËL LE GIGAN, 2015

Doktorsavhandlingar vid Chalmers tekniska högskola

Ny serie nr 3970

ISSN: 0346-718X

Department of Applied Mechanics

Chalmers University of Technology

SE-412 96 Gothenburg

Sweden

Telephone +46 (0)31 7721000

Cover:

Part of brake disc assembly (top left) and simulated stress-strain response (top right)

Photo of cracked brake disc and visualization of its thermal image. Part of brake disc assembly and simulated temperature loading.

Credit: Scania CV AB, Gaël Le Gigan and Mats Löfstrand, Scania CV AB (photo)

Chalmers Reproservice

Gothenburg, Sweden 2015

On improvement of cast iron brake discs for heavy vehicles – Laboratory experiments, material modelling and fatigue life assessment

Thesis for the degree of doctor of philosophy in Solid and Structural Mechanics

GAËL LE GIGAN

Department of Applied Mechanics

Chalmers University of Technology

## ABSTRACT

Disc brakes are commonly used in motorcycles, passenger cars, commercial vehicles, heavy-duty vehicles, passenger trains and landing gears of airplanes. Depending on the application, a wide variety of brake discs have been developed, with a multitude of designs, geometries and materials. The brake disc materials used for heavy-duty vehicles are still mostly based on traditional grey cast iron, due to its favourable performance and low cost. Gradual improvements of the thermal and mechanical properties of grey cast iron for production of brake discs have been introduced over the years through fine-tuning of the alloying elements. Nevertheless, because of a material behaviour that comprises non-linear elasticity and non-symmetric yield stress in tension and compression, the mechanical properties of grey cast iron are not as well established as those of steel or aluminium alloys.

The subject of the present work is a better understanding of the mechanisms that control the life of cast iron brake discs. In the end, the aim is an enhanced vehicle performance and reduced maintenance costs of heavy-duty vehicles. *First*, a state-of-the-art survey has been carried out with a review of brake disc technology and mechanisms related to brake disc life. *Second*, full-scale brake dynamometer experiments have been carried out and analysed, with brake discs made from eight different grey cast iron alloys, at controlled torque, speed and cooling conditions. Crack propagation and disc temperatures have been studied. Disc temperatures were recorded by use of a thermocamera and embedded thermocouples. Detailed analyses were performed on temperature data to clarify characteristics of the tested brake discs. The main phenomena influencing the life of brake discs were identified, and the spatial fixation of bands and/or hot spots was found to have a major impact on disc life.

*Third*, a constitutive model useful for grey cast iron was implemented for use with a commercial finite element software. The model was calibrated for temperatures relevant for braking applications using dedicated isothermal tests and, finally, validated against monotonic tensile tests, isothermal fatigue tests and thermomechanical fatigue tests. *Fourth*, a parametric study was performed to explore potential improvements of the cooling channels of a brake disc design when considering an established fatigue criterion. The thermal loading of the brake discs was chosen to represent the full-scale experiments. In the end, a response surface methodology was applied to optimize six types of cooling arrangements (one with straight vanes and five with different numbers of pillar rows) in order to minimize brake disc mass and/or maximize fatigue life.

Finally, *fifth*, some fatigue life models useful for grey cast iron were calibrated and used to assess brake disc design. In the calibration process, results from both isothermal and thermomechanical experiments were exploited. The life models were used to study the reference brake disc.

**KEYWORDS:** brake disc, cast iron, rig experiment, drag braking, elevated temperatures, hot spots, cracking, material testing, material modelling, finite element analysis, fatigue assessment



## PREFACE

This work has been performed as part of the FFI project “Improved performance of brake discs” (Vinnova projects 2009-01449 and 2012-03662; stages 1 and 2) which is a collaboration between the Department of Applied Mechanics at Chalmers University of Technology and the company Scania CV AB with financial support from Vinnova (the Swedish Governmental Agency for Innovation Systems). The project started during the spring 2010. The project is associated with the activities in the Swedish National Centre of Excellence CHARMEC (CHAlmers Railway MEChanics, see [www.chalmers.se/charmec](http://www.chalmers.se/charmec)).

I want to express my special gratitude and thanks to Professor Roger Lundén and Dr Tore Vernersson for their help, support and discussions that assisted my process of learning. I also would like to thank my colleagues at Scania and, especially, Dr Peter Skoglund for initiating this collaboration project and for his full commitment as project leader and co-ordinator. Mats Löfstrand was responsible for the full-scale experiments performed on the Scania brake dynamometer and Alessandro Cadario supported the implementation at Scania. The support from the project reference group, chaired by Mr Lars Wigren of Scania, is gratefully acknowledged. Moreover, it has been a very fruitful and enjoyable experience both to participate in the rig experiments and to work at Scania for three months at the end of my project. Professor emeritus Bengt Åkesson assisted in improving my manuscripts.

The fruitful collaboration with the co-authors in the appended papers: Dr Peter Skoglund, Professor Magnus Ekh, Lic Eng Viktor Norman and Docent Johan Ahlström is gratefully acknowledged.

I would like to thank my colleagues and the administrative staff at the Department’s Division of Dynamics and Division of Material and Computational Mechanics for the nice working atmosphere. Dr Shahab Teimourimanesh is gratefully acknowledged for valuable help and discussions and for his kindness that was really enjoyable.

I deeply express my appreciation to Lisa Brutti, Philippe Joachim, Olivier Le Douarin, Andrea Ricci Persson, Maxime Corbion, Maxime Bordes, Petra Ekstedt and other friends for their support and all happy moments. Thanks to Parisa Panahi for being such a wonderful person.

Finally, I would like to express my love to my mother who never stopped believing in my ability to take up challenges and who supported me along all these years.

Gothenburg, November 2015

Gaël Le Gigan



## THESIS

This thesis consists of an extended summary and the following appended papers:

- Paper A** Le Gigan G, Lundén R and Vernersson T. Improved performance of brake discs: State-of-the-art survey, *Chalmers Applied Mechanics*, Gothenburg Sweden, 2011, 55 pp.
- Paper B** Le Gigan G, Vernersson T, Lundén R and Skoglund P. Disc brakes for heavy vehicles: An experimental study of temperatures and cracks. *Proceedings of the Institution of Mechanical Engineers, Part D: Journal of Automobile Engineering* 2015; 229(6): 684-707.
- Paper C** Le Gigan G, Ekh M, Vernersson T and Lundén R. Modelling of grey cast iron for application to brake discs for heavy vehicles, *Chalmers Applied Mechanics*, Gothenburg Sweden, 2015, 20 pp. Submitted for international publication.
- Paper D** Le Gigan G. Improvement of brake disc design for heavy vehicles by parametric evaluation, *Chalmers Applied Mechanics*, Gothenburg Sweden, 2015, 18 pp. To be submitted for international publication.
- Paper E** Le Gigan G, Norman V, Ahlström J and Vernersson T. Thermomechanical fatigue of grey cast iron brake discs for heavy vehicles, *Chalmers Applied Mechanics*, Gothenburg Sweden, 2015, 19 pp. To be submitted for international publication.

## CONTRIBUTIONS TO CO-AUTHORED PAPERS

Four of the five appended papers were prepared in collaboration with co-authors.

Paper A is an extensive literature survey on brake discs with focus on material properties, numerical models, disc geometry and design optimisation. The author of the thesis was responsible for gathering of information related to the subject and writing of the paper.

In Paper B, the author was involved in the design of the test instrumentation, carried out the analyses of the experimental data and wrote the main parts of the paper. In addition, the author was present during parts of the rig experiments and actively contributed to improvements of the testing procedure in collaboration with the Brake Performance Group at Scania CV AB.

In Paper C, the author implemented, calibrated and validated the Gurson type material model, applied it in a numerical example on a standard brake disc design and wrote the main part of the paper.

In Paper E, four fatigue models were proposed and implemented, of which one model, and also the cyclic plasticity concept, were developed by the co-authors. The author contributed the remaining three models, evaluated the four models in a numerical example and wrote most of the paper.



## CONFERENCE PAPER AND PATENT

The following paper is not included in the present thesis.

Le Gigan G, Lundén R and Vernersson T. Thermomechanical fatigue brake disc materials – Results from modelling and experiments, In: *Proceedings Eurobrake 2012*, Dresden Germany, 2012, 11 pp (also given in the reference list<sup>44</sup>).

The rig tests on brake discs reported in Paper B has resulted in a patent owned by Scania on a cast iron alloy (patent document SE 535 043 C2, dated 2012-03-27).



## CONTENTS

Abstract .....	i
Preface .....	iii
Thesis.....	v
Contributions to co-authored papers .....	v
ConFERENCE paper and Patent .....	vii
Contents.....	ix
Review and summary .....	1
1 Introduction.....	1
1.1 Braking of trucks - overview .....	1
1.2 Aim and scope of study.....	4
1.3 Method of research .....	4
2 Literature.....	6
2.1 General.....	6
2.2 Brake discs .....	8
2.3 Materials for brake discs.....	10
2.4 Loading and temperatures at braking.....	13
2.5 Fatigue and cracking of brake discs.....	15
2.6 Material modelling.....	18
3 Summary of appended papers.....	20
3.1 Paper A.....	20
3.2 Paper B.....	22
3.3 Paper C.....	24
3.4 Paper D.....	25
3.5 Paper E.....	26
4 Concluding remarks and Future developments.....	28
4.1 General.....	28
4.2 Discussion of results .....	28
4.3 Future developments.....	30
5 References.....	32

### Appended papers

Paper A: .....	55 pp
Paper B: .....	24 pp
Paper C: .....	20 pp
Paper D: .....	18 pp
Paper E: .....	19 pp



## REVIEW AND SUMMARY

An introduction to the subject of the thesis is given and **Papers A – E** are referred to. The present summary and reference list are intentionally made short. Further background information and references can be found in the state-of-the-art survey, which has been compiled in **Paper A**.

## 1 INTRODUCTION

The expansion of the commercial automotive market is due to the general increase in global transport.<sup>1</sup> This means a growing demand for commercial cars (trucks and busses) and industrial vehicles (heavy vehicles for farms, mines, etc). International competition calls for cost reductions, improvements of performance regarding maintenance, safety and reliability, and also general improvements of technologies embedded in such vehicles. Improvements of brake discs respond to most of these aspects, although some traditional technologies and materials are still employed.

### 1.1 Braking of trucks - overview

Heavy-duty vehicles such as commercial vehicles, see Figure 1 (left) are built for a high utilization. The life of a commercial car is designed for a minimum of 15 years (2 000 000 km) and during this time some of its components must be replaced at planned intervals. A costly and potentially dangerous situation may arise when specific observations are made for a component, demanding unintended replacement causing immobilization and downtime of the vehicle.

Possible axle arrangements of a vehicle are shown in Figure 1 (right). At braking, the brake force is evenly shared between the front axle, drive axle and any tag axle (also called dead axle). In case of very high decelerations (which are uncommon events in practice), the front axle takes a somewhat higher brake force than the other axles. Two types of friction braking systems are used in heavy vehicles: drum brakes or disc brakes.

At braking of, e g, a heavy-duty vehicle, a pair of pads is pressed against a rotating disc, so-called brake disc or brake rotor, see Figure 2. By doing so, the kinetic or potential energy of the vehicle is converted into thermal energy.<sup>4</sup> The braking constitutes a complex loading that results

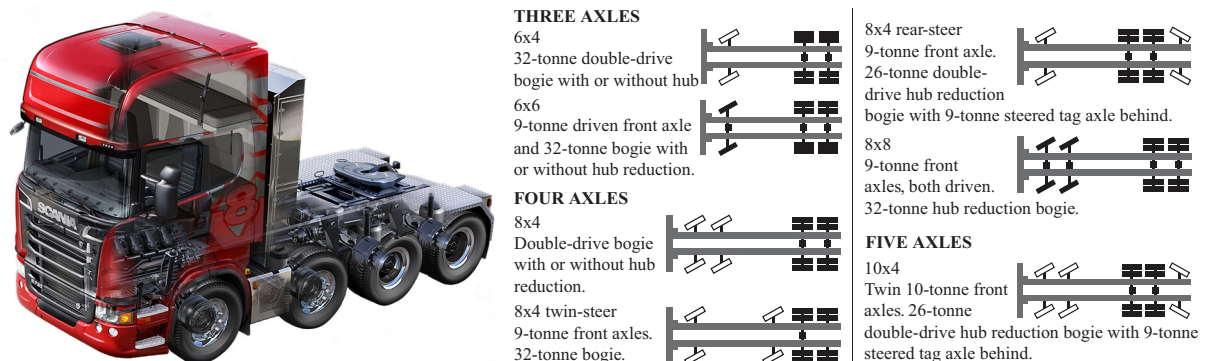


Figure 1. Over-view of a truck equipped with drum brakes (front axles) for heavy haulage without trailer<sup>2</sup> and examples of front axle arrangements (driven axles are black and non-driven axles are white).<sup>3</sup>

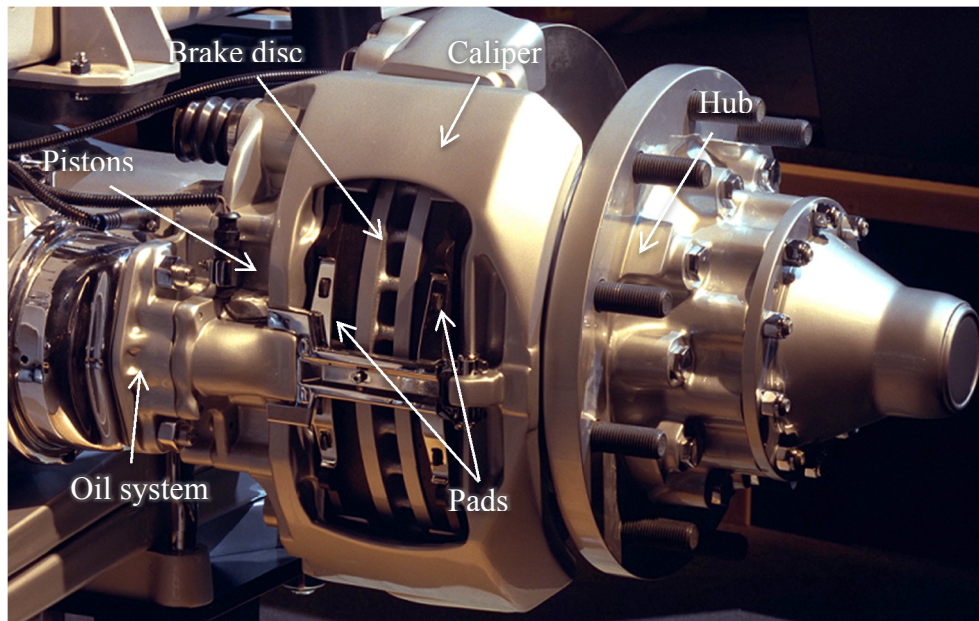


Figure 2. View of a disc brake system and hub of a commercial vehicle.<sup>6</sup>

in a rapid increase of temperatures at the disc surfaces and generally a non-uniform contact between the brake pads and the disc is developed.<sup>5</sup> This leads to wear of the disc and the pads. It may also cause initiation and growth of cracks in the brake disc as induced by stress and strain variations that follow the cyclic heating and cooling processes.

Brake discs are apart from the thermal loading, also subject to mechanical loads introduced at the pad contact. The pads introduce a contact pressure on the disc friction surface and also tractions. The stresses that are introduced in the disc material near the contact surface are generally low (some MPa) because of the rather high compressibility of the pad material and they are generally neglected in comparison with thermally induced stresses. However, for the disc and the neck supporting structures they will produce substantial stresses. Brake discs are structurally designed using a maximum torque (in the order of 30 kNm for heavy vehicles) that will control the minimum allowed dimension of the neck area.

Three different types of braking can be defined. The first kind is “stop braking” where the speed is reduced until stop. The second is “normal braking”, also known as ‘snub braking’, where the speed is decreased at general driving for safety reasons (e g, keeping the distance between vehicles) or changes in speed limits. The third one is “drag braking”, also referred to as downhill braking, as the brakes are used for preserving speed when travelling down a gradient.

The benefit of brake rig testing at controlled conditions is that it allows for improved instrumentation and make possible the study of separate influencing parameters. Characterization of brake disc lives at full-scale dynamometer testing often uses standardised testing methods and load cases of drag braking type. Such tests are designed to give accelerated testing as compared to in-service conditions and are considered to provide relevant life predictions. Naturally, results and solutions obtained from laboratory testing need to be verified for in-field conditions, which is normally done during a given time period on a limited number of vehicles. In the end, correlating rig results to in-service performance and building of knowledge on loading histories makes this simplified testing possible.<sup>7</sup>

The thermal energy generated at braking is transferred by conduction inside the brake components and by convection and radiation to the surrounding, see Paper A. The performance of a given brake disc design (with respect to phenomena such as wear, friction coefficient, brake fade and fluid vaporization) is controlled by the thermomechanical material properties and the tribological environment. Moreover, the brake disc design controls global disc deformations and convection cooling performance, and influences the build-up of thermal stresses. Hence, improvements of brake disc performance can be realised by modifying the disc material and/or disc design in appropriate ways. In Figure 3, the different phenomena involved in brake disc performance and their interactions are shown.

The most commonly used brake disc material is grey cast iron<sup>8</sup> even though materials such as aluminium metal matrix composites and carbon ceramics also are used. Grey iron is a good compromise when considering the cost to performance ratio. For heavy vehicles, the main focus for many years has been to improve grey iron, so-called flake graphite iron, by alloying it with other chemical elements. Grey irons used in brake disc materials are defined by their chemical composition (percentage of, e.g., carbon, silicon, manganese, sulphur and phosphorus) but not by their manufacturing processes which are similar for all alloys. A valuable feature of grey iron is that it is 100 % recyclable.<sup>9</sup>

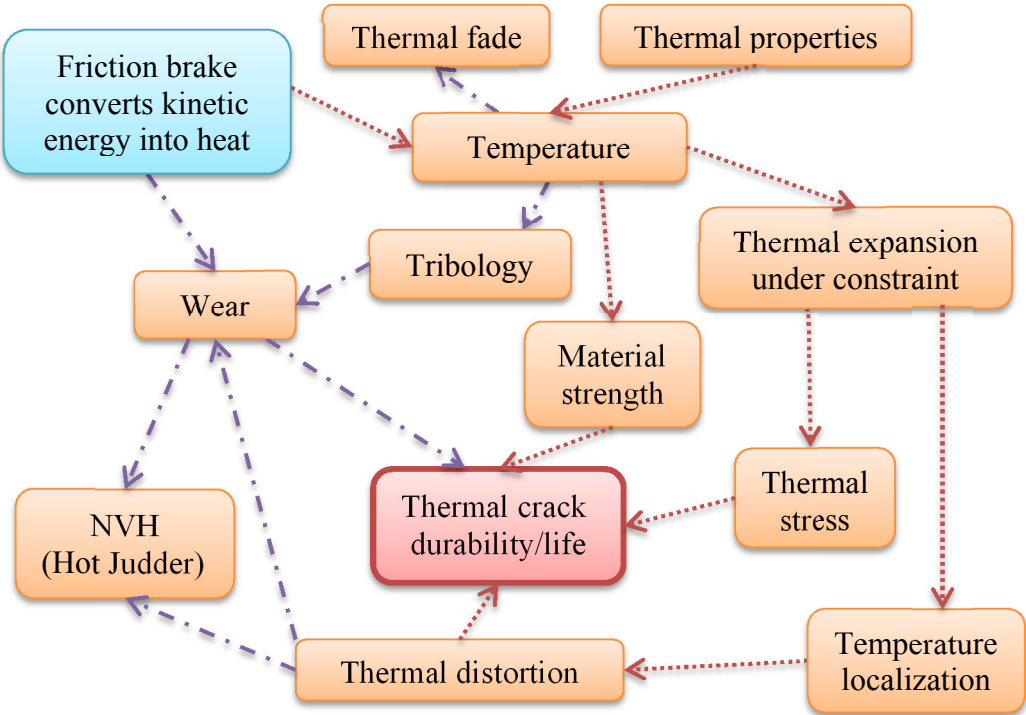


Figure 3. Function and performance of brake discs. The red dotted lines represent the contribution to thermal cracking while the magenta dashed-dotted lines define links with other phenomena. Adapted from the Power Point presentation related to a conference paper.<sup>10</sup>

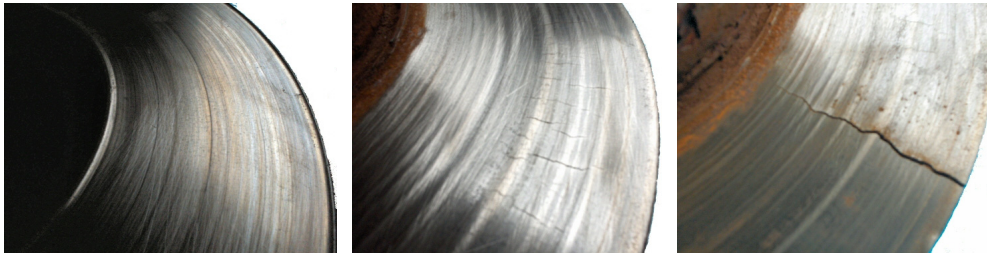


Figure 4. Example of wear (left), heat crazing (middle) and heat cracking (right).<sup>11</sup>

## 1.2 Aim and scope of study

A brake disc with better resistance to thermal cracking and preserved wear and friction properties, see Figure 4, would lead to significant savings, particularly in the form of a higher utilization rate of the vehicle. In order to increase the performance of brake discs, thereby reducing the number of disc replacements during the life of the vehicle, Scania CV AB has initiated this work aimed at understanding the mechanisms that control cracking and disc life.

Three main phenomena that affect the life of a brake disc are: 1) thermal loading of disc material from frictional sliding, 2) material stress-strain response and 3) evolution of damage and cracks. For all three of these factors the behaviour of the disc material is central, especially for 2) and 3) and, indirectly, also for 1).

The present study concerns improvement of both the material composition and the geometry of the brake discs. Full-scale dynamometer tests are used to investigate the thermal loading and to study the cracking behaviour of brake discs of different grades of grey cast iron materials. Laboratory experiments are performed to characterize cast iron materials exposed to cyclic loading and elevated temperatures and are used to calibrate a material model. Finite element simulations of brake disc are used to study brake disc behaviour for realistic thermal loads and material loading conditions. Attempts are made to optimize the disc geometry of the brake discs and to assess the fatigue life. Global cracking is studied only by observation at the brake rig tests. Cooling performance is not in the scope of the present study.

## 1.3 Method of research

In the present work, various methods of investigation have been used: literature studies, full-scale rig experiments and laboratory testing of material specimens, and also modelling and numerical simulations.

The state-of-the-art survey, see **Paper A**, provides a thorough background to key parameters that are important for braking when it comes to thermomechanical aspects, temperature behaviour, wear, cracking and related testing and numerical simulations. Cooling performance and mechanisms are described. Fatigue and crack phenomena are investigated and common approaches to life prediction are given with special consideration related to grey cast iron. Thermomechanical fatigue with damage models is described and crack initiation and propagation are discussed.

Detailed results and analyses of full-scale brake rig experiments are reported in **Paper B**. Severe drag braking applications with cooling-down between cycles are performed for several grades

of grey cast iron materials for brake discs. The measured temperature responses as registered by thermocouples and a thermocamera are thoroughly analysed. Differences in temperature phenomena are identified and related to the life of the discs with respect to crack growth.

Implementation of a Gurson type material model is performed in **Paper C** and application to a brake disc sector is given. The implemented material model is calibrated by use of a designed isothermal experiment performed at six temperature levels from room temperature up to 650 °C. Validation is then accomplished using results from monotonic tensile testing at three different temperature levels and from out-of-phase thermomechanical fatigue experiments at different ranges of mechanical strain with temperature variation from 50 °C to 700 °C. For some of the tests, a dwell time of 30 s is applied at the maximum temperature.

The material routine implemented in Paper C is applied in **Paper D** aiming at optimization of brake disc design. A total of six types of cooling arrangements are studied by a Design-of-Experiments (DOE) approach. A response surface methodology is used which enables optimization. Two aspects are studied where either the total mass of the brake disc is decreased at a given fatigue load or the life is increased for a given a brake disc mass.

Finally, in **Paper E**, four fatigue life models for grey cast iron were calibrated and validated using isothermal and thermomechanical experiments. The results from numerical simulations are used to estimate the life of brake discs exposed to thermal loading as observed in Paper B.

## 2 LITERATURE

Friction is a well-known physical process for decreasing the velocity of a vehicle to standstill even if engine braking can be used at first place. As mentioned above, in automotive applications, friction is accomplished by contact between fixed pad(s) which are pushed towards a rotating disc (disc brake) or brake shoe(s) pushed towards a rotating drum (drum brake). Friction between two bodies releases energy in terms of heat,<sup>4</sup> thus, the brake discs or drum brakes must be designed to withstand high thermomechanical loads. Both types of friction brakes have advantages/disadvantages<sup>12</sup> and the vehicle usage will favour one or the other. For example, if the vehicle is employed in a dusty environment like mining, drum brakes will be preferred as they are a closed component limiting the amount of dust entering into the system. However, for repeated or prolonged braking, temperatures can become high and brake discs with their better cooling will be preferred.

Severe braking induces high thermal loads on the brake disc leading to high local temperature (hot spots and / or hot bands), wear and possible cracking. In Europe, disc brakes are widely used in heavy-duty applications (total vehicle mass greater than 3.5 tonnes), both for freight and passenger transport. Brake discs work in pair together with the pads that are specified by the brake lining material. Brake linings should have suitable friction coefficient, constant friction coefficient (e.g., at different temperatures, in wet conditions, when exposed to salt or contamination) and a suitable compressibility.<sup>13</sup> It is well known that the pad material has an influence on the brake disc thermal loading.<sup>14</sup> However, in the present work, focussing on the brake disc material, this has not been considered, except for studying two types of pads in Paper B and using thermal load cases that are based on the here used pads of organic composite type.

### 2.1 General

A vehicle in motion is exposed to forces. The primary force is the gravitational. So-called aerodynamic drag resistance is induced by the vehicle moving in the air. Also, friction forces from the ground are acting on the wheels. The frictions forces are induced by traction, braking, rolling resistance and the slope or unevenness of the road. The forces are summarized in Figure 5.

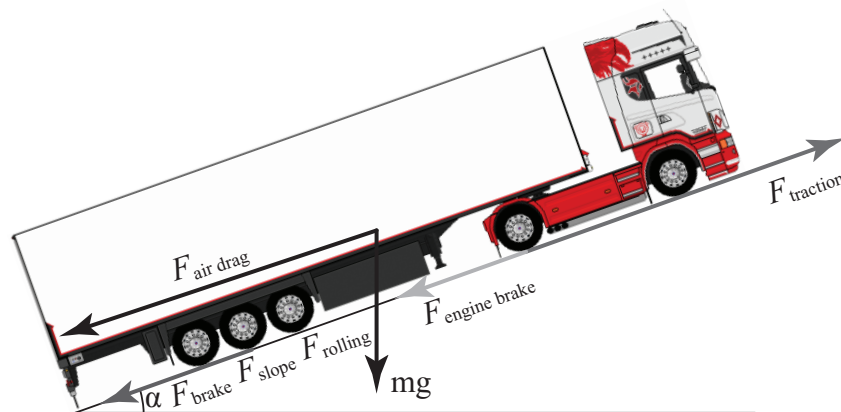


Figure 5. Illustration of the forces acting on a truck.

On the market, several types of friction braking systems are available and a selection is given in Figure 6. Drum brakes have brake shoe(s) with pad(s) that are pushed towards the drum. Conventional brake discs and full friction brake discs use a brake pad that is pushed towards the brake disc. Contrary to a conventional brake disc where the pad(s) cover(s) about 70° of the friction surface, full contact disc brakes have one or a pair of pads covering almost 100 % of the friction surface.

An example of a brake pad is given in Figure 7. Today, there are four different families of brake pad materials: 1) non-asbestos organic, 2) low metallic, 3) semi-metallic and 4) ceramic. The friction surface of a brake pad is often equipped with slots or grooves, mainly introduced in order to reduce surface temperatures and wear.<sup>15</sup> For special brake pads used in the railway industry, like for the French high speed train TGV, the friction material consists of pins that do not cover 100 % of the pad area. For high torque braking, Smith and Hudson<sup>16</sup> suggested to add an extra disc and pair of pads while reducing the size of the components compared to a single brake disc. In the rig tests reported in Paper B, two types of standard non-asbestos organic pads were used and thermal properties of the material are given in the paper.

Currently, focus on braking technology is significant as the market is growing, see Figure 8. Despite the “traditional” technology, friction braking is still used and will still be applied in the future. Thus, improvement of the current technology must be achieved either by change of material or change of design.

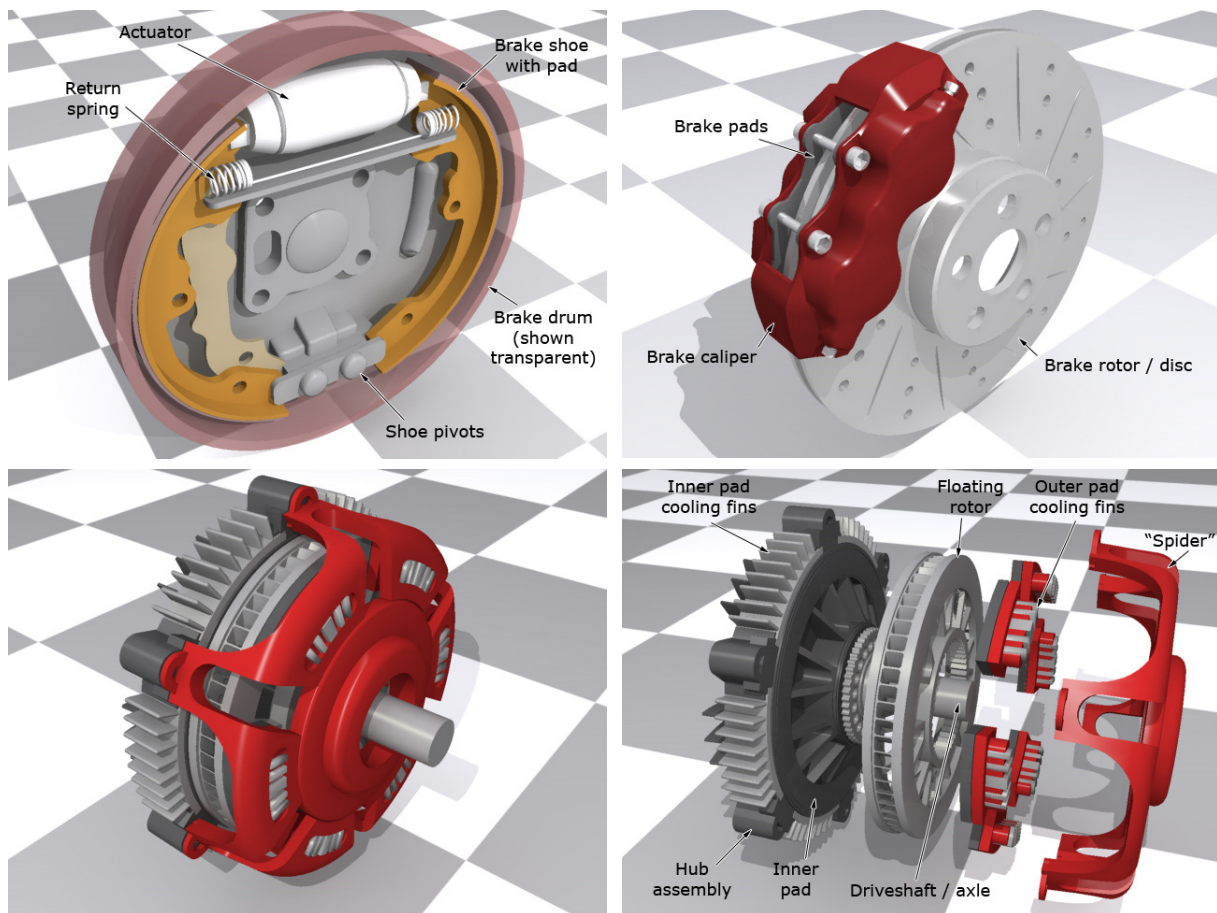


Figure 6. Brake drum (top left), brake disc (top right) and full friction brake (bottom left and right).<sup>17</sup>

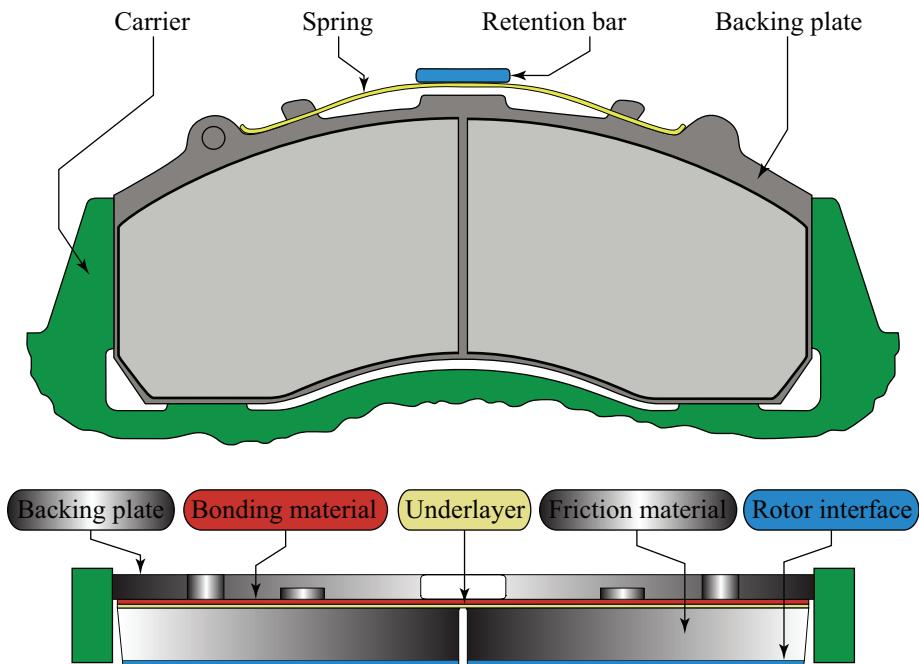


Figure 7. Brake pad description.<sup>18</sup>

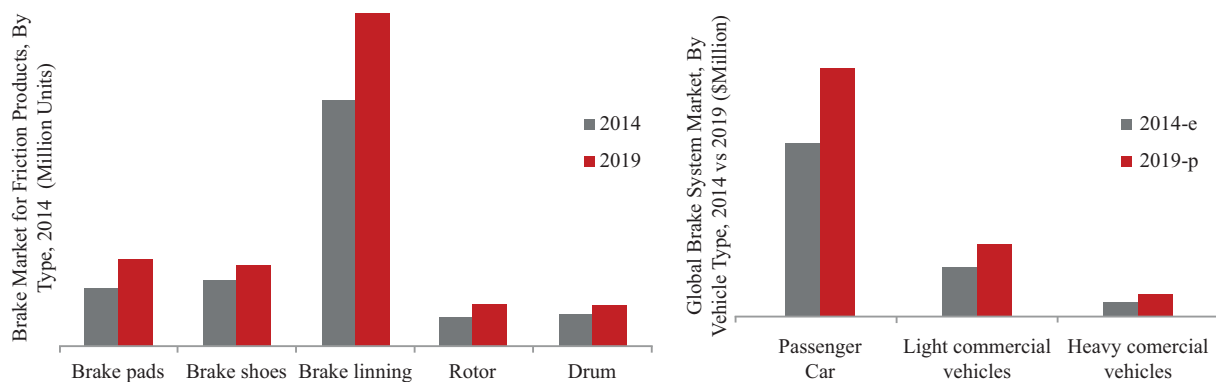


Figure 8. Brake current market and forecasts.<sup>19, 20</sup>

## 2.2 Brake discs

Today five brake disc designs are defined as 1) outer hat without neck, 2) outer hat with neck, 3) inner hat without holes in hat, 4) inner hat with holes in hat and a bit aside 5) floating discs cast in two pieces, see Figure 18 in Chapter 3.<sup>21</sup> Such designs feature either straight vanes, tangential vanes, curved vanes or pillars. In addition, extra features like groove/slots and/or holes drilled at the friction surfaces can be used. However, such features can result in stress concentration as they behave like notches. All brake discs are cast in one piece except for the floating disc which has either a bell mounted on a ring (disc) or a disc mounted on a bell, see Paper A. The floating disc exists in two versions: the semi-floating and fully-floating brake disc. The two floating disc types are very similar but the fully-floating disc is not used in heavy duty applications. The difference can be found at the connection between the bell and the disc. For the semi-floating brake disc, the disc is attached to the bell while for the fully-floating brake disc, the disc is sitting on the bell (allows for complete movement of the outer ring). The main advantage of the floating disc is to provide better flexibility of the disc as “gaps” and “joints”

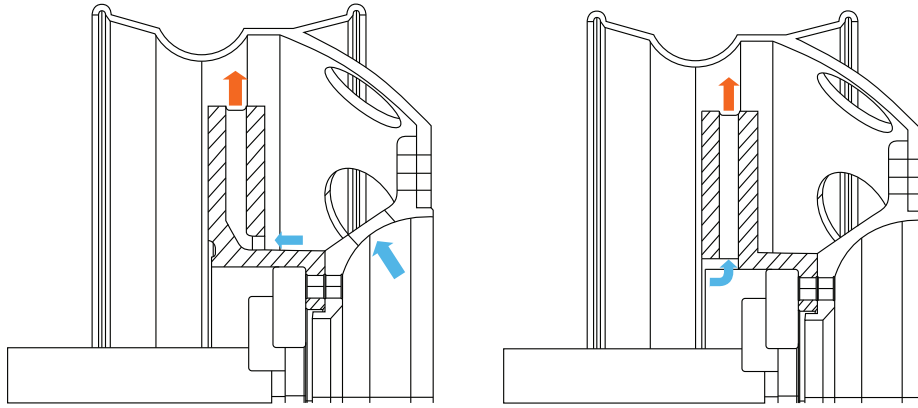


Figure 9. Anti-coning brake disc with straight vanes and improved cooling performance mounted in a wheel carrier (left), and outboard attachment brake disc of hat type mounted in a wheel carrier (right).<sup>14, 22</sup> The blue arrows represent the cold air flow entering the disc and the orange arrows represent the hot air flow going out of the disc. The brake disc is shown dashed.

allow for free expansion in the radial direction and reduce heat transfer to carrier and wheel. The disadvantage of floating discs is that the brake disc is weaker at the area where the two parts are linked together compared to a disc cast in one piece.

An important aspect when designing a brake disc is to reduce its coning at braking and possibly limit the permanent deformation after cooling. An example of an anti-coning brake disc is given in Figure 9 (left) while a traditional brake disc of hat type is shown in Figure 9 (right). A disadvantage of the anti-coning disc is a bad airflow circulation that reduces cooling between the wheel carrier and the disc.<sup>14</sup> In Figure 9 (left), the anti-coning brake disc is shown with an improved cooling design by introducing a hole in the wheel carrier so that the airflow is facilitated.

For each disc type, cooling is normally accomplished by use of different types of vanes (straight, tangential or curved) and/or pillars, see Figure 10. Curved vanes increase the cooling performance<sup>23</sup> by increased air flow (pumping), which induces higher aerodynamic losses at high speeds. However, this is mainly a problem in high-speed railway applications. Moreover, the brake disc with curved vanes has to be mounted on the correct side of the axle in order to fulfil the designed rotation for the air flow.

Comparisons of aerodynamic power loss, convective heat dissipation and cooling to aerodynamic efficiency ratio for different types of brake discs have been investigated by Tirovic<sup>24</sup> The study shows that radial/pillared disc types constitute a good compromise. The radial/pillared discs have the best cooling to aerodynamic efficiency ratio up to 800 rpm becoming the second best behind the solid disc above 800 rpm. For heavy vehicles, however, speed is about 80 km/h, which corresponds to about 425 rpm. Such a low speed means that pumping losses, which are in the order of 0.1 kW per brake disc, can be neglected.

All pad/disc couples need to be bedded-in (i.e., worn to have the entire friction surfaces in contact) to ensure heat stabilization and improved resistance to cracking. Cracking or even full

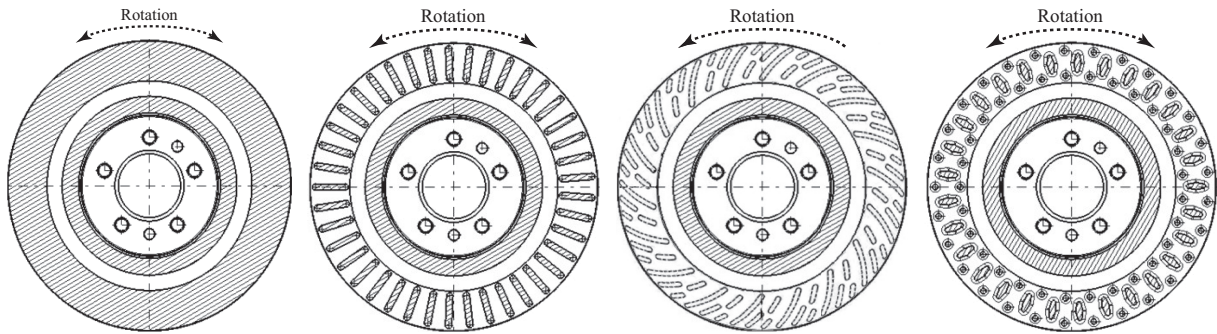


Figure 10. Solid disc (left), straight vane (second left), curved vane (second right) and pillars (right) disc design.<sup>26</sup>

disc failures can occur during the first few heavy stops if careful bedding is not carried out. In order to achieve optimum brake performance and to prolong disc life, it is essential that brakes operate at the correct temperature. In general, all the brake discs of a vehicle should have similar temperatures. Dissimilar temperatures will lead to uneven braking.<sup>25</sup>

### 2.3 Materials for brake discs

The choice of a suitable brake disc material set out from desired mechanical properties and performance related issues. Desired properties for brake discs are<sup>27</sup>

- High strength and durability to sustain torque loads from braking
- Stable mechanical and frictional properties through the range of expected service temperatures
- High wear resistance through the range of expected service temperatures
- High heat absorption capability for the braking energy
- High thermal conductivity to transport frictional heat away from braking surfaces
- High vibration damping capacity to minimize NVH (Noise, Vibration, Harshness) issues
- Minimal thermal expansion to minimize performance variability
- High degree of corrosion resistance
- Excellent machinability
- Inexpensive material and processing costs

A list of potential candidates is given in Table 1 which also corresponds to brake disc materials used today.

Table 1. Typical main mechanical and thermal properties of brake disc materials at room temperature.

	E [GPa]	$\nu$ [-]	$\rho$ [kg/m <sup>3</sup> ]	$\alpha$ [1/K]	$\lambda$ [W/mK]	c [J/kg/K]
Carbon ceramic <sup>28</sup>	30	0.6	2450	$2.8 \times 10^{-6}$	40.0	800
Aluminium <sup>29</sup>	73	0.3	2800	$23.0 \times 10^{-6}$	154.0	963.0
Steel	-	-	-	-	-	-
Stainless steel <sup>29, 30</sup>	170	0.3	7850	$18.5 \times 10^{-6}$	20.0	478
Metal-Matrix-Composite	74	-	2800	-	-	200
Grey cast iron <sup>28</sup>	90	0.4	7250	$12.0 \times 10^{-6}$	54.0	500.0

There are a number of brake disc materials or combinations available on the market today. Some examples are:

- Cast iron: Made from a single piece of iron on standard cars, or a two piece construction containing a cast iron ring and aluminium joined “hat” on upgraded versions.
- Steel<sup>35</sup>: Created from a single thin piece of steel, these brakes are lighter in weight and have a higher heat capacity. However, they are not very durable.
- Aluminium<sup>35</sup>: These brake discs transfer heat rather quickly, but have a reduced capacity to absorb heat. Aluminium is rather lightweight, but lacks the ability to be used in any frequent or prolonged braking situations because of its low melting point.
- Carbon-ceramic<sup>32</sup>: These brake discs are made from a composite material reinforced by carbon filaments within silicon carbide. Here, the silicon carbide constitutes the main matrix component that governs the great hardness characteristics of the composite material. The discs have a high resistance to thermal and mechanical loads. The major drawback is the high cost.
- Metal-Matrix-Composite<sup>37</sup>: These brake discs made from Metal-Matrix-Composites (MMCs) have improved performance in the mechanical behaviour (e.g., tensile and compressive properties, and tribology), physical properties (e.g., density, thermal expansion, and thermal diffusivity) and wear resistance. The weight is only 60 % of a traditional cast iron brake disc. MMCs are generally associated with aluminium alloy.

### Cast irons

The iron phase diagram is shown in Figure 11. Cast irons are alloys of iron, carbon, and silicon in which more carbon is present than can be retained in solid solution in austenite at the eutectic temperature. In grey cast iron, the carbon that exceeds the solubility in austenite precipitates as flake graphite. Cast iron alloys thus contain at least 2 % of carbon while steels have between 0.008 % and 2 % carbon. For cast iron, the content of pearlite, cementite, austenite or ledeburite will, for stable condition, vary with temperature according to the diagram in Figure 11. The family of cast irons include 1) white, 2) malleable, 3) grey, 4) chilled and 5) nodular cast irons. Compacted graphite iron is in between grey cast iron (graphite flake) and ductile, i.e. nodular, cast iron (graphite sphere). A summary of possible cast irons is given in Figure 12.

The composition of grey iron must be selected in such a way as to satisfy three basic microstructure requirements: 1) graphite shape and distribution, 2) a carbide-free (chill-free) microstructure and 3) the required matrix.<sup>31</sup> Grey irons usually contain 2.5 to 4% C, 1 to 3% Si, and additions of manganese, depending on the desired microstructure (as low as 0.1% Mn in ferritic grey irons and as high as 1.2% in pearlitic grey irons). Sulfur and phosphorus are also present in small amounts as residual impurities.<sup>31</sup> There exists several classes of grey iron that are found in the ASTM A48-48M standard<sup>32</sup> or European standard EN 1561,<sup>33</sup> where they are grouped according to their minimum ultimate tensile strength. Grey cast iron microstructure depends on applied cooling rates and alloying elements.<sup>34, 35</sup>

One particularity of grey cast irons should be noticed; the rather heterogeneous material structure with graphite flakes with sizes greater than 1 mm down to 0.015 mm in a metal matrix.<sup>36</sup> The presence of graphite flakes makes standard material testing susceptible to outliers. The graphite flakes have very poor mechanical properties and, in addition, they act as initiators of cracks, or can themselves be considered to constitute cracks embedded in the material. The graphite flakes can be tuned by controlling chemical composition of the material and by the cooling process at casting. Thermal conduction for cast irons depend on the graphite flakes since they have very good conductivity as compared to the base material. This also means that material conductivity can be increased while at the same time having other mechanical properties unchanged.<sup>37, 38</sup>

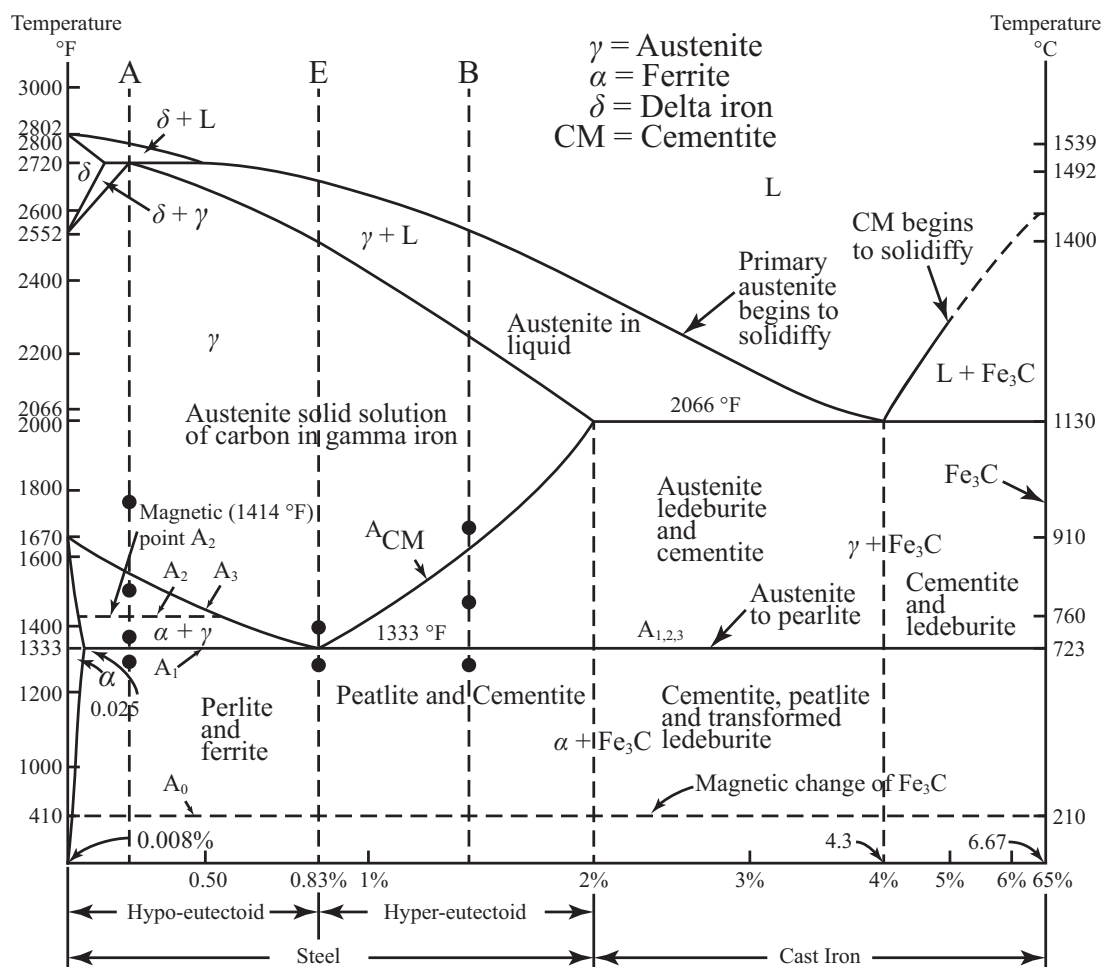


Figure 11. Iron phase diagram.<sup>39</sup>

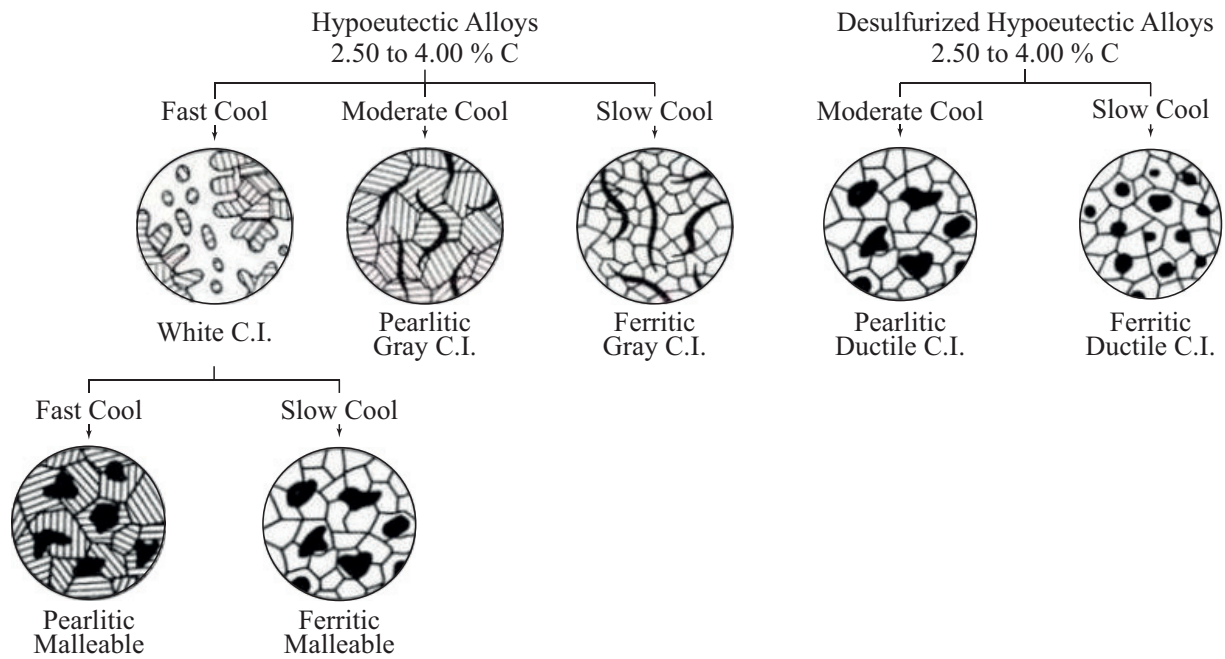


Figure 12. Summary of cast iron microstructures.<sup>40</sup>

Phase transformation is an important phenomenon when high temperature can be expected to occur. As for steel, cast iron, can form martensite by rapid cooling of austenite.<sup>41</sup> Martensite is a very hard steel crystalline structure that could cause cracking and judder in brakes. In the testing carried out in the present project, see Paper B, martensite formation has not been observed. However, hot spots are reported to cause formation of martensite in cast iron brake discs.<sup>42</sup>

#### *Grey cast iron brake discs*

Today's brake discs used for heavy vehicle applications (excluding racing) are manufactured primarily from pearlitic grey cast iron of qualities GCI 15 through GCI 25<sup>43</sup> (minimum ultimate tensile strength between 150 MPa and 250 MPa). Small amounts of chromium and molybdenum additives will give to the material a greater abrasion resistance and improved heat cracking behaviour.<sup>43</sup> A higher carbon content improves the thermal conduction,<sup>38</sup> which improves the ability to manage high brake power levels. However, the increases of free graphite at the same time impairs the mechanical properties. For these reasons, today's grey cast iron brake disc materials have balanced properties that at the end of the day give suitable braking performance. Addition of niobium will refine graphite, eutectic cell and pearlite lamellar spacing up to a certain point.<sup>44</sup>

## **2.4 Loading and temperatures at braking**

Simplified analysis of the pad/disc pressure distribution would either presume that the pressure is uniform over the nominal contact area or that the product of pressure and sliding speed is constant over the contact area as resulting from a so-called uniform wear assumption. Numerical evaluation of typical disc brakes has shown that the uniform pressure assumption results in a mean effective radius, and hence brake torque, which is approximately 2 to 3% greater than obtained for the uniform wear assumption, which is applicable for brakes at run-in conditions.

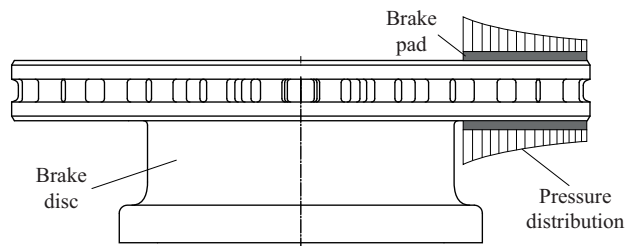


Figure 13. Brake disc pressure distribution for uniform wear.

For most practical cases the pressure would therefore be assumed to be inversely proportional to the radius. The mean effective radius would then be assumed to be equal to the average value between outer and inner radius.<sup>45</sup>

However, friction brakes are normally operated at loading conditions where thermoelastic effects are important for dimensioning and operation of the brakes.<sup>46</sup> This means that the local interface temperatures are controlled by local contact pressure, thermal expansion and eventually the local heat generation, resulting in a complex situation where material stiffness, wear, thermal characteristics and local friction will have an influence. For this reason, the pad and disc interaction will generally not be given by the simplified quasi-steady state conditions described above. Instead, local high temperatures will be induced, that may eventually lead to formation of hot bands or hot spots<sup>42</sup> on the disc surface.

Above a certain critical sliding speed, the interaction between contact pressure, heat generation and thermal expansion become unstable, leading to further localization of the contact producing so-called hot spots at the sliding contact interface.<sup>47, 48</sup> Hot spots may cause accelerated material damage<sup>49</sup>, severe wear and are closely related to undesirable low frequency vibrations, known as “hot judder”.<sup>50</sup>

Numerical analysis of the thermoelastic interaction in a brake is challenging, especially if the brake is in a state of thermoelastic instabilities. One reason for this is that contact quantities are inherently difficult to measure, thus making model calibration and verification problematic. Efforts in the field of braking that often are referenced include Barber<sup>47</sup> who pioneered the analysis of thermoelastic instabilities and later introduced finite element implementations of the stability problem together with Zagrodski<sup>51</sup>, Day<sup>49</sup> and more recent experimental work by Panier<sup>52</sup> and Dufrénoy.<sup>53</sup> At the end of the day, it is still difficult to simulate the phenomena occurring during braking in the regime controlled by frictionally induced thermoelastic instabilities. At braking of heavy vehicles, the disc temperatures may go as high as 700-800 °C.<sup>54</sup> The high temperature behaviour of the involved materials will then control the wear phenomena. For this reason, it has been chosen, in the present work, to characterize the disc thermal loading based on results from the brake rig testing reported in Paper B. This means that it can straightforwardly be modelled by use of a prescribed surface heat flux.

To add on to the above given complex picture, it has been found that the presence of a so-called third body, i.e. a “layer” built-up by wear debris and oxides between the two bodies that are in sliding contact, is important for the functioning of the tribological contact. Detailed modelling using, e.g. cellular automaton approaches<sup>55</sup> at scales bordering to size of wear particles can be

used to shed light on the processes at sliding interfaces that control both friction, heat generation and wear.

Detection of brake disc temperatures on the friction surfaces is challenging. Thermography methods are traditionally used in the form of thermocameras. Such cameras will calculate the temperature of the surface as based on detected radiation intensity of the surface within the active wavelength range of the thermocamera. However, the calculation will require that the surface emissivity, which is used to relate measured intensity with surface temperatures to be known. Recently, there has been studies published where so-called two-colour pyrometry is used to amend this problem.<sup>56, 57</sup> Thus, by detecting intensities for ranges of wavelengths, the temperature and the emissivity of the surface may be obtained. In the present work, a fixed emissivity has been used, as determined by comparison with surface thermocouples. The thermocamera has a wavelength of 1.4  $\mu\text{m}$  to 1.8  $\mu\text{m}$  and is active only for temperatures higher than 250  $^{\circ}\text{C}$ .

## 2.5 Fatigue and cracking of brake discs

Fatigue of materials relates to successive degradation of a material due to cyclic loading that compromise the intended function of a component. Fatigue of metals is generally divided into stress-based fatigue, often related to high cycle fatigue (HCF), and strain based fatigue, related to low cycle fatigue (LCF).<sup>58</sup> Basically elastic material response is considered for HCF. For LCF it is normally plastification of the material and the pertaining strains that limit the life fatigue life. HCF is often attributed to a number of cycles higher than, say, 10 000, while LCF is in the range of, say, some ten cycles up to 10 000. These two fatigue categories are in a general case overlapping and empirical models have been developed to account for the impact of stress and strain effects that have been found important at controlled tests in laboratories.<sup>59</sup>

A widely used fatigue life model to account for both low-cycle and high-cycle fatigue is the Coffin-Manson-Basquin<sup>60-62</sup> equation, displayed in Figure 14 (left) and expressed as

$$\varepsilon_a = \frac{\Delta\varepsilon}{2} = \frac{\sigma_f'}{E} (2N_f)^b + \varepsilon_f' (2N_f)^c \quad (1)$$

where  $\varepsilon_a$  is the strain amplitude,  $\Delta\varepsilon$  is the total strain range,  $\sigma_f'$  is the fatigue strength coefficient defined as the stress intercept at  $2N_f = 1$  which is roughly equal to the ultimate stress  $\sigma_f$ ,  $\varepsilon_f'$  is the fatigue ductility coefficient defined by the strain intercept at  $2N_f = 1$  which is often close to the fracture strain  $\varepsilon_f$  for many metals,  $b$  is the fatigue strength exponent which varies between -0.05 and -0.12 for most metals,<sup>63</sup>  $c$  is the ductility exponent which usually varies between -0.5 and -0.7<sup>63</sup> and, finally,  $N_f$  is the number of cycles to failure. Suggested cyclic and fatigue properties are  $\varepsilon_f' = 0.864$ ,  $c = -0.771$  for cast iron.<sup>64</sup>

Variations of this empirical equation have been introduced to account for, e g. mean stress effects on life, where Manson<sup>65</sup> introduced mean stress effect in the high-cycle fatigue term and by Manson-Halford<sup>66</sup> in both the low-cycle and high-cycle fatigue terms.

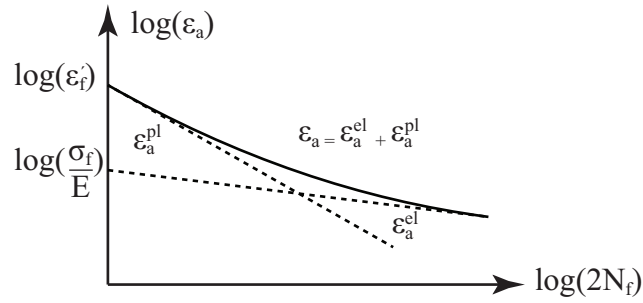


Figure 14. Coffin-Manson-Basquin low-cycle and high-cycle fatigue curves. Here  $\varepsilon_a = \Delta\varepsilon/2$  is the strain amplitude.

The lifespan can also be assessed using the Smith, Watson, and Topper (SWT) equation that in its general form<sup>67</sup> states

$$\sigma_{\max} \frac{\Delta\varepsilon}{2} = \frac{\sigma_f'^2}{E} (2N_f)^{2b} + \sigma_f' \varepsilon_f' (2N_f)^{b+c} \quad (2)$$

where  $\sigma_{\max}$  is the principal maximum tensile stress and  $\Delta\varepsilon/2$  is the principal mechanical (elastic + plastic) strain amplitude. The SWT relation, without the first high-cycle fatigue term was found useful and could be simplified when studying fatigue of cast iron in Fash and Socie.<sup>68</sup>

The material in brake discs is in principle subject to thermal loading and temperatures that induce varying stresses and strains that depend on the local confinement of the material and this is controlled by the disc geometry and mechanical boundary conditions of the disc. The result is a so-called out-of-phase thermomechanical<sup>1</sup> loading situation, where the temperature increase is combined with simultaneous material compression. Such problems are studied within the subgroup of thermomechanical fatigue (TMF).

Calibration and prediction accuracy for low cycle fatigue of cast iron materials using both traditional methods and an energy based method is studied by Gomez et al.<sup>69</sup> For a grey cast iron, with temperatures up to 450 °C, it is concluded that a Coffin-model (based on plastic strain) is the most suitable, somewhat superior to models based on plastic energy, total energy, SWT and total strain.

Fatigue of cast irons may also be modelled using mechanism-based models.<sup>70-74</sup> These models build on the assumption that the fatigue damage in the material is controlled by crack growth phenomena on a micro-scale and that models developed for study of global crack growth can be used to predict the evolution of damage. For thermomechanical situations, the model by Metzger and Seifert has been found to give good predictions of fatigue lives.<sup>71, 73</sup> The model has the advantage of requiring the fitting of only a few fatigue parameters the rest being determined from the actual stress-strain relationship. The basic life parameter is the cyclic crack tip opening displacement that is established by use of calculated variations of stresses and strains, thus requiring the use of a well-calibrated material model.

Thermomechanical loads generated at braking may result in various modes of disc failure. The two competing phenomena are cracking and wear that both are detrimental for brake disc lives.

<sup>1</sup> The term “thermomechanical” has been used for situations both with and without external mechanical load.

Cracks develop in multidirectional or unidirectional networks, see Figure 15 (right), and wear is induced by the frictional contact between the pad and the disc. A high level of disc wear will actually remove cracks on the disc surface. One could here, at least in theory, talk about a “magic wear rate” that will barely remove the cracks that start growing on the disc surface.<sup>75</sup> Brake discs that are substantially cracked or worn would call for component replacement.

The thermal localization and pertaining high temperatures will increase the risk of cracking by increased damage accumulation.<sup>76</sup> In a study on steel brake discs, the fatigue damage is related to the onset of substantial decrease in material strength and stiffness at 400 °C. Sizes of areas having temperatures higher than this temperature as compared to total area, in combination with rate of heating, are found to be related to fatigue damage for the disc.<sup>76</sup>

Laboratory testing of TMF behaviour means that temperatures and strains in a general setting are simultaneously varied and independently controlled.<sup>77</sup> This means that both variations of temperatures and strains must properly be chosen to represent / include the studied problem. The degree of material constraining is for an out-of-phase TMF situation, as for brake discs, given by the ratio between the resulting mechanical strains and the introduced thermal strains.

An example of a fully constrained experiment is given in Figure 16. This was performed within the project and reported in a conference paper.<sup>78</sup> A unidirectional temperature gradient is simulated<sup>78</sup> as part of a thermomechanical fatigue experiment aimed at reproducing the temperature gradient in the brake disc friction area. Here, cyclic temperature loading is applied to a fully constrained hour-glass shape specimen. The constrained thermal at increased temperature induces mechanical straining of the material. The controlled temperature varies from 110 °C to 600 °C at the centre of the specimen and is held at its maximum during 150 s before controlled cooling to 110 °C in 180 s. The increase in temperature is performed in 80 s.

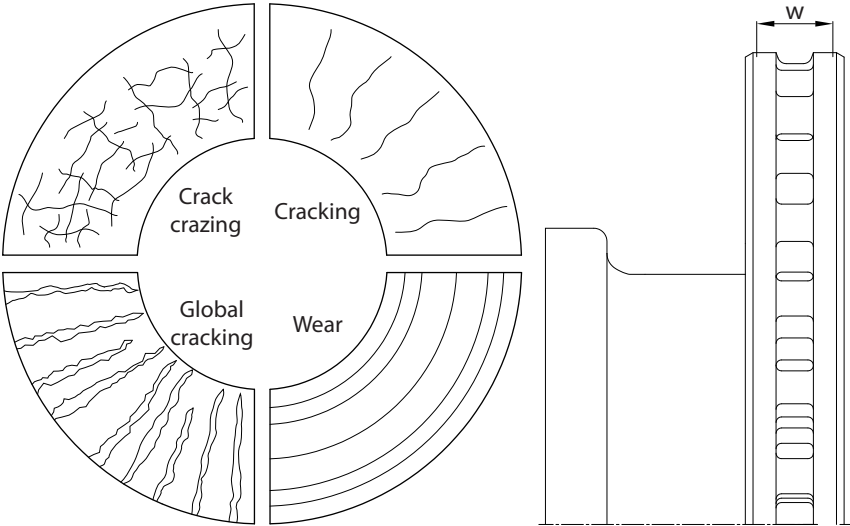


Figure 15. Types of defects occurring at the friction surfaces of brake discs (left) and permissible wear (right).

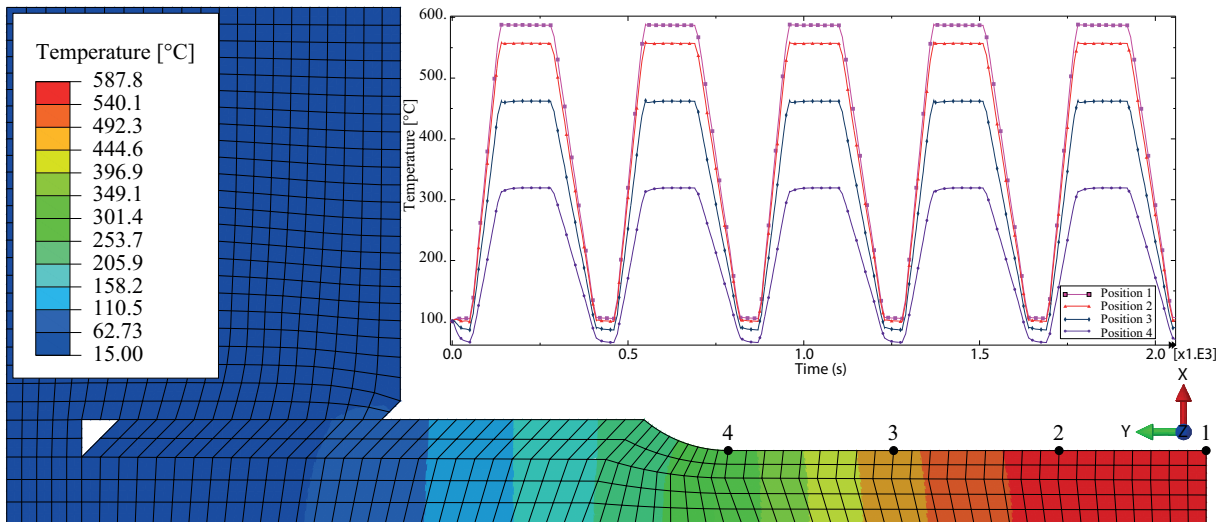


Figure 16. Thermomechanical fatigue simulation aimed at reproducing the temperature gradient in the friction surface of a brake disc at braking and cooling.<sup>78</sup>

## 2.6 Material modelling

Development of a material model able to simulate the material response of cast iron, having non-symmetric yield stress in tension and compression, for various levels of temperatures and repeated loading is a challenge. Such models are not available in commercial FE codes. The basic principle of a material response at loading, holding and unloading is illustrated in Figure 17 (a). Hardening is described by three types: isotropic, kinematic or a mix between the two. Isotropic hardening is considered when the yield surface expands symmetrically in all directions and proportionally to the plastic multiplier, see Figure 17 (b-c). Kinematic hardening assumes a constant yield surface that can translate towards the loading direction, see Figure 17 (d-e). A mixed isotropic and kinematic hardening can also be assumed, see Figure 17 (f). Viscous effects result from either relaxation or creep and are both rate-dependent and temperature-dependent. Ratcheting is a phenomenon where the material accumulates strain during each cycle. Hardening of the material may result in elastic shakedown (cycles without plastification) or plastic shakedown (steady-state plastic cycles).

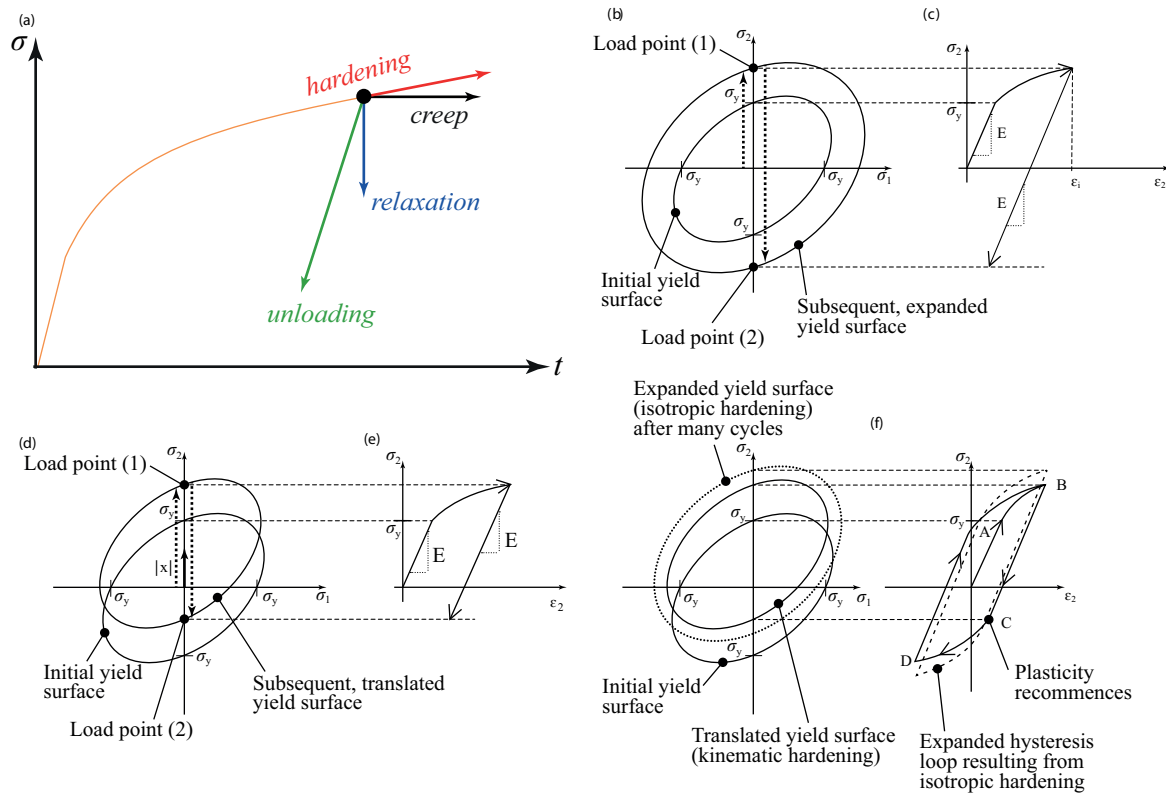


Figure 17. Material response under loading, holding and unloading (a), reversed loading with isotropic hardening showing (b) the yield surface and (c) the resulting stress–strain curve, kinematic hardening showing (d) translation of the yield surface with plastic strain, and (e) the resulting stress–strain curve with shifted yield stress in compression (Bauschinger effect) and (f) combined kinematic and isotropic hardening.<sup>79</sup>

The microstructure of grey cast iron is of lamellar type with flakes that are considered as voids of spherical types, i.e. nodules, in material models and a life model could be used on this concept. Ductile damage described by growth of cylindrical or isolated voids included in a rigid perfectly plastic matrix were first introduced by McClintock<sup>80, 81</sup>, Rice and Tracey<sup>82</sup> and then by Gurson.<sup>83, 84</sup> However, the first idea on premature fracture in metals due to a process of internal necking was introduced already in 1855.<sup>85</sup> Thomason's micromechanical model<sup>86, 87</sup>, so-called plastic limit-load model, studied the coalescence of voids by introducing a plastic limit load that improves the prediction of ductile failure. It should be noted that the Gurson concept of voids growth can be used together with Thomason's coalescence concept in order to give reasonable predictions of ductility.<sup>88, 89</sup> The concept of voids introduced by Gurson<sup>83, 84, 90</sup> for a perfectly elastic–plastic matrix material was extended by Tvergaard and Needleman to account for temperature-dependent materials with isotropic and kinematic hardening and a new formulation of the yield function.<sup>71, 91, 92</sup> The model has been successfully employed for thermomechanical loadings up to 450 °C for Compacted Graphite Iron (CGI), which has spherical nodules instead of graphite flakes.

### 3 SUMMARY OF APPENDED PAPERS

A short summary of each of the appended papers is given in the following.

#### 3.1 Paper A

*Improved performance of brake discs – State-of-the-art survey.* An overview of disc braking and phenomena related to braking performance and disc life is given. Different types of brake discs are introduced and some examples of ventilated brake discs are shown in Figure 18. It can be noted that solid disc are used for some specific applications, e.g., low-performance cars (on the rear axle) and, although for different reasons, also on the French high speed train (TGV). For a low-performance car solid brake discs constitute a low-cost and low-capacity alternative, while for the TGV trains there is a large distance / time between stops at stations that allows the disc to cool down completely between stations independently of cooling arrangements. Influence of mounting of the disc part, which can be of so-called hat (integrated bell) or floating type, is discussed and related to its importance for cracking of the discs. Discs of a floating type allow for radial and axial heat expansion which reduces stresses, cracking and distortion as compared to discs of hat type where the disc is fixed to the hub via a hat shaped structure. However, the hat type of brake discs has some advantages, e.g., easy to cast, low cost and one body (no internal vibrations induced at bell-disc interface). A brake disc of hat type (cast in one piece) is prone to coning and its constrained thermal expansion affects the contact conditions during braking as illustrated in Figure 19.

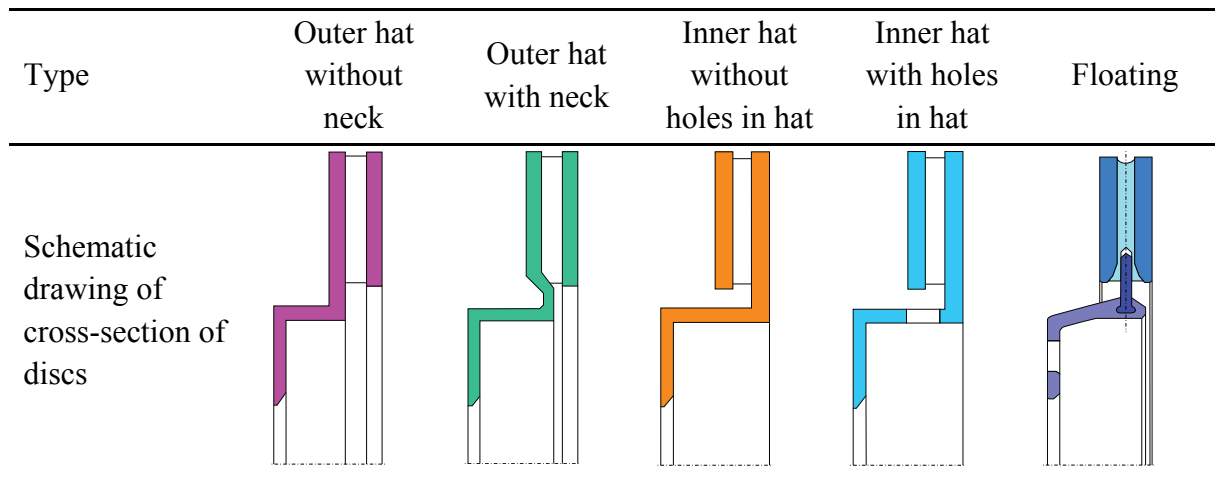


Figure 18. Basic configurations of ventilated brake discs.<sup>21</sup>

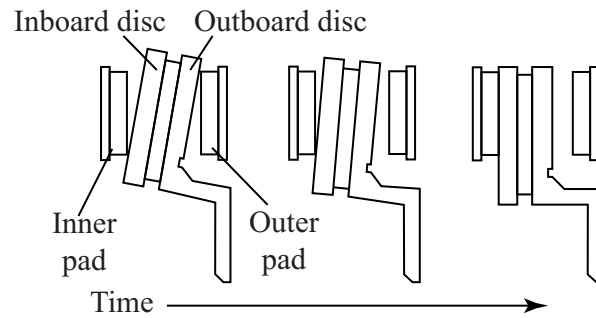


Figure 19. Schematic change in contact conditions between deformed brake disc and pads after one brake application.<sup>93</sup> The left figure shows the disc behaviour at braking, while the middle figure is the configuration when the disc is cooling down. The area of the disc near the inner radius is still in contact with the pad until the disc recovers its “normal” geometry when cooled to ambient temperature (right figure).

Ventilated brake discs as introduced in Figure 18 can have several types of cooling vane geometries and some examples are shown in Figure 20. Many variations exist for the vane shapes<sup>94</sup> and pillar shapes.<sup>95</sup> Tangential and curved vane discs are mounted in a way where the air is actively pumped. This design is also called directional vanes. The cooling influence of vanes in the discs for railway applications has been studied.<sup>23</sup>

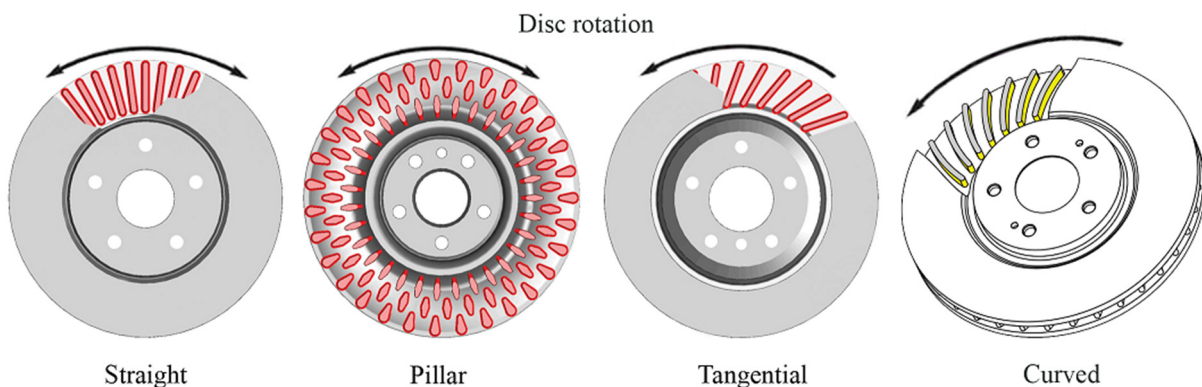


Figure 20. Examples of vane types available on the market.<sup>96,97</sup> Slotted or drilled discs can also be found, but no such configurations are shown here.

The mechanisms of heat generation and heat transfer in a disc brake system are also discussed<sup>4</sup>, see Figure 21. At braking, the major heat transfer mechanism is initially conduction through the brake disc itself and the pads. Gradually, with longer periods of braking, the temperature in the disc increases, heat is conducted to surrounding structures and cooling increases by radiation and also by convection by air flowing through the vanes.<sup>98</sup>

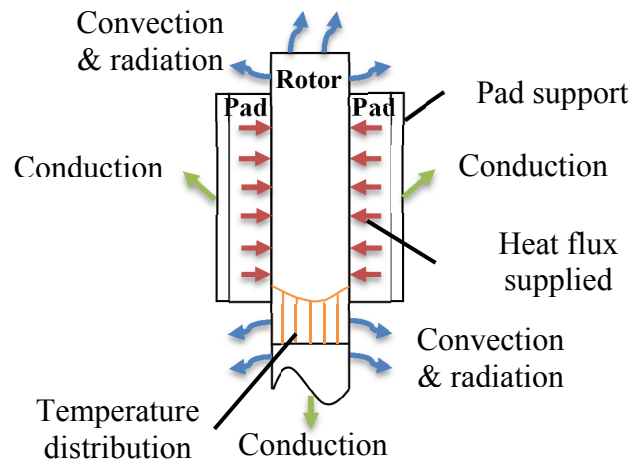


Figure 21. Heat transfer mechanism in a disc brake system.<sup>4</sup>

A description of different grey iron alloys is presented and reasons are given as to why grey cast iron is still in use nowadays, high-lighting the advantageous performance to cost ratio of this material. The role of the main chemical elements and the microstructure of grey iron alloys are discussed and thermophysical properties are introduced. The influence of temperature on the thermal properties of grey cast iron is illustrated. The manufacturing process has not been investigated. Fracture mechanisms and crack growth for grey cast iron and some relevant phenomena for this material, such as creep and thermal shocks, are surveyed.

### 3.2 Paper B

*Disc brakes for heavy vehicles – An experimental study of temperatures and cracks.* Brake rig experiments have been carried out on eight brake disc materials to measure the life of the tested discs with respect to global cracking. Drag braking is performed at a constant torque of 2800 Nm for 45 s and with a constant speed of 425 rpm (corresponding to a truck speed of about 80 km/h). Temperatures are measured in the disc and the pads (thermocouples) and on the disc surface (thermocamera). The main focus in the work was on finding the key influencing parameters which control the life of the disc. The work has been divided into two parts: analysis of data from the thermocouples and analysis of data from the thermocamera. Figure 22 shows the full-scale brake dynamometer where the discs are mounted for the accelerated drag braking crack test.

Material testing showed that seven of the eight disc materials studied show very similar thermal conductivities, at a given temperature, for the considered testing temperature range (25 °C to 900 °C). The remaining brake disc material shows a similar thermal conductivity at high temperatures while at lower temperatures it is up to 15 % lower. The chemical compositions of the tested brake discs are rather similar. The modifications mainly concern niobium and molybdenum content.

All tested brake discs exhibited hot spots and banding behaviour with more or less variations. An example of a thermal image generated at the end of the braking application is illustrated in Figure 23.

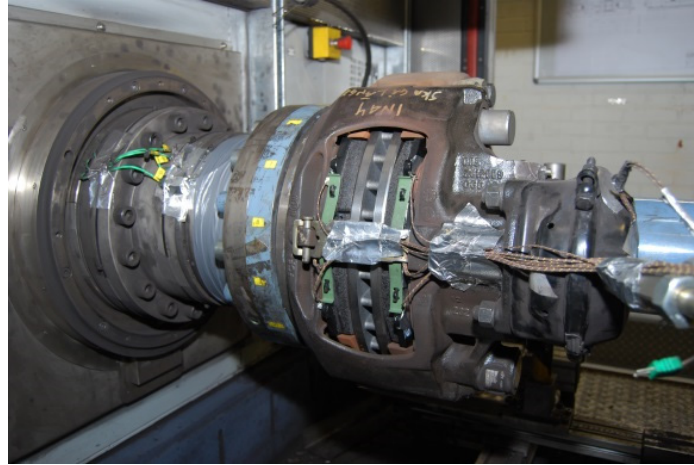


Figure 22 Brake dynamometer with a close up of brake disc and caliper.

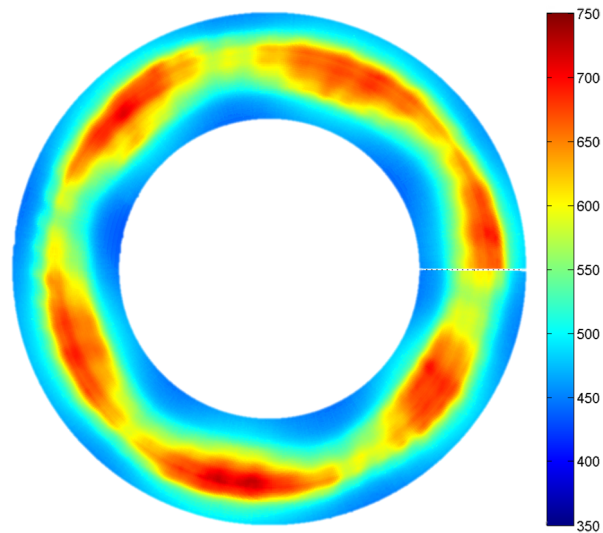


Figure 23. Example of thermal image of a brake disc showing hot spots located in one band.

It was found that the level of temperatures reached in the discs cannot be related to disc life as some discs showed high maximum temperatures but still resulted in a longer life than some other discs with lower maximum temperatures. However, discs having long lives showed migration of hot spots and/or of alternating bands, see examples in Figure 24. A general observation is an antisymmetric temperature behaviour between the two sides of brake disc. A main result of this study is that spatial fixation of hot spots and band(s) on the disc is detrimental for the brake disc life. In addition to those findings, the pad material is important for the hot spot formation regarding fixation and peak disc temperatures.

The results for crack growth show a rather stable evolution of the crack length up to 60 mm after which the crack growth rate increases substantially. However, the disc with the shortest life (a “pirate disc”) shows a much higher crack growth rate than the other discs. This disc was the one with the lower thermal conductivity than the others and which also was inclined to towards fixation of hot spots and bands.

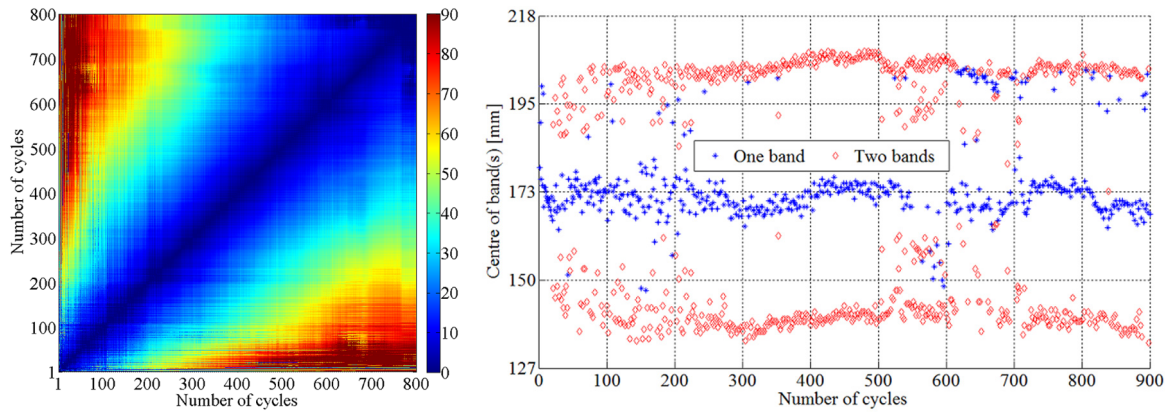


Figure 24. Example of angle shift (in degrees) showing hot spot migration (left) and variation of band(s) location (right).

### 3.3 Paper C

*Modelling of grey cast iron for application to brake discs for heavy vehicles.* In the present work a Gurson-Tveergaard-Needleman type (GTN) model was chosen as it accounts for “voids” naturally present in grey cast iron materials. Here, the graphite flakes are represented by spherical voids. This simplifying assumption is acceptable when the global response of the material is of interest. The material model accounts for non-linear elasticity, plasticity, viscoplasticity, kinematic hardening, asymmetric yielding in tension and compression and porosity introduced by void nucleation. The material model is calibrated by use of dedicated isothermal experiments and validated by monotonic tensile tests and thermomechanical fatigue experiments. In a numerical example it is applied to a brake disc FE sector. It is found that the material model is suitable for brake disc materials allowing for further improvement of brake disc design and life. It is noted that fatigue life is not studied here but is later addressed in Paper D and Paper E.

Some simplifications of the model have been introduced compared to the original formulation given by Seifert<sup>71</sup> and Metzger<sup>99</sup>, such as adoption of the classical Norton’s law for relaxation. In addition, small strains are considered and porosity evolution is assumed to be a slow process.

The material model is implemented and after this calibrated by use of dedicated uniaxial strain controlled isothermal experiments.<sup>2</sup> The applied mechanical strain cycles are varying in range but also in rate. This is intended to activate different features of the implemented material model. The model is calibrated at six temperature levels from room temperature up to 650 °C. Then, the model is validated by a use of three external sets of data for both isothermal and thermomechanical conditions. The results for ten simulated thermomechanically controlled cycles are given in Figure 25. The thermomechanical experiments have a cyclic temperature variation from 50 °C to 700 °C that is out-of-phase at 0.25 % mechanical strain range. The material parameters are extrapolated up to 700 °C. Moreover, the model has shown to be able to capture monotonic tensile testing up to 0.9 % mechanical strain while the material model has been calibrated only up to 0.3% mechanical strain amplitude.

<sup>2</sup> Due to variations in mechanical properties between material batches, although being of same specification, the stress response for the tests employed for the calibration has been scaled down by 20%.

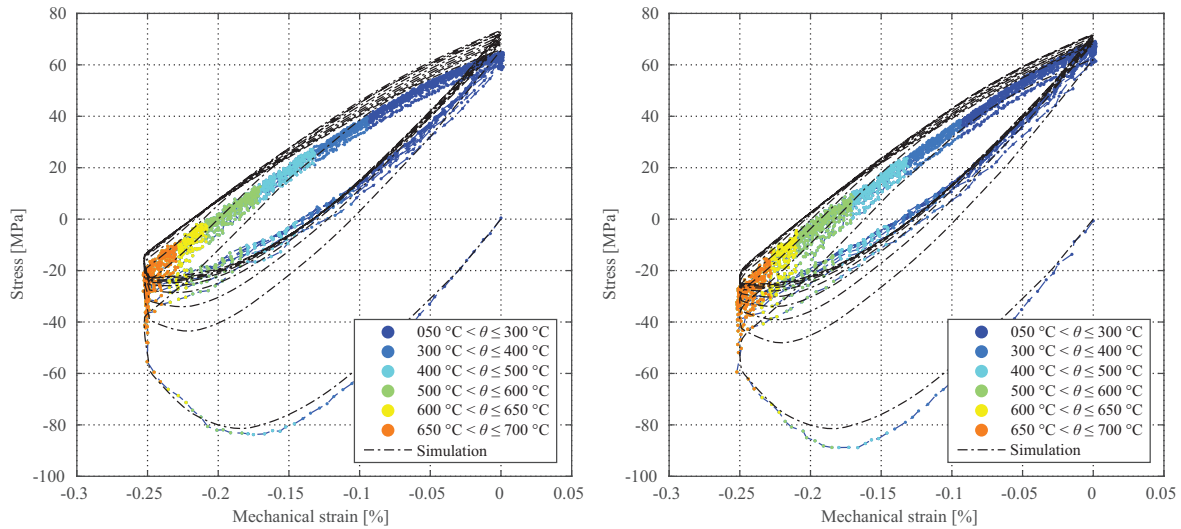


Figure 25. TMF experiments and TMF simulation for the first ten cycles at  $-0.25\%$  mechanical strain with 30 s dwell (left) and without dwell (right). Curves from experiments in colour which also indicate the temperature.

### 3.4 Paper D

*Improvement of brake disc design for heavy vehicles by parametric evaluation.* Development and implementation of material models into finite element (FE) software make possible the analysis of structures exposed to various load cases. In the present work, a parametric study is performed using a Design-Of-Experiment (DOE) approach in order to investigate the importance of cooling arrangements for mechanical fatigue. Six cooling arrangements are studied and compared to the reference brake disc used today, by use of a  $5^\circ$  sector of a brake disc and one thermal loading case. The reference disc is of hat type from the present commercial market (see Section 3.1, Figure 18 for full description of the terms) and is studied in more detail with three types of thermal loadings observed in previous experimental work in Paper B. The reference brake disc has 36 vanes equally spaced and has axial distance 18 mm between disc cheeks. The six cooling arrangements are shown in Figure 26.

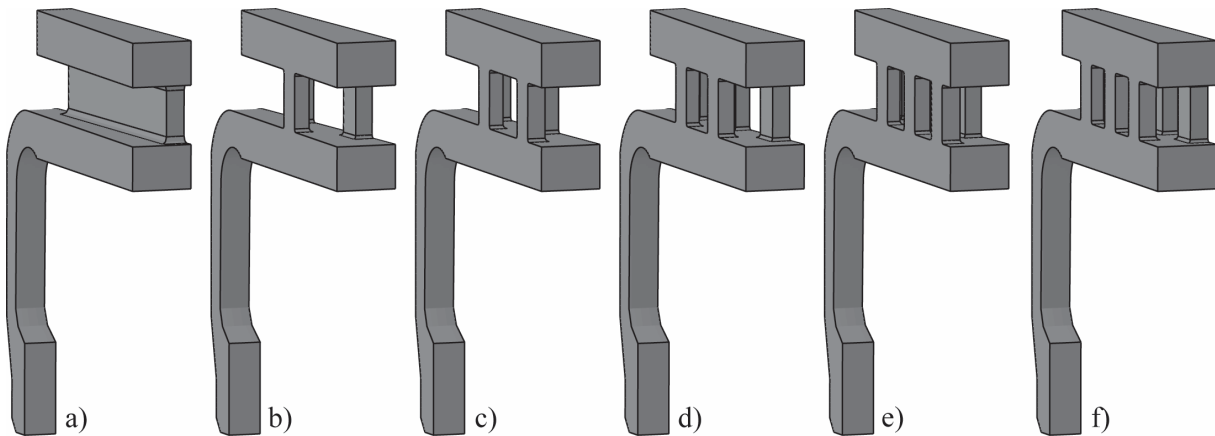


Figure 26. Geometries of brake discs for a five degree sector with a) a vane, b) three pillar rows, c) four pillar rows, d) five pillar rows, e) six pillar rows, and f) seven pillar rows. Note that some pillars are (partly) hidden.

A total number of four parameters were defined to parametrize the pillar cooling arrangement: 1) axial thickness  $t$  of the cooling channel, 2) width  $w_i$  at inner radius of the vane/pillars, 3) width  $w_o$  at outer radius of the pillars and 4) length  $L$  of each pillar. The parametrization of the vane design is chosen to only consider a single width parameter corresponding to an angle  $\alpha$ , thus controlling the width. In the present study the vanes or pillars are assumed to have even spacing  $10^\circ$  in the circumferential direction. The geometries are assessed for a chosen thermal loading that corresponds to a severe temperature pattern found in the study of full-scale experiments in Paper B for the simulated brake disc material. It is composed of one hot band on the hat surface and two hot bands having lower intensity on the piston surface. A succession of three identical brake cycles are performed with cooling to  $50^\circ\text{C}$  between cycles.

Fatigue damage is assessed for the last simulated cycle using a so-called “fatigue load” parameter based on the Smith- Watson-Topper (SWT) criterion, defined as the maximum stress in tension and the mechanical strain amplitude. Optimization, based on response surfaces, is performed for the total mass of the brake disc or for the “fatigue load” so that either the mass is improved at a life corresponding to that of the reference brake disc or the life is improved given the mass of the reference disc. The assessment of the “fatigue load” showed that the critical point is at the centre of the hot band and located at the vane. This is not 100 % in line with the experimental findings where the cracks have been seen to develop at the edge of the vane. However, the analyses do not account for the potential residual stresses after casting that could locally modify the material response.

For the brake disc with vanes, optimization using response surfaces shows that the reference brake disc can be improved by either decreasing the mass or increasing the life. In the best cases, 2.1 kg can be saved as compared to the 30.0 kg reference brake disc or life can be increased by 55 %. For the optimized pillar row cases, the maximum reduction in mass is 4.0 kg for the three pillar rows. Lives of optimized cooling arrangements show a clear improvement, with an increase of about 50% for all cases, as compared to the reference brake disc. In a search for a geometry having a balance between brake disc mass and life, three or four pillar rows seem to be the best candidates. It was also shown that it is possible to gain life by up to 80 % if one would allow for an increase of brake disc mass by 2 kg. The analyses on the reference brake disc indicate that a banding load case can be more detrimental than hot spot load case, due to a lower cyclic strain range, even if the hotspot case has higher temperature.

### **3.5 Paper E**

*Thermomechanical fatigue of grey cast iron brake discs for heavy vehicles.* Being able to predict the life of mechanical components is critical for maintenance planning and safety. Various life models are available in the literature, but not all will be useful to represent the life of grey cast iron materials. Some traditional empirical life models can, after proper calibration of their parameters, be useful for brake disc applications. More recently, fatigue models for cast irons have been proposed that are based on a fracture mechanics approach, then taking advantage of the free graphite acting as cracks inside the metal matrix.

The choice of a life model is influenced by how well it can account for the fatigue phenomena at hand, but also by how complex it is to use and calibrate and the required amount of

experimental results. For this reason, the traditional fatigue models are normally preferred. In the present paper, four models for predicting the life of specimens, exposed to uniaxial strain controlled tests, are studied and compared. Two of them are mechanisms based damage models while the other two are the Smith-Watson-Topper (SWT) and the Coffin-Manson models.

Simpler models, such as stress-strain loop shape analysis, can be used for analysing plastic work, strain energy density, stiffness evolution, etc. In order to characterise the material behaviour at different temperatures, the shapes of the stress strain loops were analysed under given strain controlled loading. Development in peak and trough stresses, tangent stiffness evolution and estimates of plastic work are presented.

The four fatigue models are presented and calibrated using results from isothermal tests (at 300 °C and 600 °C) and thermomechanical tests (out-of-phase test, 50 to 700 °C with compressive strain down to -0.3%). The life model based on Paris' law, which is intended for use at a given temperature range at the TMF test, is calibrated only using TMF data. Resulting relationships are compared and discussed to find out the testing required for predicting TMF life using the models.

Finally, the predictions of the four life models are applied to the results from an FE simulation of the full-scale brake disc experiments, reported in Paper B. The predicted lives are discussed and compared to the brake disc experiments, then considering onset of global cracking. Failure criteria for simulations and experiments are discussed.

## 4 CONCLUDING REMARKS AND FUTURE DEVELOPEMENTS

### 4.1 General

The present thesis has reported the results of a doctoral project which is part of the collaboration project “Improved performance of brake discs” between the Department of Applied Mechanics at Chalmers University of Technology and the truck manufacturing company Scania CV AB. The project was formulated in 2009 and in 2013 (Stage 1 and Stage 2) with the aim at enhancing the performance of cast iron brake discs and at gaining a better understanding of the mechanisms that control cracking and disc life. For Chalmers a main focus in the project has been to assess experimental results and to work with computational models for temperatures, stresses, strains and fatigue/cracking and for optimization of mass and life of the brake discs.

The study is motivated by the fact that cast iron brake discs are common in braking systems for heavy vehicles. These brake discs provide favourable performance at low cost. However, the life of the disc is often limited by formation of cracks due to thermal stresses that arise during the repeated heating and cooling. A brake disc with better resistance to thermal cracking, with preserved wear and friction properties would lead to significant savings by reducing the number of disc replacements during the lifetime of the vehicle. Therefore, the understanding of the mechanisms that control cracking and disc life are of great importance.

### 4.2 Discussion of results

The present work has resulted in a state-of-the-art study (Paper A), one journal paper (Paper B) one paper which is submitted for international publication (Paper C) and two papers (Papers D and E) which later will be submitted for international publication. Further, a paper on thermomechanical fatigue for brake disc materials resulted in a conference presentation /proceeding publication, which, however, is not included in the present thesis. In the following, condensed summaries and some results and aspects of the five papers and how they contribute to the project, are highlighted.

*Paper A: Improved performance of brake discs – State-of-the-art survey.* The paper was written in the beginning of the project and gives an extensive overview of aspects of the complex phenomena that influence the life of brake discs: heat transfer, temperatures, stresses, plastification, residual stresses, fatigue cracks, wear, material properties, cast iron alloys, etc. Further, it shows the wide topics involved in braking applications e g, tribology and squeal noise. The survey contain 98 references and has been very useful in the project as an information source on braking problems and related fields. There has been no intention or plan to submit this paper for publication.

*Paper B: Disc brakes for heavy vehicles – An experimental study of temperatures and cracks.* The brake rig experiments and the detailed analyses of the measured temperatures reveal some key phenomena affecting disc life. It has been demonstrated that the temperatures reached in the disc are not by themselves determining the disc life. It was found that hot spots and band fixation, as generated by thermoelastic instabilities (TEI), contribute to development of cracks. The results made it possible to establish some typical thermal loading cases that were used in

the optimization and fatigue studies in Papers C, D and E. The rig tests were performed on several materials and resulted in a patented material specification for brake discs.

*Paper C: Modelling of grey cast iron for application to brake discs for heavy vehicles.* A major effort in the project has been to develop and implement a constitutive model of Gurson type for grey cast iron to be used with a commercial finite element software. The model accounts for cyclic loading with asymmetric yielding in tension and compression, kinematic hardening effects, viscoplastic response and temperature dependence. The model was calibrated for temperatures relevant for braking applications using dedicated isothermal tests and, finally, validated against monotonic tensile tests, isothermal fatigue tests and thermomechanical fatigue tests. The agreement is deemed as good up to 500 °C and 0.3% strain and as satisfactory up to 650 °C and 0.2% strain. The material model has proven to be operative in FE simulations of braking cycles for cast iron brake discs. The simulations in Papers D and E have been made possible through this work. There are obvious applications of the model, after proper calibration, for other cast iron components exposed to temperature loads, e.g. cylinder heads of diesel engines.

*Paper D: Improvement of brake disc design for heavy vehicles by parametric evaluation.* A parametric study was performed to explore potential improvements of the cooling channels of a brake disc design considering fatigue life. The thermal loading of the brake discs was chosen to represent typical loading recorded in the full-scale experiments in Paper B. The material model in Paper C was employed in extensive FE simulations. In the end, a response surface methodology was applied to optimize six types of cooling arrangements (one with straight vanes and five with different numbers of pillar rows) in order to minimize brake disc mass or maximize fatigue life. The parametric study and the optimization provide useful trends regarding brake disc geometry. The study demonstrates the potential to simulate, in a realistic manner, cast iron brake discs exposed to brake loads.

*Paper E: Thermomechanical fatigue of grey cast iron brake discs for heavy vehicles.* Four fatigue life models were selected and calibrated. The models were compared to full-scale testing based on simulated results generated in Paper D using the material model implemented in Paper C.

Studying results from isothermal and TMF tests on specimens, it is found that it is not possible to predict lives for the thermomechanical situation when using the models only calibrated to isothermal tests. Large variations in predicted lives are found, that generally are overestimating the life for the TMF situation. This includes the DTMF-model and also the Coffin-Manson models. These two models have previously been proven to be useful for temperatures up to 425 °C. But for both TMF and isothermal cases, they substantially overestimate the lives of the brake disc experiment. However, it should then be noted that the analysis of stress strain hysteresis loops showed that the mechanical properties drop substantially at high temperature (above 500 °C). It can be concluded that the mechanisms occurring at elevated temperatures need further considerations.

In an application example, the predicted fatigue lives are compared to the brake disc experiments in Paper B. The studied fatigue life models are calibrated to tests on specimens where failure is defined as a given decrease in load carrying capacity. Straightforward comparison with brake disc experiments, where global cracking is of main interest, is not

possible and needs further considerations. Failure according to the fatigue models could indicate the coalescence of microstructurally small cracks and the appearance of a macroscopic crack. This would then, in approximate way, correspond to some 10 cycles, after which a macroscopic crack growth takes place (estimated from crack lengths on the friction surface of about 10-30 mm when first inspected after 100 cycles). After this the “life” in the experiments corresponds to macroscopic crack propagation. If one studies the onset of cracking only (not global crack growth), using parameters for the models calibrated for TMF specimen tests, a rather good agreement between models and the full-scale tests is found. This could be attributed to the rather similar temperature-strain cycling at TMF specimen testing and at full-scale experiment.

### **4.3 Future developments**

Naturally, there are a number of aspects of the present work that could be worth developing further. Ten such aspects are mentioned in the following along with some short comments.

*Rig test and field conditions.* Presently, brake discs are developed using standard rig tests which are considered to represent some common field conditions. A thorough study of how representative such rig tests are, and what condition in field conditions that might / might not be covered by the rig tests, would be valuable.

*Temperature patterns.* It would be interesting to further develop the analysis of the rig test results in Paper B. More typical loading cases could be identified and developed into loading cases for assessment of brake discs. Possibly, migration patterns for hot spots could be included.

*Numerical modelling of interaction between brake pad and brake disc.* The complicated thermoelastic interaction between the brake pads and the brake disc is a great challenge to simulate in an accurate way. The required computer capacity is very high. Nevertheless, such simulations would be very useful for the understanding and combating TEI phenomena like banding and hot spots.

*Tribology.* The tribological phenomena in the pad/disc interface are important for wear, friction and thermoelastic interaction and also for generation of noise and vibration. This has not been a focus of the present project but would be a natural area to exploit further.

*Properties of cast iron.* There is a substantial scatter in material parameters of cast iron. This fact has caused some problem in the calibration of the material model in the present project. More knowledge and methods to handle such scatter would be very useful.

*Phase transformation of cast iron.* Phase transformation of cast iron caused by the thermal loading at braking could be a major importance for disc life. This phenomenon has not been investigated in the present project. It would be interesting and useful to establish under which conditions this would be a major problem.

*Improvement of material model.* The material model in Paper C could be further developed to make it more user friendly, with a faster search for material parameters based on experimental data. Improvement of the numerical efficiency of the code would be useful, e.g., by developing an analytical version of the so-called ATS tensor.

*Crack growth in brake discs.* In Paper B, some data on crack growth observed in the brake rig tests were given and discussed. However, further work, also involving modelling, would give more knowledge and might provide tools for suppressing or limiting the crack growth.

*Influence of severe loadings.* The fatigue models employed in Paper C, D and E indicate that even a single severe brake cycle could have a major detrimental effect on disc life. This would be interesting to investigate further, both by simulations and by experiments.

*Hat disc design.* There seems to be opportunities to optimize hat discs by modifying the neck area in order to allow for more expansion of the cheeks and thus to reduce the build-up of high compressive stresses during braking. A challenge is then to meet the requirements on static strength. Further, it has not been found out in the present project why there is such a big difference in the temperatures and life between the hat side and the piston side of a disc.

## 5 REFERENCES

1. Truck market 2024 - Sustainable growth in global markets. Deloitte Consulting GmbH; 2014. p. 54.
2. Scania R 730 8x4 twin-steer V8 Streamline, Topline cab, Heavy haulage tractor.: Scania CV AB; 2013.
3. Scania heavy-haulage tractors – on top of every task. Scania CV AB; 2013.
4. Talati F and Jalalifar S. Investigation of heat transfer phenomena in a ventilated disk brake rotor with straight radial rounded vanes. *Journal of Applied Sciences* 2008; 8(20): 3583-3592.
5. *Braking 2004: Vehicle braking and chassis control*. Barton DC, Blackwood A, editors: Wiley-Blackwell; 1st edition, 2004.
6. Scania CV AB. Taking a look back at the development of Scania Retarder. <http://newsroom.scania.com/en-group/2013/02/22/a-brake-with-history> (2013, accessed September 2013).
7. Marsh KJ. *Full-scale fatigue testing of components and structures*. London: Butterworths, 1988.
8. Chatterley TC and Macnaughtan MP. Cast iron brake discs - Current position, performance and future trends in Europe. In: *SAE International Congress and Exposition*. Detroit, Michigan, USA, March 1-4, 1999 1999: SAE International, Warrendale, Pennsylvania, USA. 10 pp.
9. Maleque MA, et al. Material selection method in design of automotive brake disc. In: *Proceedings of the World Congress on Engineering 2010*. London, UK, June 30 - July 2, 2010: Newswood Limited. 5 pp.
10. Toshikazu O and Masanori I. Increasing thermal strength of brake discs by improving material homogeneity. In: *27th Annual Brake Colloquium and Exhibition*. Tampa, Florida, USA, October 11-14, 2009: SAE International, Warrendale, Pennsylvania, USA. 7 pp.
11. Thos Winnard & Sons Ltd. Brake Discs Service Guide. [http://www.winnard.co.uk/prod\\_disc\\_service\\_guide.html](http://www.winnard.co.uk/prod_disc_service_guide.html), accessed September 2013).
12. Gilles T. *Automotive Chassis: Brakes, Suspension, and Steering*: Delmar Cengage Learning, 2004.
13. Emmett R and Paul HG. Brake lining set having different compressibility. Google Patents; 2010.
14. Day A. *Braking of road vehicles*. Oxford: Butterworth-Heinemann, 2014, 472 pp.
15. Santini JJ and Kennedy Jr FE. Experimental investigation of surface temperatures and wear in disk brakes. *ASLE Prepr* 1974.
16. Smith AC and Hudson SM. A New, High Torque Brake Design Using Sliding Discs. 2003: SAE International.
17. Longhurst C. The brake bible. [http://www.carbibles.com/brake\\_bible.html](http://www.carbibles.com/brake_bible.html) (2014, accessed october 2015).
18. The compelling case for air disc brakes in heavy truck braking: A white paper. Elyria, Ohio: Bendix Spicer Foundation Brake LLC; 2011.
19. Brakes Market for Friction Products by OE & Aftermarket (Brake Pads, Shoes, Lining, Rotor, Drum), Material type (Pads-Non Metallic, Semi-Metallic, Ceramic & Lining-Organic, Semi-Metallic & Synthetic) & Two-wheelers - Trends & Forecast to 2019. 2015, [marketsandmarkets.com](http://marketsandmarkets.com), AT 3214.

20. Brake System Market by Application (PC, LCV, HCV, Off-Highway, Wagon, Locomotive, and RTV), Type (Disc and Drum), Technology (ABS, TCS, ESC, and EBD), Rolling Stock and Locomotive (Air, EP, ECP, and others), and Region - Global Forecast to 2020. 2015, marketsandmarkets.com, AT 3016.
21. Okamura T and Yumoto H. Fundamental study on thermal behavior of brake discs. In: *24th Annual Brake Colloquium and Exhibition*. Grapevine, Texas, USA, October 8-11 2006: SAE International, Warrendale, Pennsylvania, USA. 16 pp.
22. Tirovic M. Development of a lightweight wheel carrier for commercial vehicles. *International Journal of Vehicle Design* 2012; 60(1/2): 138-154.
23. Tirović M and Voller GP. Heat dissipation from high speed train brakes - the efficiency compromise. In: *TILT 2003 conference*. Lille, France 2003, 8 pp.
24. Tirović M. Energy thrift and improved performance achieved through novel railway brake discs. *Applied Energy* 2009; 86: 317-324.
25. AP RACING. Brake discs. 2014.
26. Tirovic M. Research into Brakes and Braking Systems [PowerPoint presentation]. 2014, 98 pp.
27. Ihm MK. Introduction to gray cast Iron brake rotor metallurgy. SAE Brake Colloquium & Exhibition - 21st Annual - lecture notes, 2003, 97 pp.
28. Carbon-ceramic brake disks.  
[https://www.sglgroup.com/cms/international/products/product-groups/cc/carbon-ceramic-brake-disks/index.html?\\_\\_locale=en](https://www.sglgroup.com/cms/international/products/product-groups/cc/carbon-ceramic-brake-disks/index.html?__locale=en), accessed october 2015).
29. Skrzypek JJ, et al. *Advanced Materials and Structures for Extreme Operating Conditions*: Springer Berlin Heidelberg, 2008.
30. Odqvist FKG. *Mathematical theory of creep and creep rupture*: Oxford : Clarendon, 1974.
31. *Properties and Selection: Irons, Steels, and High-Performance Alloys* ASM International, 1990, 1063 pp.
32. ASTM standards. Standard specification for gray iron castings. Designation: A48/A48M-03(2012): ASTM International; 2012. 6 pp.
33. EN 1561: Grey cast iron. European Standard; 1997. 19 pp.
34. Jabbari Behnam MM, et al. Effect of cooling rate on microstructure and mechanical properties of gray cast iron. *Materials Science and Engineering A* 2010; 528: 583–588.
35. *Springer Handbook of Mechanical Engineering*. Grote K-H, Antonsson EK, editors: Springer Berlin Heidelberg, 2009, 1576 pp.
36. ISO 945-1:2008. Microstructure of cast irons - Part 1: Graphite classification by visual analysis. International Organization for Standardization, 2008.
37. Holmgren D, et al. Influences of the graphite growth direction on the thermal conductivity of cast iron. *Metallurgical and Materials Transactions A* 2007; 38(A): 268-275.
38. Holmgren D, et al. Effects of carbon content and solidification rate on the thermal conductivity of grey cast iron. *Tsinghua Science and Technology* 2008; 13(2): 170-176a.
39. Pollack H. *Materials Science and Metallurgy (4th Edition)*. Englewood Cliffs, NJ: Prentice Hall, 1988.
40. Shah KP. Cast irons. <http://practicalmaintenance.net/?p=1611>, accessed october 2015).
41. Dossett JL and White CV. Heat Treating of Gray Irons. ASM Handbook. 4D: ASM International; 2014. p. 493–507.

42. Anderson AE and Knapp RA. Hot spotting in automotive friction systems. *Wear* 1990; 135: 316-337.
43. *Chassis Handbook: Fundamentals, Driving Dynamics, Components, Mechatronics, Perspectives*. Heißing B, Ersoy M, editors: Vieweg+Teubner, 2011.
44. Wenbin Z, et al. Niobium alloying effect in high carbon equivalent grey cast iron. *China Foundry* 2011; 8(1): 36-40.
45. Engineering Design Handbook - Analysis and Design of Automotive Brake Systems: (DARCOM-P 706-358). U.S. Army Materiel Command.
46. Kennedy Jr FE. Thermal and thermomechanical effects in dry sliding. *Wear* 1984; 100(1-3): 453-476.
47. Barber JR. Thermoelastic instabilities in the sliding of conforming solids. *Proceedings of the Royal Society of London - Mathematical and Physical Sciences* 1969; 312(1510): 381-394.
48. Kennedy Jr FE and Ling FF. A thermal, thermoelastic and wear simulation of a high energy sliding contact problem. *ASME Pap* 1973(73 -Lub-6).
49. Day AJ, et al. Thermal effects and pressure distributions in brakes. *IMechE Journal of Automobile Engineering* 1991; 205(34): 199-205.
50. Inoue H. Analysis of brake judder caused by thermal deformation of brake disk rotors. *SAE 865131* 1986.
51. Zagrodzki P, et al. Simulation of a sliding system with frictionally-excited thermoelastic instability. *Thermal Stresses* 1999; Cracow, Poland.
52. Panier S, et al. An experimental investigation of hot spots in railway disc brakes. *Wear* 2004; 256(7-8): 764-773.
53. Dufrénoy P and Brunel JF. Thermal Localizations in Friction Brakes. 2008: SAE International.
54. Pevec M, et al. Elevated temperature low cycle fatigue of grey cast iron used for automotive brake discs. *Eng Fail Anal* 2014; 42: 221-230.
55. Wahlström J, et al. A cellular automaton approach to numerically simulate the contact situation in disc brakes. *Tribology Letters* 2011; 42(3): 253-262.
56. Thevenet J, et al. Measurements of brake disc surface temperature and emissivity by two-color pyrometry. *Applied Thermal Engineering* 2010; 30(6-7): 753-759.
57. Kasem H, et al. An emissivity-corrected method for the accurate radiometric measurement of transient surface temperatures during braking. *Tribology International* 2010; 43(10): 1823-1830.
58. Dahlberg T and Ekberg A. *Failure fracture fatigue - An introduction*: Studentlitteratur AB, 2002.
59. Suresh S. *Fatigue of Materials, 2nd Edition*: Cambridge University Press, 1998.
60. Coffin LF. A study of the effect of cyclic thermal stresses on a ductile metal. *Transaction of American Society of Mechanical Engineering* 1954; 76:931-50.
61. Manson SS. Fatigue: A complex subject-some simple approximations. *Experimental Mechanics* 1965; 5: 193-226.
62. Basquin BO. The exponential law of endurance tests. *Proceedings - American Society for Testing Materials* 1910; 10: 625-630.
63. Campbell FC, editor. *Elements of Metallurgy and Engineering Alloys*. Materials Park, Ohio 44073-0002: ASM International; 2008.

64. Zoroufi M. *Manufacturing process effects on fatigue design and optimization of automotive components – An analytical and experimental study*. The University of Toledo, 2004.
65. Morrow J. Fatigue properties of metals, Section 3.2. *Fatigue Design Handbook*. Warrendale, PA: Society of Automotive Engineers, Pub. No. AE-4; 1968.
66. Halford G and Manson SS. Life prediction of thermal–mechanical fatigue using strain range partitioning. In: Spera DA, Mowbray DF, editors. *Thermal Fatigue of Materials and Components*. 612: ASTM STP; 1976.
67. Weinacht DJ. Fatigue behavior of Gray Cast Iron under Torsional Loads. College of Engineering, University of Illinois at Urbana-Champaign, Department of Mechanical and Industrial Engineering MaDD; 1986.
68. Fash J and Socie DF. Fatigue behaviour and mean effects in grey cast iron. *International Journal of Fatigue* 1982; 4(3): 137-142.
69. Gocmez T, et al. A new low cycle fatigue criterion for isothermal and out-of-phase thermomechanical loading. *International Journal of Fatigue* 2010; 32(4): 769-779.
70. Uihlein A, et al. Entwicklung von Rechenmodellen zur Lebensdauervorhersage von Motorbauteilen unter thermisch-mechanischer Ermüdungsbeanspruchung. Frankfurt: Forschungsvereinigung Verbrennungskraftmaschinen e.V. = FVV, Abschlussbericht Vorhaben Nr. 825, Heft 860: 2008.
71. Seifert T and Riedel H. Mechanism-based thermomechanical fatigue life prediction of cast iron. Part I: Models. *International Journal of Fatigue* 2010; 32(8): 1358-1367.
72. Schweizer C, et al. Mechanisms and modelling of fatigue crack growth under combined low and high cycle fatigue loading. *International Journal of Fatigue* 2011; 33(2): 194-202.
73. Metzger M, et al. Lifetime prediction of cast iron materials under combined thermomechanical fatigue and high cycle fatigue loading using a mechanism-based model. *International Journal of Fatigue* 2013; 53: 58-66.
74. Norman V, et al. Thermo-mechanical and superimposed high-cycle fatigue interactions in compacted graphite iron. *International Journal of Fatigue* 2015; 80: 381-390.
75. Kalousek J and Magel E. Achieving a balance: The "magic" wear rate. *Railw Track Struct* 1997; 93(3): 50-X54.
76. Dufrenoy P, et al. Quantitative identification of braking disc cracking parameters: hot spots, pad type, disc material. In: *6th European Conference on Braking, (JEF 2010)*. Lille, France 2010, 8 pp.
77. ASTM standards. Standard Practice for Strain Controlled Thermomechanical Fatigue Testing. Designation: ASTM E2368-10: ASTM International; 2010.
78. Le Gigan G, et al. Thermomechanical fatigue of brake disc materials - Results from modelling and experiments. Eurobrake 2012; 2012; Dresden, Germany.
79. Dunne F and Petrinic N. *Introduction to Computational Plasticity*. Oxford, GBR Oxford University Press, 2005.
80. McClintock FA, et al. Ductile fracture by hole growth in shear bands. *Int J Fract* 1966; 2(4): 614-627.
81. McClintock FA. A Criterion for Ductile Fracture by the Growth of Holes. *Journal of Applied Mechanics* 1968; 35(2): 363-371.
82. Rice JR and Tracey DM. On the ductile enlargement of voids under triaxiality. *Journal of the Mechanics and Physics of Solids* 1969; 17: 201-217.

83. Gurson AL. Continuum theory of ductile rupture by void nucleation and growth: Part I: Yield criteria and flow rules for porous ductile media. *Journal of Engineering Materials and Technology, Transactions of the ASME* 1977; 99 Ser H(1): 2-15.
84. Gurson AL. Porous rigid-plastic materials containing rigid inclusions - Yield function, plastic potential, and void nucleation. *Fract 1977 adv in res on the strength and fract of mater, Int Conf on Fract, 4th* 1978; 2 A: 357-364.
85. Argon AS, et al. Cavity formation from inclusions in ductile fracture. *Metallurgical Transactions A* 1975; 6(3): 825-837.
86. Thomason PF. A theory for ductile fracture by internal necking of cavities. *Journal of Institute Metals* 1968; 96: 360-365.
87. Thomason PF. Theory for the effects of strain-rate-sensitivity on ductile fracture. *Metal Science J* 1969; 3: 139-141.
88. Zhang ZL and Niemi E. A new failure criterion for the Gurson-Tvergaard dilational constitutive model. *International Journal of Fracture* 1995; 70(4): 321-334.
89. Betegón C, et al. Implicit integration procedure for viscoplastic Gurson materials. *Computer Methods in Applied Mechanics and Engineering* 2006; 195(44-47): 6146-6157.
90. Gurson AL. *Plastic flow and fracture behavior of ductile materials incorporating void nucleation, growth, and interaction*. Ph.D. Thesis, Brown University, Providence, Rhode Island, USA, 1975.
91. Hao S and Brocks W. The Gurson-Tvergaard-Needleman-model for rate and temperature-dependent materials with isotropic and kinematic hardening. *Computational Mechanics* 1997; 20(1): 34-40.
92. Ristinmaa M. Void growth in cyclic loaded porous plastic solid. *Mechanics of Materials* 1997; 26(4): 227-245.
93. Kubota M, et al. Development of a lightweight brake disc rotor: a design approach for achieving an optimum thermal, vibration and weight balance. *JSAE review* 2000; 21(3): 349-355.
94. Galindo-Lopez CH and Tirović M. Understanding and improving the convective cooling of brake discs with radial vanes. *Proceedings of the Institution of Mechanical Engineers, Part D: Journal of Automobile Engineering* 2008; 222(7): 1211-1229.
95. Palmer E, et al. An optimization study of a multiple-row pin-vented brake disc to promote brake cooling using computational fluid dynamics. *Proceedings of the Institution of Mechanical Engineers, Part D: Journal of Automobile Engineering* 2009; 223(7): 865-875.
96. Jay C. Project Nissan 350z - Brake Guru 101. <http://www.modified.com/tech/modp-0908-project-nissan-350z-stoptech-brakes/viewall.html> (2009, accessed September 2013).
97. RacingBrake 2 Piece Rotor Review! <http://www.e90post.com/forums/showpost.php?p=8653991&postcount=1> (2011, accessed October 2013).
98. Eisengräber R, et al. Comparison of different methods for the determination of the friction temperature of disc brakes. In: *International Congress and Exposition*. Detroit, Michigan, March 1-4, 1999 1999: SAE International, Warrendale, Pennsylvania, USA. 498-504 pp.
99. Metzger M and Seifert T. On the exploitation of Armstrong-Frederik type nonlinear kinematic hardening in the numerical integration and finite-element implementation of pressure dependent plasticity models. *Computational Mechanics* 2013; 52(3): 515-524.

# **Paper A**

## **Improved performance of brake discs: State-of-the-art survey**



# IMPROVED PERFORMANCE OF BRAKE DISCS: STATE-OF-THE-ART SURVEY

Chalmers University of Technology, Gothenburg, Sweden, 2011

<sup>1</sup>Le Gigan, Gaël, <sup>2</sup>Lundén, Roger, <sup>2,3</sup>Vernersson, Tore

<sup>1</sup>Chalmers University of Technology, Applied Mechanics, Gothenburg, Sweden

<sup>2</sup>Chalmers Applied Mechanics / CHARMEC, Gothenburg, Sweden

<sup>3</sup>Epsilon, Gothenburg, Sweden

## ABSTRACT

Brake discs are exposed to high thermomechanical loads when the brake pads are pressed onto the rotating disc during braking and the vehicle's kinetic energy is converted into thermal energy. The complex load case causes disc wear, but also the formation of cracks due to thermal stresses that arise in the surface layers of the disc during repeated heating and cooling. These cracks often determine the life of the disc. A brake disc with better resistance to thermal cracking and preserved wear and friction properties would lead to significant savings, particularly in the form of a higher utilization of the vehicle. In order to enhance the performance of brake discs, thereby reducing the number of disc replacements during the life of the vehicle, Scania has initiated a PhD project aimed at a deeper understanding of the mechanisms that control cracking and the of the discs.

The present state-of-the-art survey is the result of the first efforts to gather and compile information useful for the PhD project. An overview of general aspects of braking is given. The study focusses on brake discs made from cast iron material. For traditional and new such materials thermal and mechanical properties have been studied: heat conduction, heat capacity, static strength, fatigue strength and wear resistance. An overview of the influence of different alloying elements on the microstructure and other properties of the material is presented. Further, aspects of modelling of the thermomechanical behaviour of the disc brake system are reported. It is concluded that due to the complex phenomena and the large number of parameters involved, a total optimization of brake discs is a very difficult task.

***Keywords: disc braking, thermomechanical fatigue, cracking, thermal stress, residual stress, wear, heat transfer, cast iron alloy***

## 1 INTRODUCTION

The present state-of-the-art survey reports on the initial efforts in the FFI-project “Improved performance of brake discs”. The project is a collaboration between the truck manufacturer Scania and the Department of Applied Mechanics at Chalmers University of Technology. In this chapter the background to the project, the aim of the present study, a general overview of disc braking and information on different disc designs are given.

### 1.1 BACKGROUND

When a driver presses the brake pedal, the contacting brake discs and pads are exposed to high thermomechanical loads while converting the kinetic energy of the vehicle into thermal energy. The thermal loading, generated by the friction between the brake disc and its two pads, induces stresses which lead to crack initiation and crack propagation [1]. Compressive stresses are induced at high temperatures during braking due to restrained thermal expansion of the surface layers of the disc material, and as a result of plastification during braking, tensile residual stresses appear in the surface layers when the brake disc has cooled down. During their life, discs and pads are subjected to repeated heating and cooling, which induces thermal stress cycling in the

discs, promoting surface cracking. Ideally, the heat generation between disc and pad can be assumed to be uniformly distributed over the contacting surfaces. However, thermomechanical phenomena such as thermoelastic instabilities causing banding, hot spotting and wear, and the fact that the brake pads cover only a part of the disc surfaces, make the heat generation non-uniform. The resulting complex loading reduces the lifespan of discs and pads. Locally increased heat generation in the disc surface means severe temperature gradients and thereby severe stresses in the disc.

With the aim to increase the vehicle performance and to reduce the number of replacements of discs, and hence the costs, particularly in the form of inactive vehicles, Scania has initiated this work aimed at enhanced understanding of the mechanisms that determine the lifespan of brake discs. Today's brake discs for trucks are made from grey cast iron with suitable characteristics such as high thermal conductivity and preserved mechanical properties at elevated temperatures. Other important characteristics are disc friction and wear and these properties are directly related to the type of pad used. Different load cases can result in various modes of failure and a disc that meets certain requirements may be worse in other respects. Depending on where and how the truck is running, also the load on the disc will vary. To optimize the performance of a brake disc is therefore very difficult. The present project focusses on maximizing the life of the disc with respect to resistance against thermal cracking. However, other properties such as friction and wear must still be satisfactory.

The work on brake discs previously carried out at Scania has focussed on examining different material microstructures of the discs and their relationship to the mechanical and thermodynamical properties. In the future the results from this work should also be linked to the component testing of discs and pads in a brake dynamometer. In addition, computational models should be developed that can be used for ranking of candidate disc materials, for example, using realistic analyses of life expectancy. Calculation tools should also be developed to allow for optimization of the geometry and weight of the discs.

The project is expected to generate:

- Methods for ranking (disc) friction materials with respect to
  - friction properties
  - wear properties
  - resistance to thermal cracking
- Methods for measuring the distribution of brake power between disc and pads
- Computational models for lifespan calculations of brake discs with respect to thermal cracking
- Models for optimizing geometry and weight of brake discs
- Proposals of new alloys for brake discs with increased life expectancy and improved overall performance
- Enhanced competence in tribology and thermomechanical fatigue and also in computational modelling

In summary, a brake disc with improved resistance to thermal cracking and with preserved wear and friction properties, would lead to significant savings, particularly in the form of higher utilization of the vehicle. In order to increase the performance of brake discs, thereby reducing the number of disc replacements during the life of the vehicle, Scania has initiated the present PhD project "Improved performance of brake discs" aimed at a better understanding of the mechanisms which influence the cracking and life of brake discs.

## *1.2 AIM OF STUDY*

The aim of the present literature survey is to report on the results of the first efforts to gather and compile information useful for the project "Improved performance of brake discs". An overview of general aspects of braking will be given including braking modes, designs of pads and discs, interaction pad/disc, heat transfer, thermal behaviour, mechanical behaviour, thermoelastic instabilities and wear of pads and discs. The study should focus on brake discs made from cast iron material. For traditional and new such materials thermal and

mechanical properties will be studied: heat conduction, heat capacity, static strength, fatigue strength and wear resistance. An overview of the influence of different alloying elements on microstructure and material properties will be given. Methods for material testing will be reviewed and described. Overall, an attempt will be carried out to describe the state-of-the-art of the thermomechanical behaviour of the disc brake system.

### 1.3 OVERVIEW OF DISC BRAKING

Three types of braking cycles may be defined. The first one is here referred to as “repeated braking” which is very common at normal service conditions. Repeated braking could be in the form of “snubs”, where the speed is partially reduced, or stop braking where the speed is reduced to standstill. The second one is drag braking (downhill) with constant brake application at constant speed during a long time. The third one is emergency stop braking with extreme (maximum possible) deceleration, which seldom occurs but is important for safety and brake life.

Apart from the deterioration of the structural integrity caused by disc cracking, also other problems are related to the extreme resulting temperatures, such as brake fade, premature wear, brake fluid vapourization, bearing failure and also thermally excited vibrations [2]. These problems are not discussed in the present literature survey.

According to Degallaix and Wicker [3, 4], there are three mechanisms for transferring heat (see Section 2.3): convection, conduction (through the support) and radiation. Convection is normally the most important mechanism for cooling. Radiation is significant only for very high temperatures. The contribution of conduction is less important since it is a slow process [5]. Only a few studies consider conduction through the disc support.

In order to gain a better overview of braking for different applications, Table 1 gives the order of magnitude of typical braking data.

Table 1 Comparison of braking for different modes of transportations, adapted from [6]. All data are for one brake disc.

	<b>Motorbikes</b>	<b>Cars</b>	<b>Trucks</b>	<b>Buses</b>	<b>Trains<sup>(1)</sup></b>	<b>Aircraft</b>
<b>Average disc mass (kg)</b>	-	-	-	-	150	-
<b>Brake power (kW)</b>	-	-	-	-	500	-
<b>Kinetic energy (MJ)</b>	-	5.0	23	-	13.89	25
<b>Heat flux (MW/m<sup>2</sup>)</b>	-	6.0	-	-	10.29	2.5
<b>Apparent pressure (MPa)</b>	-	5.0	2.0	-	0.4082	2.5

(1) X2 trainling wheelset “X2 1997-2005”

### 1.4 DISC GEOMETRIES

Okamura and Yumoto [7] show different disc geometries commonly used for ventilated brake discs, see Figure 1-1. Optimization of the disc geometry is discussed in Section 6.3.

There exist two families of brake discs containing three to four different types of geometry. The common brake disc has a “hat” directly bolted to the hub while the floating disc is divided into two parts.

Four configurations of ventilated brake discs with hat (non-floating brake discs) are shown in Figure 1-1. Configurations 1 and 2 correspond to a positioning of the hat as shown in Figure 1-2 or Figure 1-3 while Configurations 3 and 4 can be obtained with the floating disc if the hat is fixed inside the brake disc itself. Scania uses the Configuration 1 “outer-hat without neck” geometry.

Floating discs (see Figure 1-2 and Figure 1-3) are used for heavy duty applications and allow axial and radial heat expansion. Expansion is allowed by “radial floating disc” and “float in the bell disc” and both arrangements reduce stresses, cracking and distortion [8].

In a "perfect" system with minimal disc movement relative to the calliper, the amount of float need only be around 0.15 - 0.20 mm. In most actual installations where the mountings are less than ideally rigid, a float of 0.40 - 0.45 mm for "float in the disc" systems and 0.20 - 0.30 mm for "float in the bell" systems is more appropriate [8].

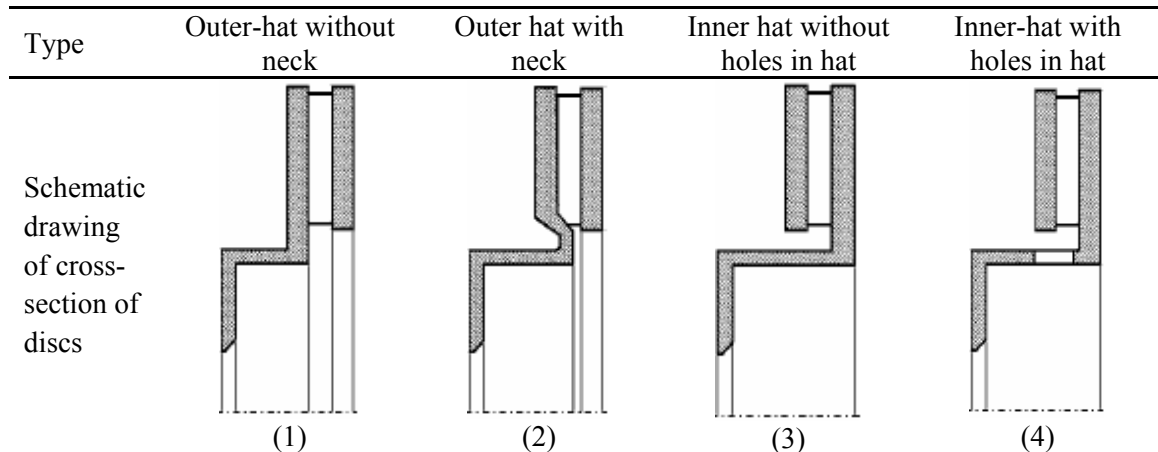


Figure 1-1 Basic configurations of ventilated brake discs with hat (nonfloating brake discs) [7].



Figure 1-2 Photo of a floating discs (without and with bell).

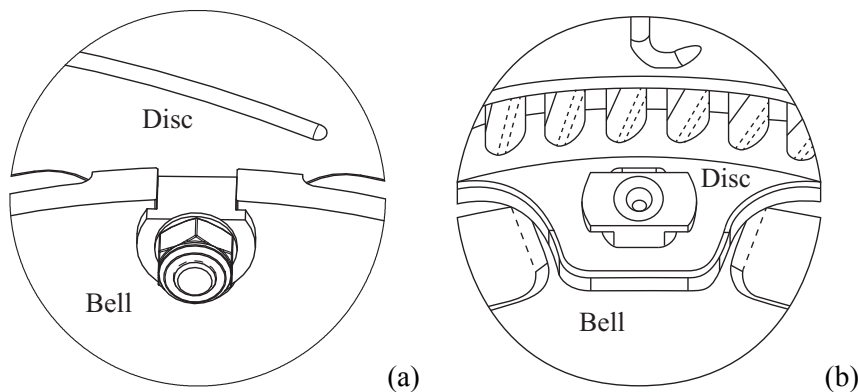


Figure 1-3 (a) Float in the bell (allowing radial expansion of the disc), (b) Float in the disc [8].

## 1.5 VANE GEOMETRIES

Palmer et al [9] tried to optimize a multiple-row pin-vented brake disc regarding its cooling performance. Ventilated discs have two rubbing surfaces separated by vanes. There exist three families of types of vane geometries: straight radial vanes, tangential vanes and pins (pillars/columns). Brake discs with different vanes are shown in Figure 1-4 to Figure 1-7. In order to have a good cooling efficiency of a brake disc, three main characteristics have to be taken into consideration: the flow of air through the disc, the average heat transfer coefficient of the surfaces of the disc and the wetted area of the rotor. It should be noted that Scania uses the straight vaned disc.



Figure 1-4 Straight vaned brake disc [10].



Figure 1-5 Tangential, straight vaned disc [10].



Figure 1-6 Tangential, curved vaned disc [10].



Figure 1-7 Pillar-type disc [10].



Figure 1-8 Radial vaned and tangential vaned discs used for train [11].

It has been shown that tangential curved vanes give improved cooling characteristics. However, a drawback is that the two discs on an axle have to be mirror images of each other. In order to avoid such a constraint while keeping the heat transfer rate of the curved vane disc, the pin-vented discs have been designed [12], see Figure 1-7. Another advantage of the pin-vented disc is that it has a higher resistance to thermal deformation which results from lower thermal stresses inside the rotor due to the material distribution.

It is important to note that the geometry of the pins can be different within the disc depending on at which row the pins are located as shown in Figure 1-8.

At high speed, the initial disc temperature has to be as low as possible because heat dissipation during braking is low [11]. It is then tempting to maximize the convection cooling of the brake discs by using vanes that exhibit better cooling performance and a low mass. However, at high speeds such discs generate substantial aerodynamic (pumping) effects which create losses, see Figure 1-9. In [11], discs with radial vanes, tangential vanes, novel radial vane/pillared and a solid disc made of steel for a high speed train with an outside disc diameter of 640 mm have been studied for high speed conditions.

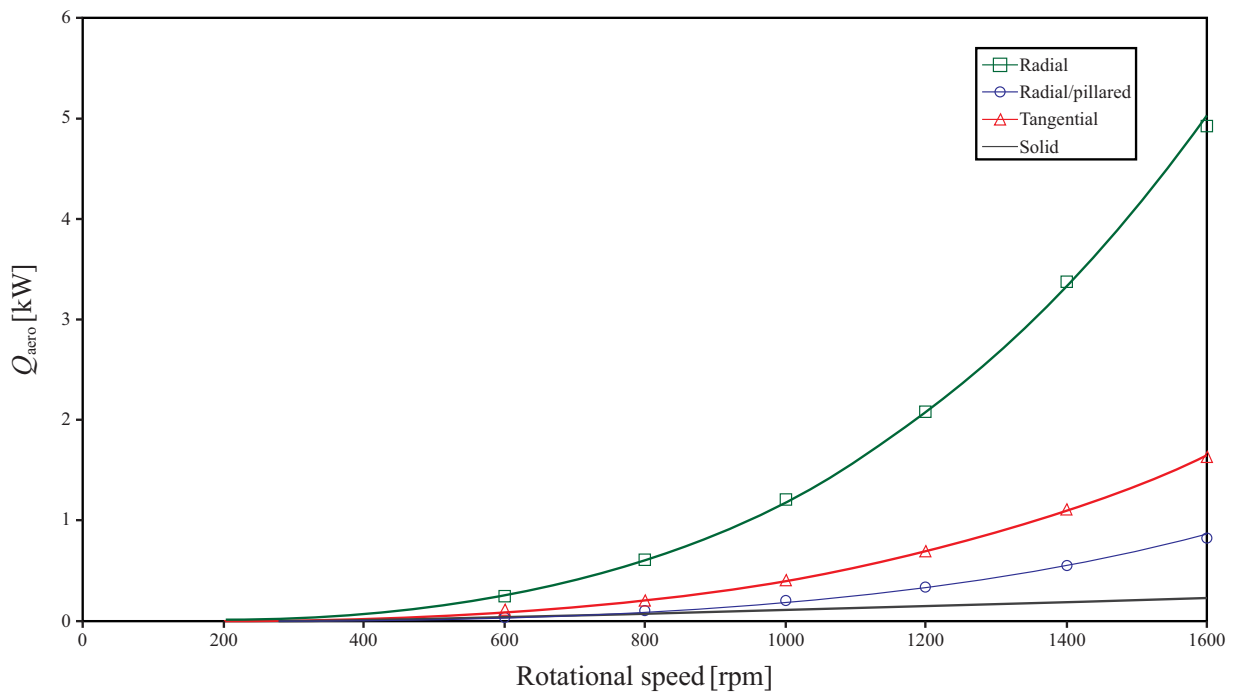


Figure 1-9 Comparison of aerodynamic losses of four disc designs [13].

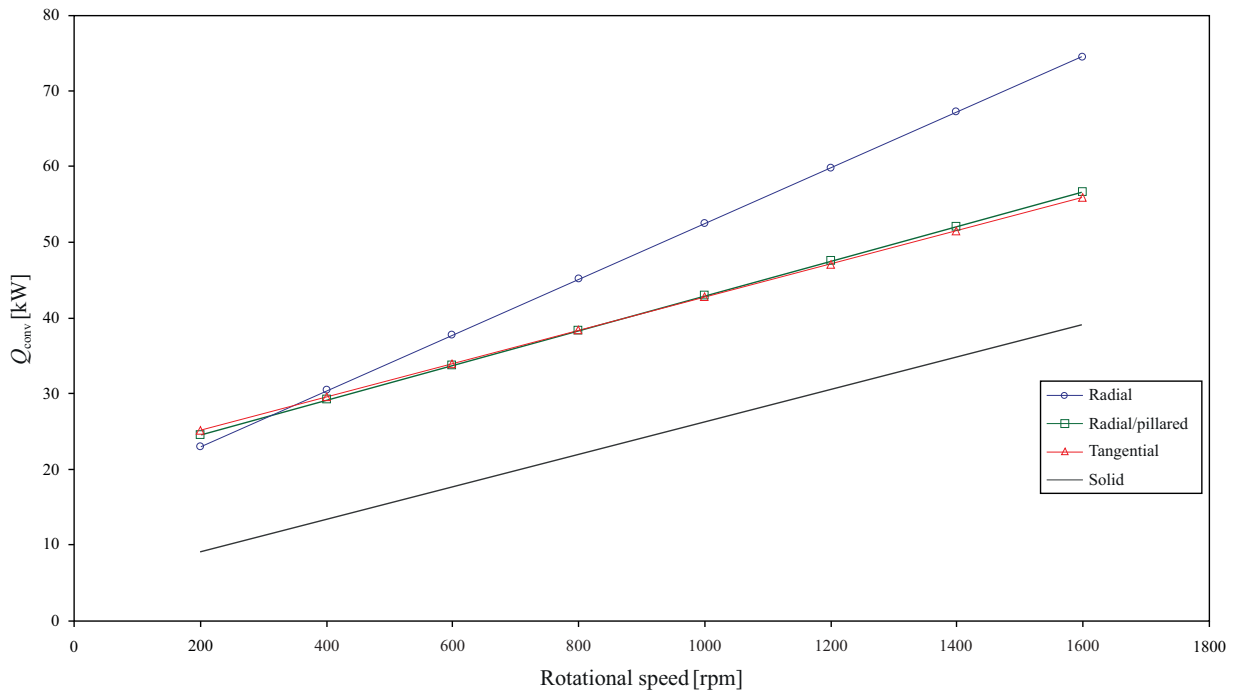


Figure 1-10 Comparison of convective thermal power loss at constant disc temperature ( $T_{at}$  the disc surface -  $T_{\infty} = 180^{\circ}\text{C}$ ) [13].

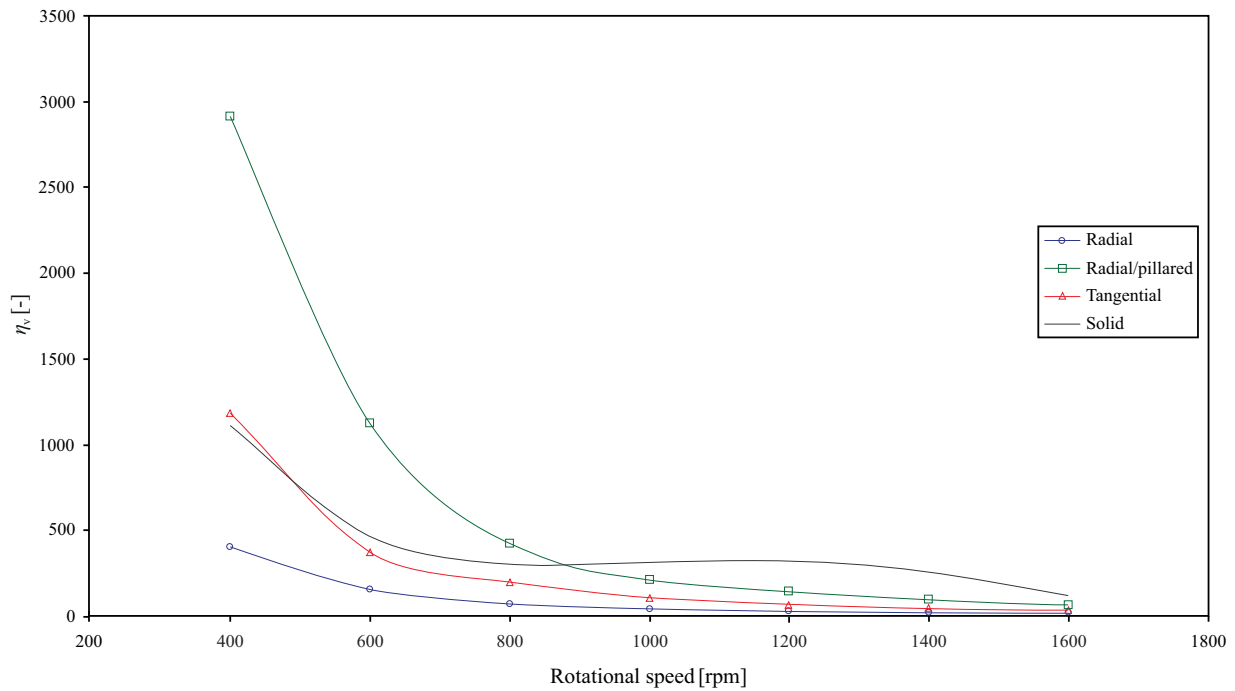


Figure 1-11 Comparison of cooling/aerodynamic efficiency ratios for four disc designs [13].

As shown in Figure 1-9, a solid disc has the lowest value of aerodynamic resistance  $Q_{aero}$  (aerodynamic power losses) while a radial vane disc has the highest value at high rotating speed. Figure 1-10 shows that a radial disc has the best convective heat dissipation ( $Q_{conv}$ ) while the solid disc has the lowest value. It has to be noted that tangential and radial/pillared discs have the same behaviour close to the radial disc performance. Figure 1-9 and Figure 1-11 show that the radial/pillared disc gives the best compromise between low losses and high cooling at low and high speed using equation (1.5.1) [11, 13]. In Figure 1-11,

$$\eta_v = \frac{Q_{conv}}{Q_{aero}} = \frac{(a\omega + b)\Delta T}{\omega^c} \quad \text{disc cooling/aerodynamic efficient ratio [nondimensional]} \quad (1.5.1)$$

where  $a$  is a constant forced-convection component,  $b$  is a constant accounting for natural-convection,  $c$  is a constant accounting for pumping-power,  $\Delta T$  [°C] is the difference between the temperature at the disc surface and the ambient air temperature, and  $\omega$  [rad/s] is the angular velocity.

## 2 TEMPERATURES AND STRESSES

### 2.1 INTRODUCTION

During braking, the kinetic energy of a truck is converted into heat. Talati and Jalalifar [2] describe the heat generation between the disc and the pad. At braking to full stop, the kinetic energy converted into thermal energy is  $E_c = \frac{1}{2}MV_0^2$  where  $M$  is the total mass and  $V_0$  is the initial speed of the vehicle. For each of the two brake discs of the front wheels of the vehicle, the energy is  $E = \frac{1}{4}mV_0^2$  where  $m$  is the mass braked by the front axle of the vehicle.

From the kinetic energy and its time variation (from vehicle deceleration), the braking power to be dissipated by the discs at every time instant is established. However, the spatial distribution of the heat flux  $q$  over the disc is given by  $q = \mu p v$  where  $\mu$  is coefficient of friction,  $p$  is local pressure and  $v$  is local sliding speed. The coefficient of friction is generally assumed to be constant and the local sliding speed varies linearly with the radius on the disc and the speed of the vehicle. The distribution of pressure between pad and disc may either be determined from some *a priori* assumptions or be found as part of the simulation.

Two models for the pad-disc contact have been considered by Talati and Jalalifar [2]:

- uniform pressure distribution:  $p = p_{\max} = \text{constant}$  where  $p_{\max}$  is the maximum pad-disc pressure
- uniform wear distribution:  $\delta = k p \omega r = \text{constant}$  which gives  $p = p_{\max} \frac{r_2}{r}$  where  $\delta$  is wear rate,  $r$  is the constant radius,  $k$  is the wear coefficient and  $\omega$  is the angular velocity, see Figure 2-1 where  $r_1$ ,  $r_4$  are the inner and outer radius of the disc respectively, and  $r_2$ ,  $r_4$  are the inner and outer radius of the pad respectively.

### 2.2 HEAT GENERATION

In order to determine the heat flux on pad and disc for the two assumptions *uniform pressure distribution* and *uniform wear*, one sets out from the heat generation for the area  $dA = \phi_0 r dr$ , see Figure 2-1, which is calculated as [2]

$$d\dot{E} = dP = V dF_f = \omega \mu p \phi_0 r^2 dr \quad (2.2.1)$$

and,

$$d\dot{E} = d\dot{E}_{\text{pad}} + d\dot{E}_{\text{disc}} = (1 - \sigma)dP + \sigma dP \quad (2.2.2)$$

respectively. Here  $\mu$  is the coefficient of friction (dimensionless),  $\omega$  ( $s^{-1}$ ) is the instantaneous angular velocity of the disc and  $\phi_0$  (rad) is the pad contact angle. Further,  $d\dot{E}$  is the rate of heat generated due to the friction between the two sliding components,  $V = \omega r$  is the relative sliding velocity and  $dF_f$  the friction force. The terms  $d\dot{E}_p$  and  $d\dot{E}_d$  are the amounts of heat absorbed by the pad and the disc, respectively, where the heat partitioning factor  $\sigma$  (dimensionless) denotes the part of the total generated heat that goes to the disc. We find the heat flux distribution into the pad on the area  $S_{\text{pad}} = dA = \phi_0 r dr$  of the pad as

$$q_{\text{pad}}(r, t) = \frac{d\dot{E}_{\text{pad}}}{dS_{\text{pad}}} = (1 - \sigma)\mu p r \omega(t) \quad (2.2.3)$$

$$q_{0\text{pad}}(r) = q_{\text{pad}}(r, 0) = (1 - \sigma)\mu p r \omega_0 \quad (2.2.4)$$

and the heat flux into the disc on area on the area  $S_{\text{disc}} = dA = 2\pi r dr$  of the disc as

$$q_{\text{disc}}(r, t) = \frac{d\dot{E}_{\text{disc}}}{dS_{\text{disc}}} = \frac{\phi_0}{2\pi} \sigma \mu p r \omega(t) \quad (2.2.5)$$

$$q_{0\text{disc}}(r) = q_2(r, 0) = \frac{\phi_0}{2\pi} \sigma \mu p r \omega_0 \quad (2.2.6)$$

Here,  $\omega_0$  ( $\text{s}^{-1}$ ) is the initial angular velocity of the disc. Talati and Jalalifar [2] and Mazidi et al [14] give the boundary conditions, including loading, for the pad and the disc at stop braking with constant retardation, see Figure 2-2 and Figure 2-3.

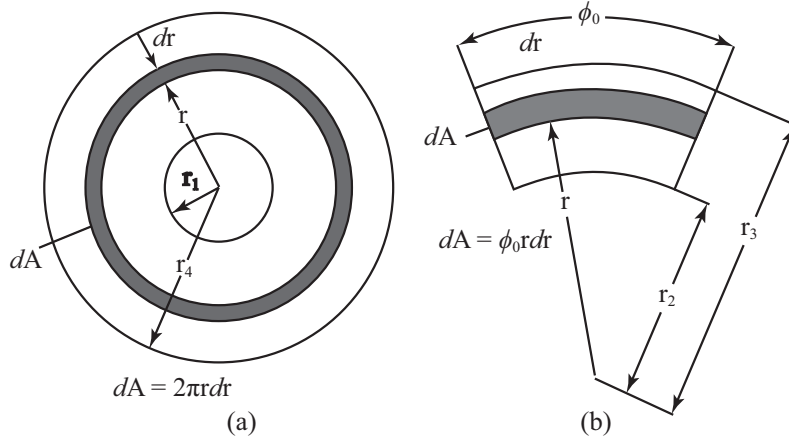


Figure 2-1 Contact surface element of two components (a) the disc, (b) the pad [14].

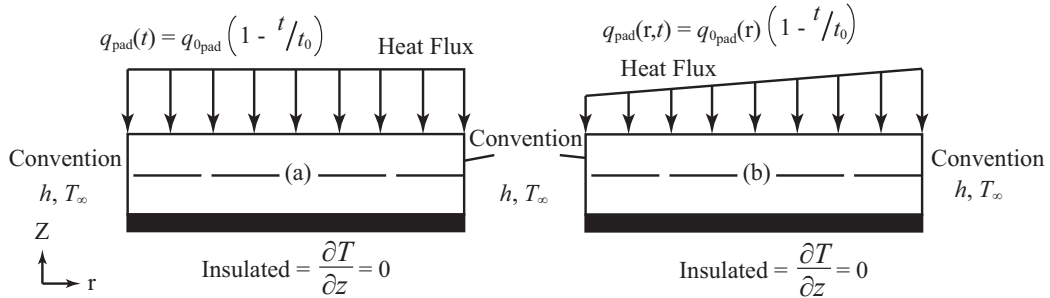


Figure 2-2 Boundary conditions for the pad. (a) Uniform wear, (b) uniform pressure [14].

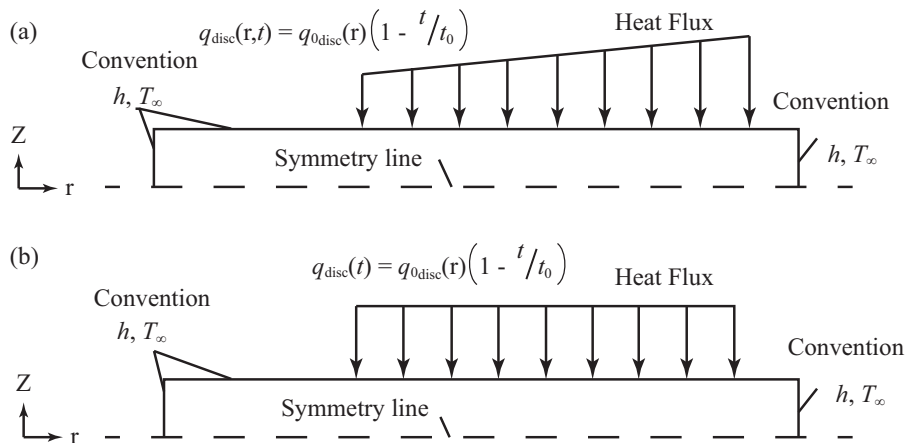


Figure 2-3 Boundary conditions for the disc. (a) Uniform pressure, (b) uniform wear [14].

The study concludes that the surface temperatures depend on the heat partitioning between the disc and the pad which can be affected by such a factor as accumulation of wear particles at the contact surface. The surface temperatures are also affected by heat transfer and ventilation.

Brake temperatures can hence be studied using an *a priori* assumption on heat partitioning assuming that a constant part of the heat enters the disc, see eg [15] and [16]. When the heat partitioning has been determined, the thermal analysis is straightforward with known heat fluxes applied to the components studied. However, by using this approach, the heat partitioning cannot account for the evolution of generated temperatures resulting from different cooling conditions of the components. Another approach is to introduce a thermal contact conductance between the two sliding bodies. By doing this, the partitioning of heat can account for the temperatures of the sliding bodies at the common interface, see [17]. Models of this type have the capability to account for geometrical design and cooling by convection and radiation from surfaces.

One model of this type assumes that the heat is generated on the surface of the friction material (pad) and is conducted to the disc via

$$q_{\text{disc}} = h_{\text{contact}}(T_{\text{pad}} - T_{\text{disc}}) \quad (2.2.7)$$

where  $h_{\text{contact}}$  [ $\text{W} / ^\circ\text{C m}^2$ ] is the thermal contact conductance of the pad and disc interface. The model is implemented for railway disc braking by Dufrenoy and Weichert [18]. Another model of the same type, but allowing for a more flexible heat partitioning, is found by introducing two thermal contact resistances  $R_{\text{pad}}$  and  $R_{\text{disc}}$  [ $^\circ\text{C m}^2 / \text{W}$ ] at the interface using an electrical analogy, see Figure 2-4.

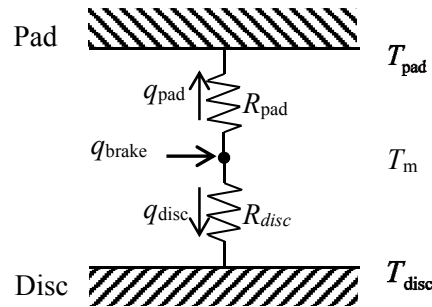


Figure 2-4 Schematic view of heat partitioning model for a unit surface area of pad and disc in contact. Of a total generated heat flux  $q_{\text{brake}}$ , the flux  $q_{\text{disc}}$  goes to the disc and  $q_{\text{pad}}$  to the pad. Surface temperatures are  $T_{\text{disc}}$  and  $T_{\text{pad}}$  for disc and pad, respectively, and the common interface temperature is  $T_m$ . Thermal resistances are denoted  $R_{\text{pad}}$  and  $R_{\text{disc}}$ , adapted from [19].

The heat partitioning between the two bodies is then found from the equations

$$q_{\text{disc}} = \frac{(T_{\text{pad}} - T_{\text{disc}})}{R_{\text{pad}} + R_{\text{disc}}} + \frac{R_{\text{pad}}}{R_{\text{pad}} + R_{\text{disc}}} q_{\text{brake}} \quad (2.2.8)$$

$$q_{\text{pad}} = \frac{(T_{\text{disc}} - T_{\text{pad}})}{R_{\text{pad}} + R_{\text{disc}}} + \frac{R_{\text{disc}}}{R_{\text{pad}} + R_{\text{disc}}} q_{\text{brake}} \quad (2.2.9)$$

The above model has successfully been employed for railway tread braking in the work by Vernersson [19]. The thermal resistances were in that work assumed to be constant for a given friction couple. However, the same model has also been employed when the thermal resistances are assumed to be inversely proportional to the contact pressure [20], ie  $r_i = R_i / p$  where  $R_i$  [ $^\circ\text{C}/\text{WN}$ ] is a reference parameter.

### 2.3 HEAT TRANSFER

As mentioned in [3, 4], there are three mechanisms for transferring heat (see Figure 2-5): convection (air flow through the disc), conduction (through the support) and radiation. Convection is normally the most important mechanism for cooling. Radiation is significant only for very high temperatures. The contribution of conduction through the support is less important, since it is a slow process [5].

Voller et al [5] have described the mechanisms of conduction, convection and radiation for transferring heat away from a disc which are summarized here.

*Convective heat transfer.* The thermal power  $Q_{\text{conv}}$  [W] transferred by convection is determined by

$$Q_{\text{conv}} = h_{\text{conv}} A_{\text{D,conv}} (T_{\text{D}} - T_{\infty}) \quad (2.3.1)$$

where  $A_{\text{D,conv}}$  is the area transferring heat by convection and  $h_{\text{conv}}$  [W/m<sup>2</sup> °C] is the convective heat transfer coefficient which may be determined using cooling curves, see Figure 2-6.  $T_{\text{D}}$  and  $T_{\infty}$  are the average disc surface and ambient temperatures, respectively.

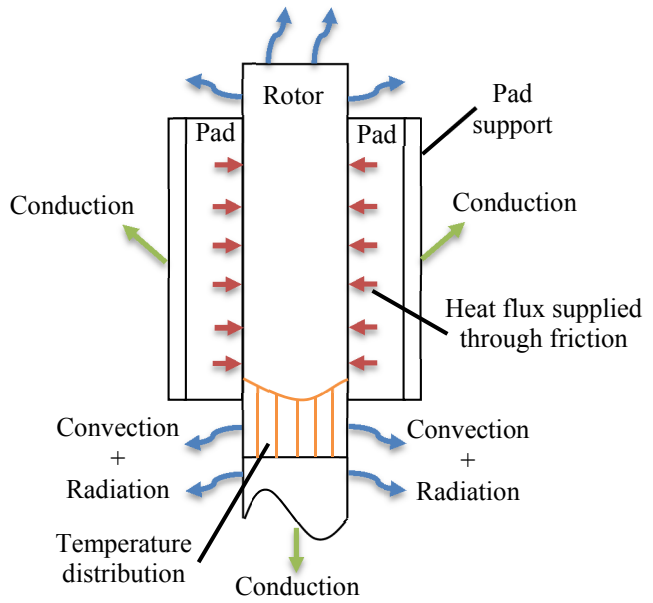


Figure 2-5 Heat transfer mechanism in a disc brake system [21].

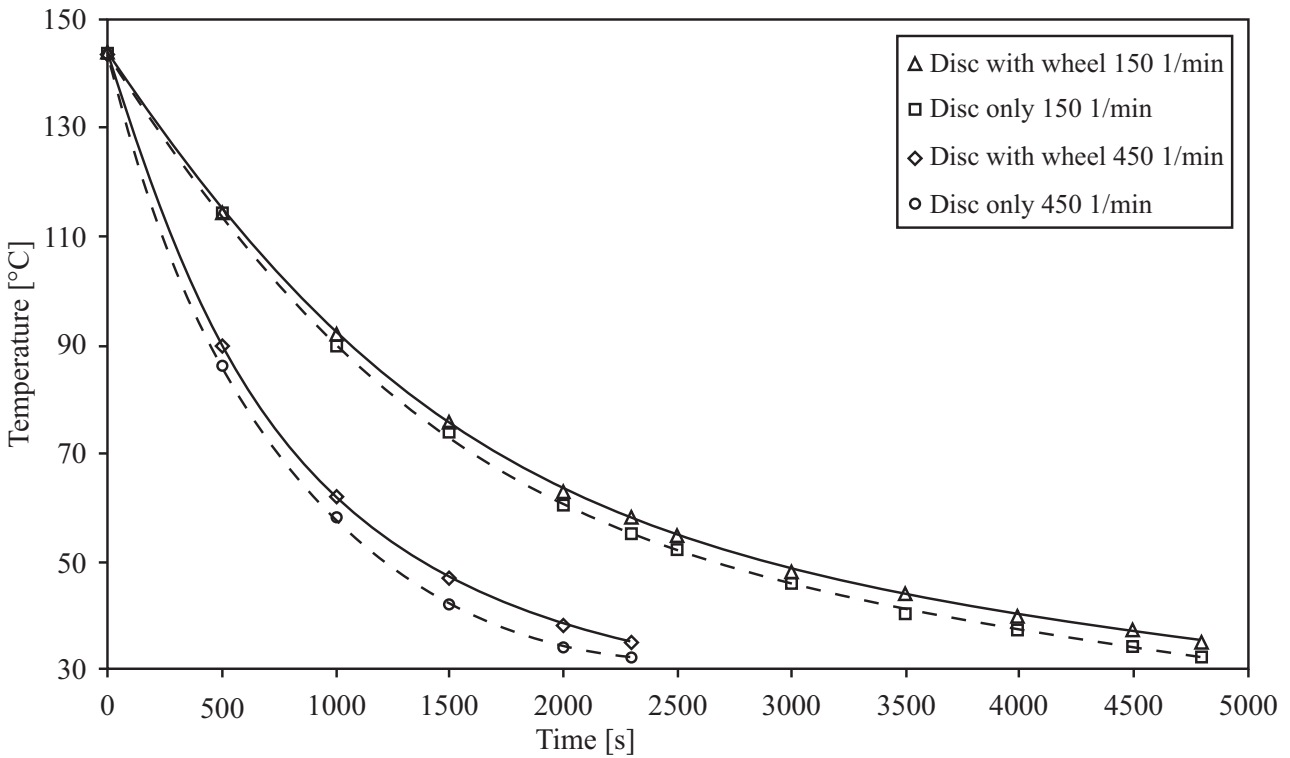


Figure 2-6 Cooling curves of brake disc on a truck [5].

*Conductive heat transfer through the supports.* The heat flow inside a body is determined by Fourier's law of heat conduction,

$$Q_{\text{cond}} = -kA \frac{dT}{dx} \quad (2.3.2)$$

where  $k$  [W / m °C] is the thermal conductivity,  $A$  [m<sup>2</sup>] is the area and  $T$  [°C] is the temperature. However, at the interface between two bodies there exists a discontinuity in the temperature field, a temperature jump, caused by eg surface roughness or oxides.

The thermal power transferred by conduction at an interface between the disc hub and the support (carrier) can be modelled using an equation of convection type,

$$Q_{\text{cond}} = h_{\text{cond}} A_{\text{D,cond}} (T_{\text{D}} - T_{\text{C}}) \quad (2.3.3)$$

where  $A_{\text{D,cond}}$  [m<sup>2</sup>] is the area of interface between the disc hub and the support,  $h_{\text{cond}}$  [W / m<sup>2</sup> °C] is the conductive heat transfer coefficient (thermal contact conductance) and  $T_{\text{D}}$  and  $T_{\text{C}}$  are the surface temperatures of the disc and wheel carrier, respectively. In Figure 2-7 the thermal contact conductance is shown as a function of interface pressure at a location close to bolts or in-between bolts.

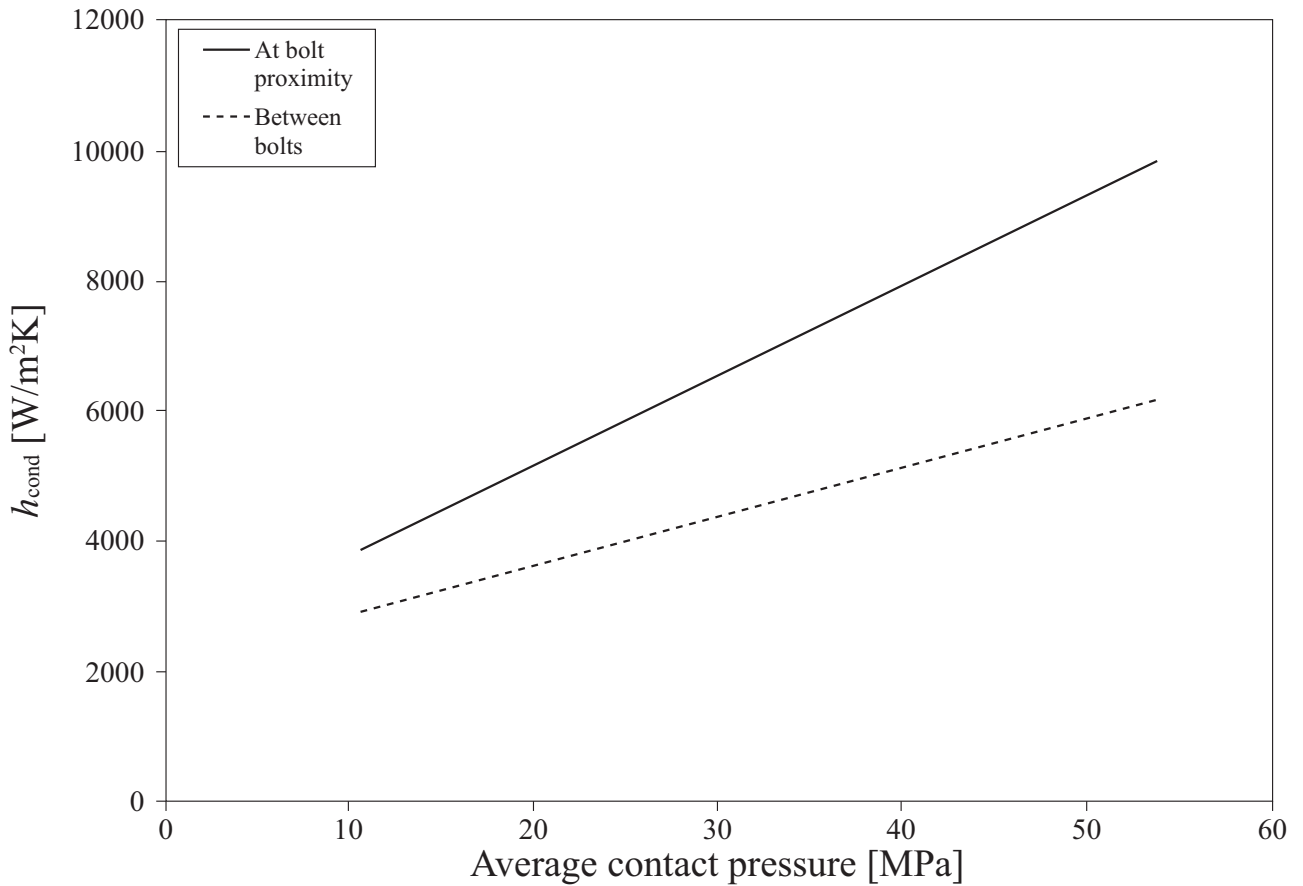


Figure 2-7 Thermal contact conductance  $h_{\text{cond}}$  at the disc/wheel support interface [5].

The thermal contact conductance in Figure 2-7 is determined using measurements of the temperature gradients in disc and wheel carrier to find the temperature drop at the interface. It is important to note that the  $h_{\text{cond}}$  as shown in Figure 2-7 is a function of the average contact pressure (total bolt clamp force divided by the contact area). It should be noted that in some literature the thermal contact resistance  $R$  is used instead of the thermal contact conductance used in Figure 2-7, where  $R$  is the inverse of  $h_{\text{cond}}$ . Hence

$$R = \frac{\Delta T_{\text{int}}}{Q_{\text{cond}}/A_{\text{int}}} \quad (2.3.4)$$

where  $\Delta T_{\text{int}} = T_{\text{D}} - T_{\text{C}}$  is the temperature drop at the interface and  $A_{\text{int}}$  is the interface area.

*Radiative heat dissipation.* Radiative heat dissipation is defined by

$$Q_{\text{rad}} = \sigma \varepsilon A_{\text{D,rad}} (T_{\text{D}}^4 - T_{\infty}^4) \quad (2.3.5)$$

where  $Q_{\text{rad}}$  [W] is the thermal power transferred by radiation,  $\sigma = 5.67 \times 10^{-8} \text{ W/m}^2 \text{ K}^4$  is the Stefan–Boltzmann constant,  $\varepsilon$  is the emissivity,  $A_{\text{D,rad}}$  is the surface area of the disc radiating heat,  $T_{\text{D}}$  [K] is the average disc surface temperature and  $T_{\infty}$  [K] the ambient air temperature. However, a radiative heat transfer coefficient can be defined as

$$h_{\text{rad}} = \vartheta \lambda (T_{\text{D}}^3 + T_{\infty}^3 + T_{\text{D}} T_{\infty}^2 + T_{\infty} T_{\text{D}}^2) \quad (2.3.6)$$

which can be rewritten using the temperature dependent factor  $h_{\text{rad}}$  (compare convective heat transfer above) as

$$Q_{\text{rad}} = h_{\text{rad}} A_{\text{D,rad}} (T_{\text{D}} - T_{\infty}) \quad (2.3.7)$$

It has been found that the emissivity of the surface of a brake disc depends on temperature. For drag braking, the emissivity has to be adjusted [22] since it varies between 0.4 and 0.7. Formation of hot spots will contribute to even higher values of the emissivity (up to 0.9 when hot spots occur). Figure 2-8 was plotted using equation 2.3.7 on the basis of emissivity values from [22].

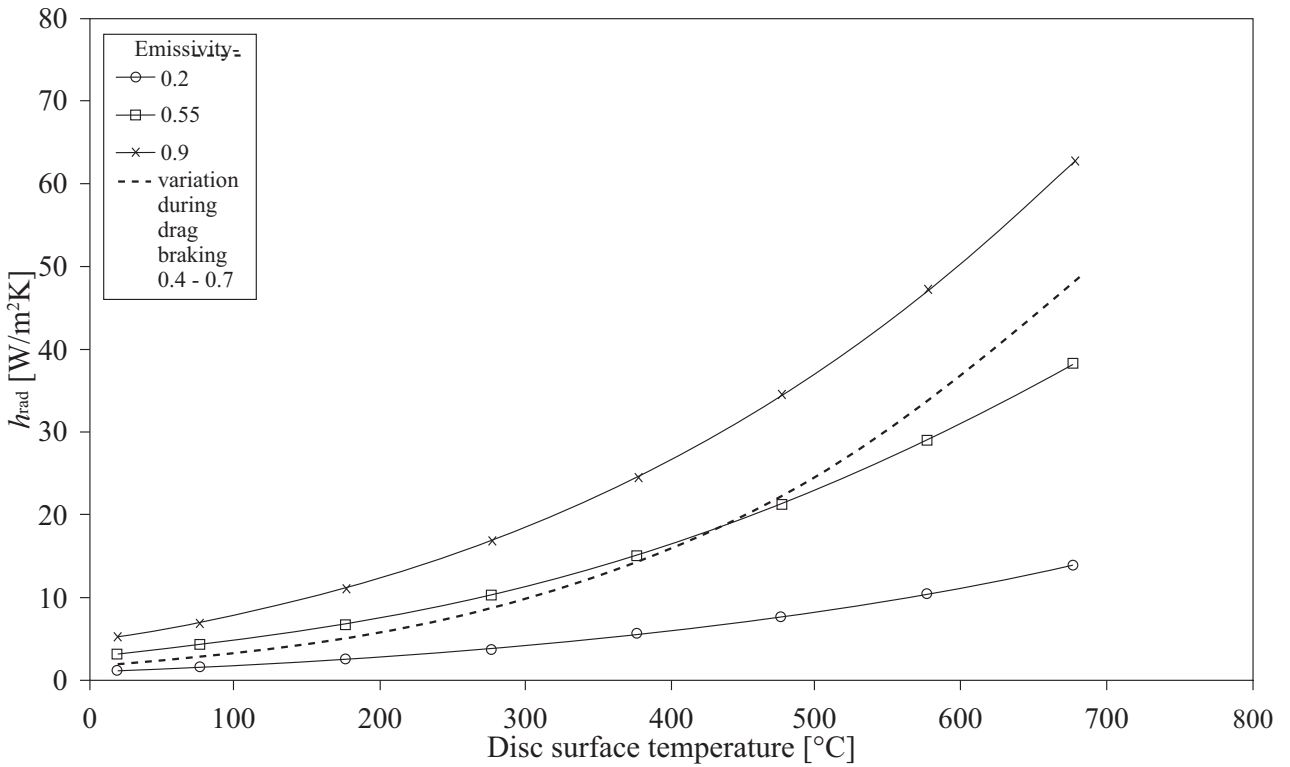


Figure 2-8 Radiative heat transfer coefficient change with disc temperature during drag application [5].

An example of a study of brake disc temperatures is given by Siroux [23]. A reduced-scaled experimental set-up for measuring temperature gradients in a brake disc is described. The aim was to reproduce the contact pressure observed between disc and pad for full-scale railway braking at stop braking conditions. The parameters for the testing condition are given in [23] and have to be scaled in order to correspond to the full-scale disc [24]. In [23], the thermal resistance at the sliding contact between the disc and the pad is neglected and the brake disc temperature is only estimated. A one-dimensional analytical model of the disc was used for periodic sliding contact with the pad. The analytical model gave good agreement with the experiments.

## 2.4 THERMAL STRESSES

Rukadikar and Reddy [25] wrote a brief literature review on thermal fatigue resistance of grey cast irons and described the parameters controlling the thermal stress  $\sigma_{th}$  in grey cast iron, assuming elastic conditions, as

$$\sigma_{th} = \left( \frac{\alpha E \Delta T}{1-\nu} \right) F \quad (2.4.1)$$

where  $\alpha$  is the coefficient of thermal expansion,  $E$  is the modulus of elasticity,  $\Delta T$  is the temperature difference (which depends on the cycle conditions and thermal conductivity,  $\lambda$ ),  $\nu$  is Poisson's ratio and  $F$  is a shape factor (which depends on specimen geometry).

## 2.5 PLASTIFICATION AND RESIDUAL STRESSES

Plastification is associated with irreversible deformation due to slip, mechanical twinning and creep [26]. Plastification introduces residual stresses which may delay the onset of plastic deformation [27]. Residual and applied stresses can only be added together until the yield strength of the material is reached. When a component is externally loaded, the applied stresses are added to the residual stresses and the combination of the stresses will control the plastification of the material [27]. Residual stresses in the component may be compressive or tensile, which may be beneficial or detrimental to its fatigue life. Brake discs made from grey cast iron have residual stresses from the casting of the component. At braking, compressive stresses appear in the disc close to the pad contact due to the heating. As a result of the locally high temperatures, temperature gradients and the restraining, the material will deform plastically in compression. Hence tensile stresses will result during cooling of the disc. Generally, *“tensile residual stresses may reduce the performance or cause failure of manufactured products. They may increase the rate of damage by fatigue, creep or environmental degradation”* [28]. Figure 2-9 shows the interaction process between microstructure, time, temperature and deformation (stress, strain). Stresses are influenced by thermal conduction, heat capacity, thermal expansion, elastic modulus, Poisson's ratio, plastic behaviour, thermodynamics and kinetics of (phase) transformations, mechanisms of transformations, and transformation plasticity [26].

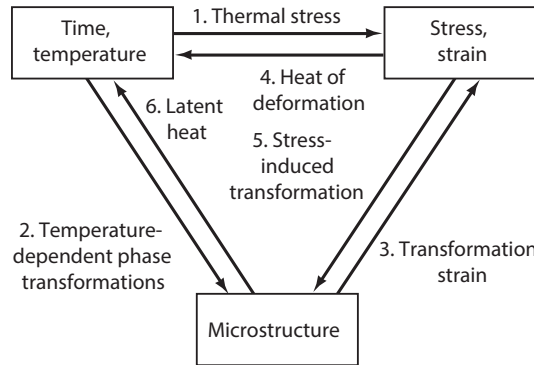


Figure 2-9 The coupling of temperature, stress and microstructure [26].

## 2.6 THERMOELASTIC INSTABILITIES AND HOT SPOTS

Hot spots appear on the surface of brake discs and are related to frictionally induced thermoelastic instabilities (commonly written TEI). TEI can be explained by the fact that a small pressure perturbation in the contact pressure between friction material and rotor is unstable if the sliding speed is exceeding the so-called critical speed [29] for the given system. This onset of TEI will cause the perturbation to grow at continued frictional sliding and localized regions of high temperatures, known as hot spots, appear on the contact surface. Hot spots should be avoided since they can cause material damage and thermal cracks, and they also induce undesirable vibrations of the disc known as hot judder.

Choi and Lee [30] proposed an axisymmetric finite element model in order to analyse the transient thermoelastic behaviour of brake discs. In the pad/disc contact model, nodes on the contact surface do not have prescribed displacement or tractions. Instead, these nodes have to fulfil two relationships: (1) continuity of normal displacements on the contact surface and (2) equilibrium conditions (traction of equal magnitude and opposite sign in pad and disc, respectively). One should note that the contact problem always is nonlinear although the contacting bodies have linear elastic properties. This means that the contact area is not a linear function of the applied loading. Figure 2-10 shows the interfaces of two adjacent subregions.

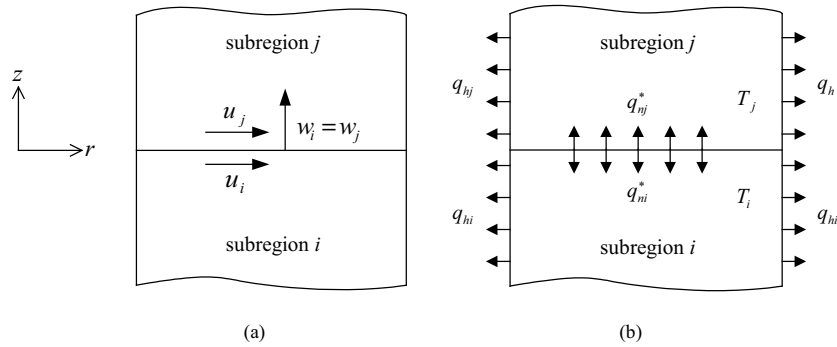


Figure 2-10 Contact model for (a) the elastic subregions i and j with  $w_i = w_j$  if  $p > 0$ , quasi-static model and (b) the heat conduction problem in the two subregions [30].

The axisymmetric thermal heat transfer equation is written

$$\rho c \frac{\partial T}{\partial t} = \frac{1}{r} \frac{\partial}{\partial t} \left( r k_r \frac{\partial T}{\partial t} \right) + \frac{\partial}{\partial z} \left( k_z \frac{\partial T}{\partial z} \right) \quad (2.6.1)$$

where  $\rho$ ,  $c$ ,  $k_r$  and  $k_z$  are the density, the specific heat and the thermal conductivities in the  $r$  and  $z$  directions of the material respectively. The boundary and initial conditions used are

$$T = T^* \text{ on } \Gamma_0, \quad q_n = h(T - T_\infty) \text{ on } \Gamma_1, \quad q_n = q_n^* \text{ on } \Gamma_2, \quad T = T_0 \text{ at time} = 0$$

here  $T^*$  is the prescribed temperature,  $h$  is the heat transfer coefficient,  $q_n^*$  the heat flux due to friction at each contact interface,  $T_\infty$  the ambient temperature,  $T_0$  the initial temperature and  $\Gamma_0$ ,  $\Gamma_1$  and  $\Gamma_2$  boundaries on which temperature, convection and heat flux, respectively, are imposed. Figure 2-11 shows the axisymmetric finite element models of the coupled thermoelastic contact problem used for the study. The hoop stresses in brake discs have the largest magnitudes of the stress components and must be considered as dominant from the viewpoint of fatigue failure.

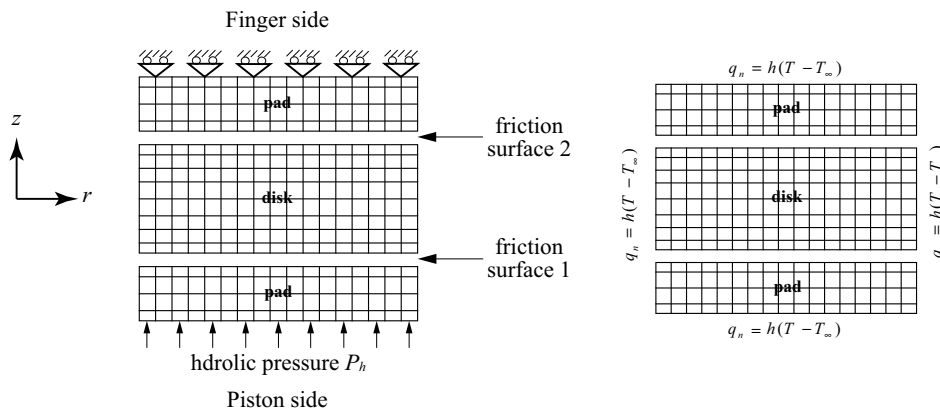


Figure 2-11 Elastic (left) and thermal (right) finite element model for the transient thermoelastic analysis [30].

The evolution of surface temperatures and interface pressures of a railway brake disc is studied by Dufrenoy and Weichert [18]. An axisymmetric model is used for the study of TEI where the variation of the bearing

surface between brake disc and pad is accounted for as induced by thermal expansion and wear. The axisymmetric assumption means that the heat flux is assumed to be uniformly distributed in the circumferential direction and that the angular temperature gradient is neglected. It is pointed out that for automotive applications, the decelerations are considerably higher which means that circumferential gradient may not be negligible. It is found for the studied stop braking cycle, that the calculated maximum surface temperatures are much higher if the variations of the bearing surfaces are accounted for than if uniform contact pressure is assumed. Furthermore, the influence of wear of the friction material is shown to lower the maximum contact temperatures.

### 2.7 THERMAL SHOCK

Thermal shock is an area of research where the reaction to a rapid and extreme temperature variation is studied. The shock results from a thermal gradient in the component. Such a temperature variation causes expansion of the molecular structure due to weakening of the bonds which hold the molecules in formation. Thermal shock tests start at ambient temperature and a specimen is exposed to an extremely low (or high) temperature within a short period of time, followed by an extremely high (or low) temperature; before going back to ambient temperature. During braking, the local temperature can reach 900°C in a couple of seconds giving two possible scenarios: thermal shocks which are responsible for thermal cracks and/or plastic deformation in the disc. It should be noted that thermal shock is normally not considered for braking applications. However, for more information, Rémy [31] gives a good overview of thermal shocks and relevant laboratory tests that can be carried out.

Failure at Thermal Shock Testing (TST) [33] and Temperature Cycle Testing (TCT) [34] depends on the following factors: 1) the difference between the high and low temperatures used. 2) the transfer time between the two temperatures. 3) the dwell times at the extreme temperatures. Failure mechanisms accelerated by thermal shock include cracking, package cracking, neck/heel/wire breaks, and bond lifting.

TCT determines both the ability of parts to resist low and high temperatures, and their ability to withstand cyclic exposures to these temperatures.

Janssens [32] made experiments of cyclic thermal shocks on notched specimens that are used in nuclear power plants. Figure 2-12 shows the arrangement of thermocouples for measuring transient temperature profiles and plots the comparison of the measured and calculated temperature profiles using the calibrated heat transfer coefficients that are given in the article. The numerical results are obtained by use of a finite element thermal stress analysis in which a calibrated, elastic-plastic material model with kinematic-isotropic cyclic hardening is employed to study stress and strain at the test. Numerical and experimental results are compared.

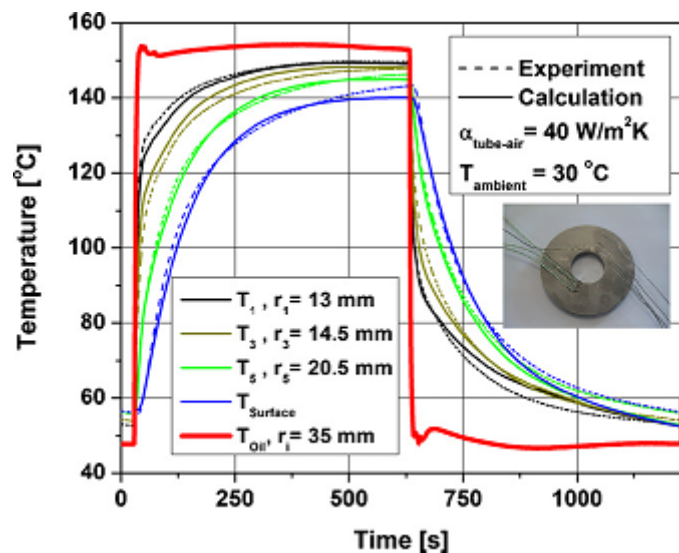


Figure 2-12 Temperature history in a notched specimen under thermal shock testing [32].

### 3 MATERIAL PROPERTIES

#### 3.1 INTRODUCTION

It should be noted that cast iron identifies a large family of ferrous alloys [35]. Several types of cast iron qualities are listed in Table 2.

Table 2 Classification of cast iron by commercial designation, microstructure, and fracture [35].

Commercial designation	Carbon-rich phase	Matrix <sup>(a)</sup>	Fracture surface	Final structure after...
<b>Grey iron</b>	Lamellar graphite	P	Grey	solidification
<b>Ductile iron</b>	Spheroidal graphite	F, P, A	Silver-grey	solidification or heat treatment
<b>Compacted graphite iron</b>	Compacted vermicular graphite	F, P	Grey	solidification
<b>White iron</b>	Fe <sub>3</sub> C	P, M	White	solidification and heat treatment <sup>(b)</sup>
<b>Mottled iron</b>	Lamellar Gr + Fe <sub>3</sub> C	P	Mottled	solidification
<b>Malleable iron</b>	Temper graphite	F, P	Silver-grey	heat treatment
<b>Austempered ductile iron</b>	Spheroidal graphite	At	Silver-grey	heat treatment

(a) F, ferrite, P, pearlite, A, austenite, M, martensite, At, austempered (bainite).

(b) White irons are not usually heat treated, except for stress relief and for continued austenite transformation.

Grey iron is commonly used for brake discs in the automotive industry (passenger cars and trucks) and railway industry. Compacted graphite iron is used for high-speed trains [36]. Also some other materials like aluminium and ceramics can be used for brake discs. Aluminium is often used in bikes. However, discs made of grey iron have better mechanical and thermal properties, which are important when the brake disc has to convert large amounts of energy into heat. Besides, grey iron is cheap and easy to cast [37]. A major drawback of brake discs made from grey cast iron is their high mass. Thus, many companies try to reduce the weight by introducing new alloyed materials since brake discs contribute to the mass of the wheel suspension which is directly linked to comfort and driving performance of the vehicle. For special cars, eg sport cars, composite materials such as metal matrix composite (MMC) are widely used for their low weight and higher thermal conductivity and diffusivity compared to grey cast iron [10]. For trucks, composite materials are considered to be too expensive.

#### 3.2 THERMAL AND MECHANICAL PROPERTIES

Due to the large number of interacting material parameters (thermal, mechanical, alloying composition ...), it is very difficult to select an “optimum” brake disc material. Different requirements on performance are in conflict and cannot be fulfilled simultaneously. The thermal characteristics are important for selecting a brake disc material and one should aim at *high thermal capacity*, *high thermal diffusivity* and *low density* [37]. The thermal diffusivity ( $\alpha$ ) is given by  $\alpha = k/c\rho$ , where  $k$  is the thermal conductivity,  $c$  is the specific heat (also called thermal capacity) and  $\rho$  is the material density. A high thermal diffusivity, quantifying the speed at which a material can transport heat from a hot source to colder parts, ensures that the surface temperatures are minimized. Further, a low density gives a low mass of the brake disc component while a high thermal capacity ( $c\rho$ ) allows the disc to absorb high amounts of thermal energy. In addition, brake discs should perform well regarding friction, mechanical strength and wear at elevated temperatures.

In Table 3 to Table 7, some information including thermal and mechanical properties for different classes of cast iron is compiled.

Table 3 Range of compositions for typical nonalloyed cast irons [38].

Type of Iron	Per cent (%)				
	Carbon	Silicon	Manganese	Sulphur	Phosphorus
Grey	2.5-4.0	1.0-3.0	0.2-1.0	0.02-0.25	0.02-1.0
Ductile	3.0-4.0	1.8-2.8	0.1-1.0	0.01-0.03	0.01-0.1
Compacted Graphite	2.5-4.0	1.0-3.0	0.2-1.0	0.01-0.03	0.01-0.1
Malleable (Cast White)	2. -2.9	0.9-1.9	0.15-1.2	0.02-0.2	0.02-0.2
White	1.8-3.6	0.5-1.9	0.25-0.8	0.06-0.2	0.06-0.2

Table 4 Grades of automotive grey iron castings, designated by Brinell Hardness as in specification SAE J431, adapted from [38]. Brinell hardness unit is in N/mm<sup>2</sup> but is usually reported with no unit.

SAE Grade	Brinell Hardness <sup>(a)</sup>	Minimum Tensile Strength		Carbon content (%)	Density (kg/m <sup>3</sup> )	Other Requirements
G1800	187 max	18,000 psi	124 MPa	3.40 - 3.70	7150	
G2500	170-229	25,000 psi	173 MPa	3.20 - 3.50	7150	
G2500 <sup>(b)</sup>	170-221	25,000 psi	173 MPa	≥ 3.40	7150	3.4% min C and microstructure specified
G3000	187-241	30,000 psi	207 MPa	3.10 - 3.40	7150	
G3500	207-255	35,000 psi	241 MPa	3.0 - 3.30	7150	
G3500b <sup>(b)</sup>	207-255	35,000 psi	241 MPa	≥ 3.40	7150	3.4% min C and microstructure specified
G3500c <sup>(b)</sup>	207-255	35,000 psi	241 MPa	≥ 3.50	7150	3.5% min C and microstructure specified
G4000	217-269	40,000 psi	276 MPa	3.0 - 3.30	7150	

(a) Hardness at a designated location on the castings.

(b) For applications such as brake drums, disc and clutch plates to resist the thermal shock.

The typical hardness ranges for grey iron are listed in Table 5. The last column called “Brinell Hardness” refers to the Brinell hardening test which is used for all iron.

Table 5 Hardness ranges for grey irons [38].

Type of Grey Iron	Matrix Microstructure around Flake Graphite	Brinell Hardness
Soft-Annealed	All Ferrite	110-140
Ordinary	Pearlite and Ferrite	140-200
Higher Strength	Fine Pearlite	200-270
Alloyed-Acircular	Bainite	260-350
Austenitic (Ni-Resist)	Austenite	140-160
Heat Treat Hardened	Martensite	480-550
Hardened and Tempered	Tempered Martensite	250-450
Chilled (white iron)	Pearlite and Carbides	400-500

Table 6 Thermal conductivity for different grades of grey iron (Specification DIN EN 1561), adapted from [39]. The number gives the tensile strength value.

	GJL 150	GJL 200	GJL 250	GJL 300	GJL 350	GJL 400
<b>Temperature ( °C )</b>	<b>Thermal conductivity (W/K.m)</b>					
<b>100</b>	52.5	50.8	48.8	47.4	45.7	44.0
<b>200</b>	51.5	49.8	47.8	46.4	44.7	43.0
<b>300</b>	50.5	48.8	46.8	45.4	43.7	42.0
<b>400</b>	49.5	47.8	45.8	44.4	42.7	41.0
<b>500</b>	48.5	46.8	44.8	43.4	41.7	40.0
<b>Tensile strength range (MPa)</b>	150 - 250	200 - 300	250 - 300	300 - 400	350 - 450	400 - 500
<b>Typical Hardness</b>	150 - 183	159 - 194	180 - 222	200 - 280	-	-

Table 7 Thermal conductivity of main metallographic phases in cast irons [39].

<b>Metallographic constituent</b>	<b>Thermal conductivity, W/m·°C</b>		
	0 – 100 °C	500 °C	1000 °C
<b>Ferrite</b>	71 – 80	42	29
<b>Pearlite</b>	50	44	40
<b>Cementite</b>	7 – 8	-	-
<b>Graphite</b>	-	-	-
<b>Parallel to basal plane</b>	293 - 419	84 – 126	42 – 63
<b>Perpendicular to basal plane</b>	84	-	-

The ability of a material to absorb vibrations is evaluated as its damping capacity. Damping capacity decreases with increasing strength since the larger amount of graphite present in the lower strength irons increases the energy absorbed. However, this damping capacity is not studied in this present state-of-the-art survey as the squeal phenomenon is not taken into consideration in the project.

Table 8 Mean specific heats of grey iron, adapted from [40]

<b>Temperature range (°C)</b>	<b>Specific heat (J/kg·°C)</b>		
	<b>Grey iron, phosphorus content</b>		
	<b>0.147% P<sup>(a)</sup></b>	<b>0.54% P<sup>(b)</sup></b>	<b>0.88% P<sup>(c)</sup></b>
<b>0–200</b>	561	377	289
<b>0–300</b>	494	435	377
<b>0–400</b>	507	465	423
<b>0–500</b>	515	481	448
<b>0–600</b>	536	502	469
<b>0–700</b>	603	553	511
<b>0–900</b>	678	653	632
<b>0–1100</b>	670	649	628
<b>0–1200</b>	871	850	833

(a) 3.71% C, 1.50% Si, 0.63% Mn, 0.069% S (b) 3.72% C, 1.41% Si, 0.88% Mn, 0.078% S (c) 3.61% C, 2.02% Si, 0.80% Mn, 0.080% S.

Table 8 gives the specific heat for standard grey cast iron. The specific heat represents the heat capacity per unit mass in J/kg·°C. A mean specific heat can be used within a temperature interval. Heat capacity represents the amount of energy required to produce a unit temperature rise [40].

### 3.3 ALLOYING ELEMENTS

Several publications are available on chemical composition of brake disc materials. An overview is given by Diószegi and Holmgren [41]. The material characteristics of a brake disc depend on the chemical composition and the production process. Several papers [10, 15, 25, 37, 42, 43] have focussed on one or several chemical elements like cobalt, carbon, copper, chromium, silicon, molybdenum, tin, etc. A result from these papers is that addition of molybdenum and/or chromium increases the strength properties at elevated temperatures since they behave as pearlite stabilizers and reduce the growth (volume expansion) of cast iron. Growth of cast iron is related to dimensional stability and long-time exposure to high temperatures. The growth of grey iron is linked to a deterioration of the mechanical properties due to structural decomposition of pearlite, decomposition of carbides and structural breakdown of the pearlite to ferrite. It is also related to internal cracking (due to differential expansions and contractions during cyclic heating) which accelerates oxidation and carbon decomposition of graphite flakes in an atmosphere containing carbon monoxide in the temperature range 350 to 550 °C [16]. Hence, deterioration of mechanical properties occurs concurrently with growth as a result of structural decomposition. For ferritic-pearlitic Compacted Graphite Iron (CGI), an increase in pearlite content has been found to increase the tensile strength at high temperatures, however, with reduced effect at very high temperatures. At high temperatures, the tensile strength is inversely proportional to the amount of vermicular graphite in pearlitic CGI and ductile iron, which means that the nodularity<sup>1</sup> is also a factor that should not be neglected.

The decomposition of the microstructure has to be prevented in order to improve the properties at high temperatures. This may be accomplished by using combinations of alloying element, eg Cr, Cr+Mo, Mo+Sn or Cr+Mo+Sn. Also thermal shocks were investigated in [41] and additions of vanadium and molybdenum in grey iron resulted in an increase of the strength at high temperatures without any decrease of the thermal conductivity. It was found that a combination of high carbon content and vanadium improves the thermal shock resistance. Influences of Mo and Si on the thermal fatigue resistance for ferritic/pearlitic CGI and ferrite ductile iron in constrained thermal cycling tests were also investigated. It was shown that a combination of Mo and Si significantly increases the thermal fatigue life which is explained by an increase of the yield strength. However, silicon and molybdenum affect the material behaviour in different aspects: silicon increases the yield strength at room temperature (RT) while molybdenum does the same thing at elevated temperatures. This is also reflected in the fatigue life where an addition of 0.6 % molybdenum to a 2.5 % silicon ductile iron increases the thermal fatigue life by three times. Moreover, the thermal fatigue life is improved by 33 % and 55 % by an addition of 0.6 % molybdenum to a 0.4 % silicon ductile CGI and to a 0.5 % copper CGI, respectively.

Another aspect of silicon, and also chromium, is that they reduce surface oxidation which is one reason for crack initiation. The downside is that silicon and chromium have a negative effect on thermal properties such as thermal conductivity, and that they may initiate high pad wear. Thus, a compromise has to be found since a high silicon level, according [10], improves certain aspects of brake disc performance.

---

<sup>1</sup> Nodularity as per Japanese International Standard refers to the number of nodular (rounded) graphite particles in microstructure over the total number of graphite particles.

According to Hecht et al [44] the thermal diffusivity of grey cast iron is influenced by the graphite flake morphology, which is linked to the carbon equivalent value, defined as  $CE = \%C + 1/3 (\%Si + \%P)$ . Figure 3-1 depicts an almost linear relationship between the carbon equivalent and the thermal diffusivity. Increasing the %C - or the CE equivalent- is the easiest way to improve the graphitization which is directly linked to the graphite flake number<sup>2</sup> and the morphology of the graphite flakes. The typical way of measuring the graphite flake morphology is given in Figure 3-2. However, the influence of the graphite flake morphology on the thermal diffusivity is reduced at higher temperatures as illustrated in Figure 3-3. At 500°C, there is practically no difference in diffusivity between the different cast iron qualities. If the temperature is kept at 500 °C for more than 100 hours, it has also been observed that the thermal diffusivity decreases with time which means that this phenomenon could be of importance for, eg drag braking.

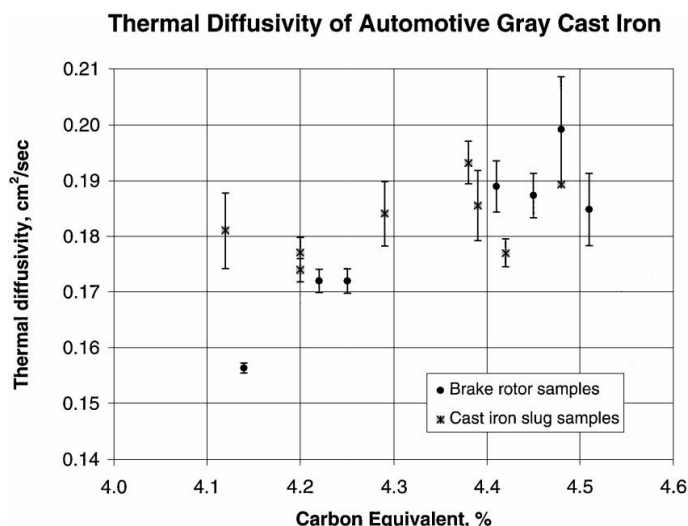


Figure 3-1 Room temperature thermal diffusivity increases as a function of carbon equivalent (CE). Error bars are  $\pm$  one standard deviation [44].

Another study on the temperature dependence of thermal diffusivity of cast irons is given by Maluf et al [37]. They showed that alloying of grey cast iron has a great influence on thermal diffusivity up to 300 °C. Above this temperature, the thermal diffusivity strongly decreases with temperature and at about 500 °C all the studied alloys have the same thermal diffusivity, which confirms the results in [44]. They explain this result by the fact that at high temperatures “*the atomic vibration is so intense that the “difficulty” of movement of the conduction electrons is practically the same regardless of the alloy element present in the crystal structure*”. They also showed that the “best performance” for the tested alloys was exhibited by the alloy containing copper even though molybdenum is usually added in grey cast iron in order to increase its heat resistance<sup>3</sup>. A compromise has to be found between molybdenum, copper and carbon content because molybdenum addition, in spite of improving heat resistance, increases degradation of the disc at elevated temperatures as well as the thermal diffusivity. They conclude that molybdenum unlike copper lowers the thermal diffusivity of grey cast iron. The best results for in-phase thermomechanical testing [37] were obtained with the specimen E which contained no molybdenum, the highest percentage of sulphur (0.11 %), copper (0.52 %) and chromium (0.29 %), and which contained the lowest percentage of silicon (1.87 %), manganese (0.53 %), phosphorus (0.03 %), and contained 3.49 % of carbon, all values with only minor deviations between the specimens. The thermal diffusivity is the highest for this material for all tested temperatures (< 650 °C). However, the resulting carbon equivalent of 4.12 % is the second lowest among the four specimens [37].

<sup>2</sup> A graphite flake is a curved graphite particle in gray cast iron. The graphite flake number corresponds to the number of those graphite flakes which can be found per unit area.

<sup>3</sup> Ability to resist degradation at high temperatures. The ultimate heat resistance is given by the temperature above which irreversible degradation occurs in the material. Up to this temperature, if the material is cooled, it will revert back to a similar or slightly higher value of the ultimate heat resistance. Above this temperature, strength is lost even after cooling.

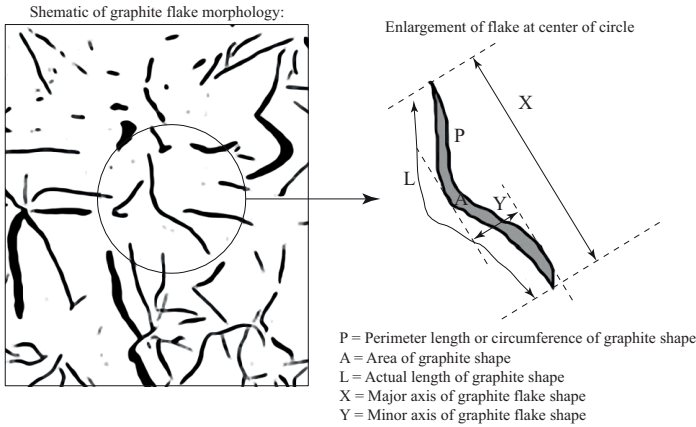


Figure 3-2 Schematic showing definition of parameters used to characterize graphite flake morphology [44].

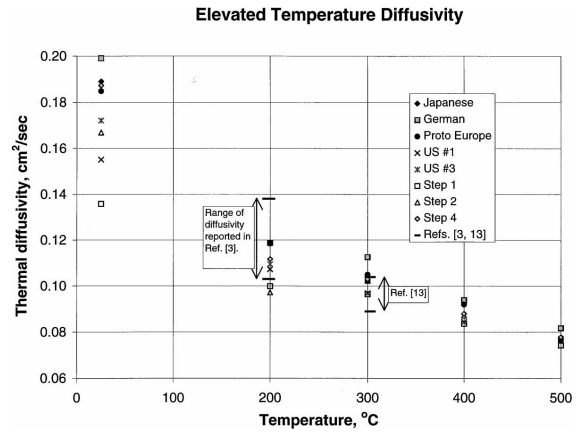


Figure 3-3 Thermal diffusivity of grey cast iron decreases with temperature [44].

Chatterley and Macnaughtan [10] found for brake discs made of grey cast iron that molybdenum increases the thermal conductivity significantly while nickel and copper additions only have a moderate effect. However, aluminium, silicon, chromium, vanadium, tin and antimony have an adverse effect on the thermal conductivity. Their study also shows that high carbon and low silicon contents improve the thermal conductivity and, if molybdenum is added, then a decline in strength at high temperatures can be prevented, ie, a better resistance to heat cracking is obtained. As already mentioned, a high silicon level improves the braking performance regarding fatigue, but unfortunately causes higher pad wear. Pad wear can be reduced by addition of manganese and phosphorus. However, no comparison can be made with [45] because Chatterley and Macnaughtan [10] use another definition of the carbon equivalent:  $(CEL = \text{Carbon} (\%) + \frac{1}{4} \text{Silicon} (\%) + \frac{1}{2} \text{Phosphorus} (\%))$ . It should be noted that all discs studied in [10] have a flake graphite structure of type “A” in a pearlitic matrix, see below. This results in good mechanical strength and high wear resistance of the discs.

A short description of the microstructure in grey cast iron is given in the following. Different subcategories have been defined for grey cast iron depending on the microstructure. An overview of these parameters is given (x100 magnification). Three main parameters are used: graphite distribution (see Figure 3-4 to Figure 3-8 [46]), graphite form (see Figure 3-9 to Figure 3-14 [46]) and graphite sizes (see Figure 3-15 to Figure 3-22 [46]). The graphite form and distribution and the size diagrams are taken from the international standard EN ISO 945:1994.

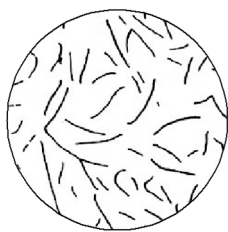


Figure 3-4 TYPE A, Random flake graphite in a uniform distribution [46].

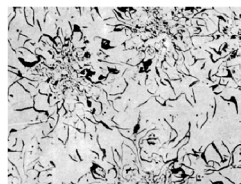
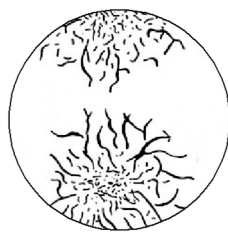


Figure 3-5 TYPE B, Rosette flake graphite [46].

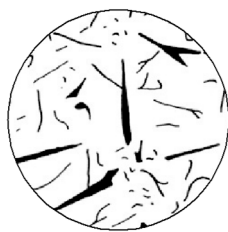


Figure 3-6 TYPE C, Kish graphite (hyper-eutectic compositions) [46].

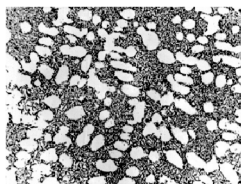


Figure 3-7 TYPE D, Undercooled flake graphite [46].



Figure 3-8 TYPE E, Interdendritic flake graphite (hypo-eutectic compositions) [46].

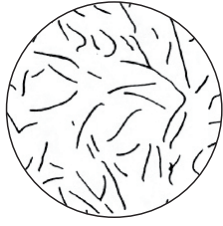


Figure 3-9 form I [46].



Figure 3-10 form II [46].

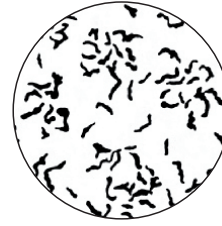


Figure 3-11 form III [46].

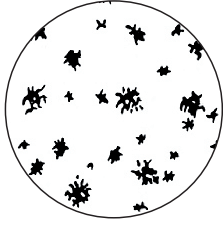


Figure 3-12 form IV [46].

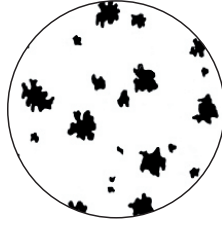


Figure 3-13 form V [46].

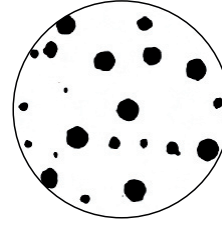


Figure 3-14 form VI [46].

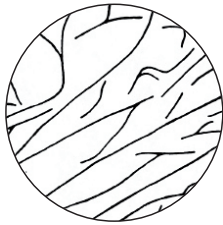


Figure 3-15 Largest flake size = 100 mm or more (x100) [46].

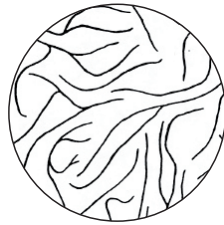


Figure 3-16 Largest flake size = 50 – 100 mm (x100) [46].

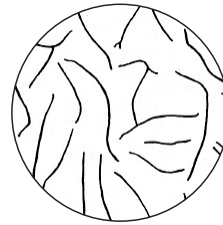


Figure 3-17 Largest flake size = 25 – 50 mm (x100) [46].

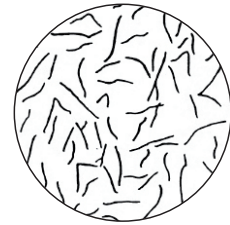


Figure 3-18 Largest flake size = 12 – 25 mm (x100) [46].

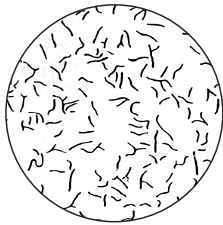


Figure 3-19 Largest flake size = 6 – 12 mm (x100) [46].

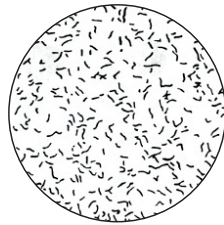


Figure 3-20 Largest flake size = 3 – 6 mm (x100) [46].

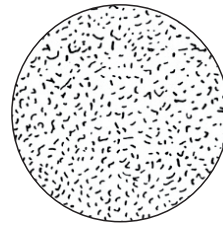


Figure 3-21 Largest flake size = 1.5 – 3 mm (x100) [46].

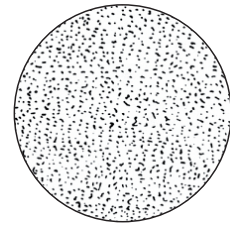


Figure 3-22 Largest flake size = less than 1.5 mm (x100) [46].

Titanium, like vanadium and molybdenum, creates carbide particles which promote an under-cooled graphitic structure and increase the amount of ferrite, which influences the material durability and friction characteristics of a brake disc. “*The friction and wear would be high if up to 0.01 % titanium is introduced and low with titanium levels of 0.03 %. Titanium levels greater than 0.15 % would appear to have little effect*” [10]. Addition of copper will make the disc thickness expand more uniformly at heating and will not affect the wear. The wear properties can be improved by increasing the carbon and phosphorous contents, or, by increasing the sulphur content and decreasing the manganese content. Addition of titanium leads to an increase of the pad wear and results in lowered braking performance. High carbon content in discs was found to give better overall performance and reduced wear compared to brake discs alloyed with titanium or brake discs made from medium carbon iron.

In grey cast iron, the thermal diffusivity has been found to be strongly anisotropic (or can be considered as orthotropic with one preferential direction for the heat conduction) at the microscopic scale. Holmgren et al [47] showed that there is a significant influence of the crystal orientation of graphite on the effective thermal

conductivity of grey cast iron. Toshikazu and Masanori [17] showed that the thermal strength of brake discs can be improved by an increase of the material homogeneity in ordinary grey cast iron. Thermal stresses can be reduced by increasing the thermal conductivity and reducing the elastic modulus, which can be accomplished by introducing a higher carbon content in the material.

The thermal conductivity (ability of a material to conduct heat), thermal capacity (ability of a material to store heat) and thermal diffusivity (determining the rate at which heat flows through a material) are often referred to since they are important for the disc fatigue life. However, some studies reveal contradictions since brake discs with high values of the thermal diffusivity do not show the best results regarding low crack growth, see also section 7.2.

### 3.4 MATERIAL MODELLING

Modelling of material behaviour is important in order to understand the influence of material parameters. Constitutive equations are established using different assumptions. Together with boundary conditions, solutions for specific problems can be obtained. A simple elastic model can be chosen if the stresses in the structure do not exceed the yield stress. Other material models, like perfect plastic, linear/non-linear isotropic hardening plastic, linear/non-linear kinematic hardening plastic, mixed linear/non-linear isotropic-kinematic hardening plastic, perfect linear/non-linear viscoelastic, linear/non-linear isotropic hardening viscoelastic, linear/non-linear kinematic hardening viscoelastic, mixed linear/non-linear isotropic-kinematic hardening viscoelastic, exist or can be defined. Creep, oxidation and fatigue damage can also be included in the mathematical models and will be described in Section 4.4. Many numerical methods exist in order to solve these kinds of problems.

Bodner et al [48] introduced a unified constitutive model having *one single inelastic strain tensor* for modelling both creep and plasticity in order to compute the stresses. At lower stresses, time dependent creep dominates the behaviour while plasticity dominates at higher stresses. A so-called drag stress has to be introduced and represents an internal state variable which is related to the strength of the material. Transition between deformation dominated by creep and plasticity is determined by the stress level and depends on the temperature. The inelastic strain rate under creep and plasticity [49] is (uniaxial conditions)

$$\dot{\epsilon}^{in} = \begin{cases} A_0 \left(\frac{\bar{\sigma}}{K_0}\right)^{n_1} e^{\left(-\frac{\Delta H^{in}}{RT}\right)} & \text{if } \left(\frac{\bar{\sigma}}{K_0}\right) \leq 1 \\ A_0 e^{\left(\frac{\bar{\sigma}}{K_0}\right)^{n_2} - 1} e^{\left(-\frac{\Delta H^{in}}{RT}\right)} & \text{if } \left(\frac{\bar{\sigma}}{K_0}\right) \geq 1 \end{cases} \quad (3.4.1)$$

where  $\Delta H^{in}$  is the activation energy for inelastic deformation,  $A_0$  is the scaling constant for inelastic deformation,  $n_1$  is the exponent for creep dominated deformation,  $n_2$  is the exponent for plasticity dominated deformation,  $K_0$  is the back stress,  $R$  is the gas constant,  $T$  is the temperature and  $\bar{\sigma}$  is the stress.

Material modelling of grey cast iron alloys can be found in the literature for brake discs used in the railway industry. Samrout [50] give a material model for 28CrMoV5-8 steel under thermomechanical thermal loading. This model uses a viscoelastic law with a double kinematic and isotropic hardening with memory effect of the plastic strains. The complete definition of this model can be found in [50]. However, such a model is computationally demanding and Dufrenoy and Weichert [51] propose a model using a simpler multisurface linear kinematic hardening behaviour depending on temperature. Calibration is performed using tension tests up to 1100 °C. This model decreases the computational time but does not account for the cyclic softening of the material.

### 3.5 MATERIAL TESTING

Kim et al [52] studied the fatigue life of a railway brake disc manufactured from GC25 grey cast iron. In order to determine the cause of the thermal fatigue cracks, the pad/disc contact pressure and the stresses in the disc and the pads were analysed. The S-N curve for the GC25 material was established using a test specimen collected from the central part of the friction plate, see Figure 3-23 and Figure 3-24. For the fatigue tests, constant amplitude loading with stress ratio  $R = \sigma_{\min}/\sigma_{\max} = -1$  and the frequency 10 Hz was used.

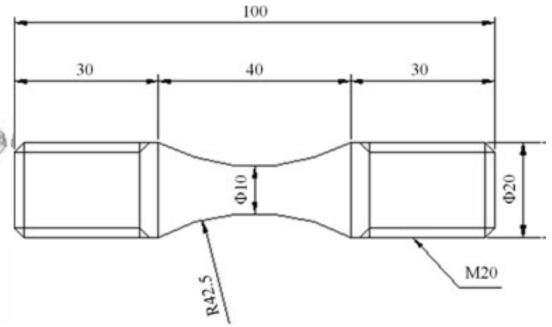
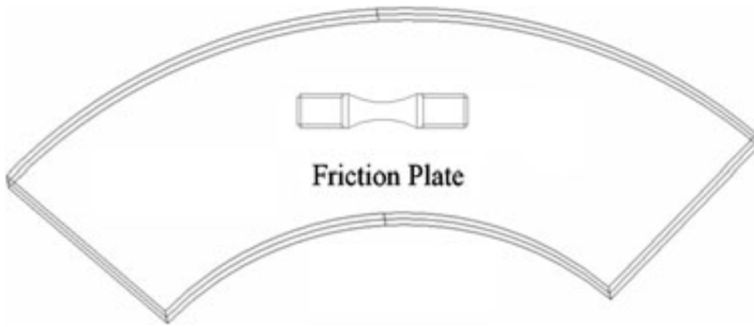


Figure 3-23 Position of specimen in the friction plate [52].

Figure 3-24 Drawing of specimen [52].

*Fatigue testing.* Results from the fatigue tests in [52] are shown in Figure 3-25 where the S–N curve for GC25 material is plotted at room temperature and at 300 °C. The fatigue strength was found to be almost independent of temperature for the interval 0–300 °C. Older studies have shown that grey cast iron can keep its mechanical properties up to 400 °C. However, temperatures resulting from braking of a truck are usually higher than 400 °C.

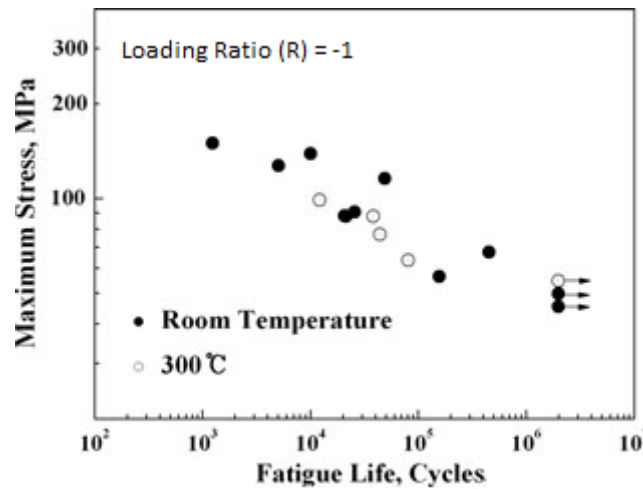


Figure 3-25 S–N data of the GC25 material [52].

*Creep behaviour and testing.* Gorash [53] described the creep phenomena in detail and gave models for the forms of damage caused by creep based on isotropic damage model, uni-axial creep model, temperature dependent model as exemplified and detailed in the thesis. Elementary descriptions of the three creep stages are shown in Figure 3-26. Creep usually occurs when the temperature reaches around 0.4 times the melting temperature of the component.

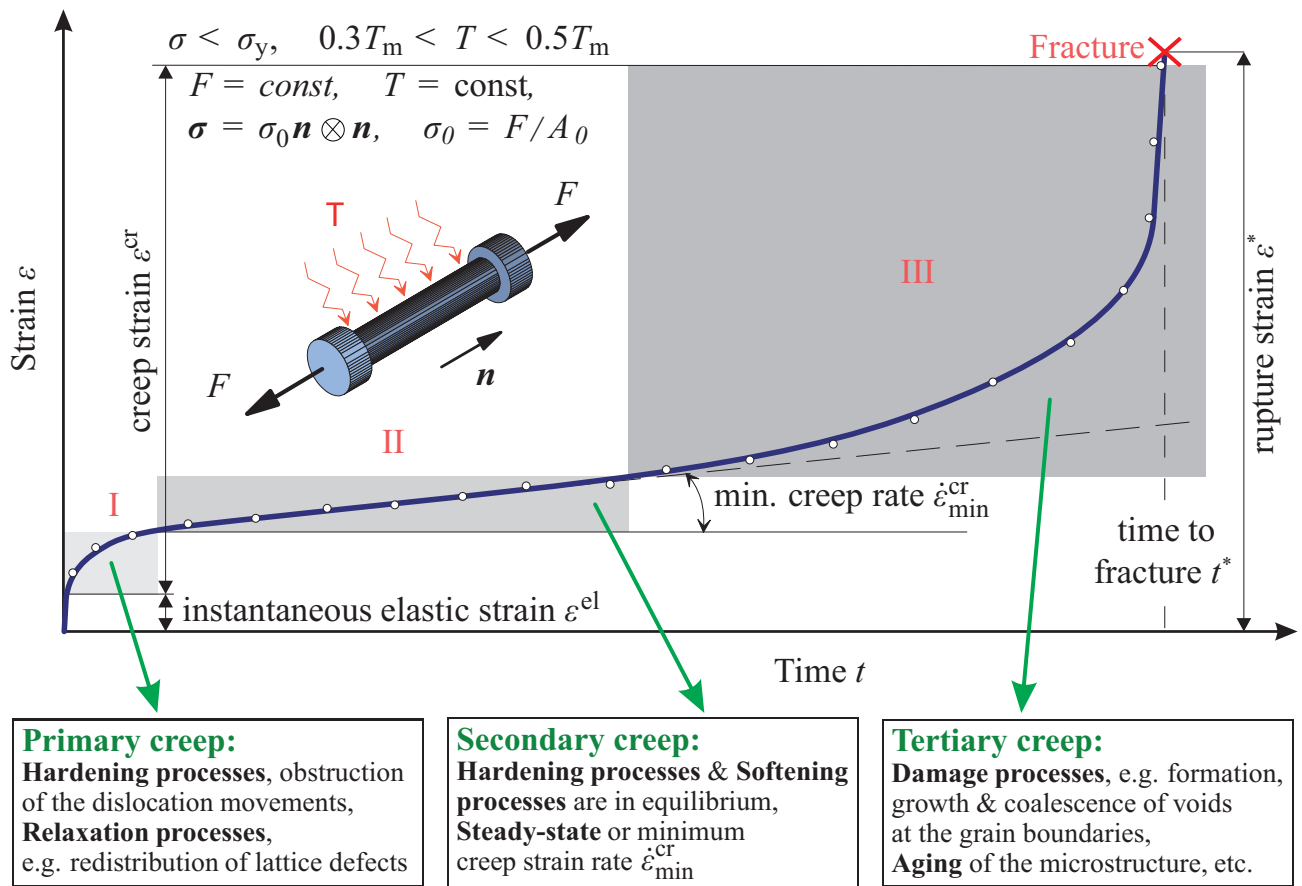


Figure 3-26 Strain vs time curve under constant load  $F$  and temperature  $T$  (I – primary creep, II – secondary creep, III – tertiary creep) [53].

It is important to note that the creep damage starts first at the end of the secondary creep stage. The creep damage starts when the slope which describes the secondary creep stage is not constant any longer. The onset of the tertiary creep is thus refined.

Different deformation mechanisms and corresponding functions are described in [53] and are shown in Table 9, where  $\dot{\epsilon}_{cr}$  is the creep strain rate,  $\sigma$  is the stress,  $Q_c$  is the activation energy for creep [J/ mol],  $R = 8.314$  [J/ K· mol] is the universal gas constant,  $T$  is the absolute temperature [K], and  $A$  and  $C$  are stress-independent constants. These equations are obtained with the basic assumptions in [53] and more response functions can be found in its reference.

Table 9 Deformation mechanisms and corresponding response functions [53].

Deformation mechanisms	Response functions
<b>Power-law creep</b>	$\dot{\epsilon}_{cr} \propto \exp\left(-\frac{Q_c}{RT}\right) \sigma^n$
<b>Diffusional flow</b>	$\dot{\epsilon}_{cr} \propto \exp\left(-\frac{Q_c}{RT}\right) \sigma$
<b>Linear + power law</b>	$\dot{\epsilon}_{cr} \propto \exp\left(-\frac{Q_c}{RT}\right) \sinh(A\sigma)$
<b>Power-law breakdown</b>	$\dot{\epsilon}_{cr} \propto \exp\left(-\frac{Q_c}{RT}\right) \exp(C\sigma)$

## 4 FATIGUE AND CRACKS

### 4.1 GENERAL

Fatigue and cracks at cyclic and/or time-dependent loading, including different fatigue failure mechanisms are studied in this chapter.

When a load is applied to a material, normal and shear stresses will be introduced and the material will change shape. This change in shape is called deformation. The microstructure of the material will be affected by the deformation in a complex way, see Figure 4-1. If the load applied is sufficiently high, the material may deform plastically which is irreversible contrary to elastic deformation. Such loading creates damage (in some cases) and residual stresses (generally). At elevated temperatures, the strength of a material decreases while the ductility increases. The opposite phenomenon occurs at low temperatures. When a structure is subjected to cyclic loading, fracture can occur even if the applied loading never exceeds the yield limit. This phenomenon is known as fatigue and is one of the primary reasons for the failure of structural components. The life of a fatigue crack has two parts, initiation and propagation. Dislocations in the microstructure of the material play a major role in the fatigue crack initiation phase.

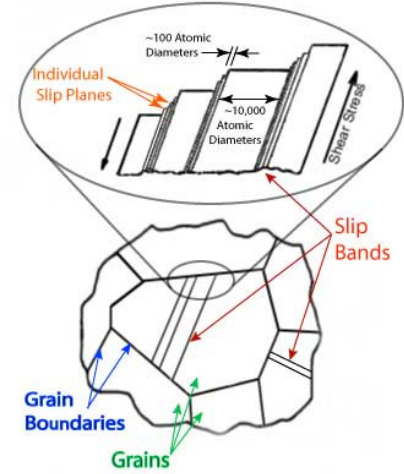


Figure 4-1 Deformation of the microstructure after loading [54].

Two different fatigue phenomena are often distinguished. Low-cycle fatigue (LCF) focusses on cyclic plasticity, including crack initiation, while high-cycle fatigue (HCF) concerns crack initiation and propagation at nominally elastic stress levels. However, it should be noted that, also in HCF, the material in front of the crack tip is exposed to LCF loading (a zone with cyclic plasticity is formed).

The stress amplitude is defined as  $\sigma_a = \Delta\sigma/2$ , where  $\Delta\sigma = \sigma_{\max} - \sigma_{\min}$ . The mean stress is defined as  $\sigma_{\text{mean}} = (\sigma_{\max} + \sigma_{\min})/2$  and the stress ratio as  $R = \sigma_{\min}/\sigma_{\max}$ . The amplitude ratio can be defined as  $A = \sigma_a/\sigma_{\text{mean}} = (1 - R)/(1 + R)$ . For fully-reversed loading conditions,  $R$  is equal to -1. Figure 4-2 summarizes all these variables. A comparison between low and high-cycle fatigue is given in Table 10.

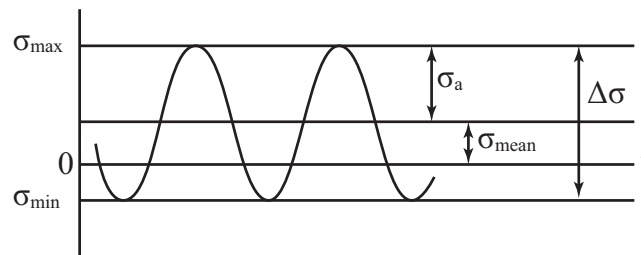


Figure 4-2 Schematic showing the imposed periodic stress and the definition of terms. Adapted from [55].

Table 10 Comparison between low-cycle and high-cycle fatigue, adapted from [56].

High-cycle fatigue (HCF)	Low-cycle fatigue (LCF)
Stress controlled, more than 50,000 cycles, crack has not started, facilitates design	Strain controlled, less than 50,000 cycles, when will crack start?
<ul style="list-style-type: none"> <li>✓ Advantages of HCF                             <ul style="list-style-type: none"> <li>• Empirical parameters for a lot of materials have been determined                                     <ul style="list-style-type: none"> <li>- Marin factors</li> <li>- Fatigue Strengths</li> </ul> </li> <li>• Easy to use for design applications</li> </ul> </li> <li>✓ Disadvantages of HCF                             <ul style="list-style-type: none"> <li>• Cannot be used for LCF applications</li> <li>• If loads are fluctuating in a pseudo-random way, HCF methods can yield non-conservative results</li> </ul> </li> </ul>	<ul style="list-style-type: none"> <li>✓ Advantages of LCF                             <ul style="list-style-type: none"> <li>• More conservative than HCF</li> <li>• Widely used in industry</li> </ul> </li> <li>✓ Disadvantages of LCF                             <ul style="list-style-type: none"> <li>• Analysis depends on testing and strain data must be available</li> <li>• Analysis is more complicated than with HCF methods</li> </ul> </li> </ul>

4.2 HIGH-CYCLE FATIGUE

Structures that are subjected to (basically) elastic stresses are dimensioned using a stress-based infinite-life approach where the fatigue limit of the material is not exceeded. *S-N* curves (also known as Wöhler curves) are commonly used for finding the fatigue life (*N*) of a material. In Figure 4-3, the fatigue life (*N*) corresponding to a certain probability of failure, normally 50 %, is plotted as a function of the stress amplitude (*S<sub>a</sub>*). This curve is plotted from experiments as described in Section 3.5. The applied stress amplitude is defined by  $S_a = (\max_t[\sigma(t)] - \min_t[\sigma(t)]) / 2$  where  $\sigma$  is the stress.

The *S-N* curve in Figure 4-3 has two asymptotes. The upper one is associated with static failure and the lower one is usually referred to as the fatigue limit (*S<sub>f</sub>*). This means that for amplitudes below the fatigue limit, failure does not occur, even after a very high number of cycles.

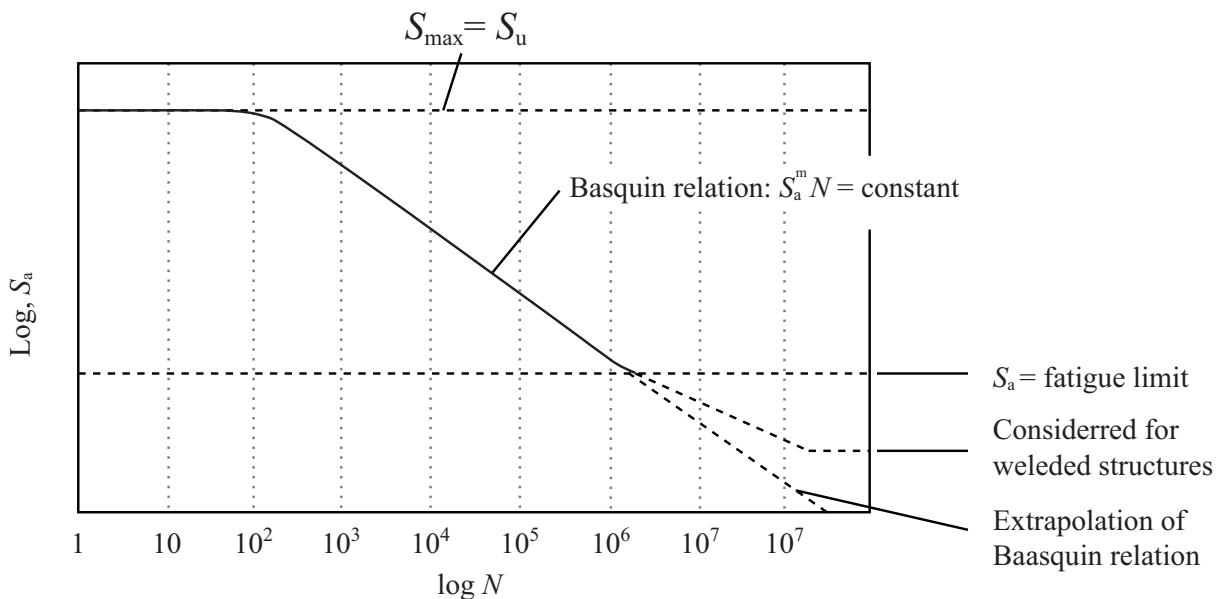


Figure 4-3 S-N curve with extrapolations below the fatigue limit [57].

Söderberg, Gerber or Goodman relations are often used to quantify the effect on fatigue life of the mean stress, see Figure 4-4.

$$\frac{\sigma_a}{\sigma_e} + \frac{\sigma_{\text{mean}}}{\sigma_{\text{yield}}} = 1 \quad \text{Söderberg (USA, 1930)} \quad (4.1.1)$$

$$\frac{\sigma_a}{\sigma_e} + \frac{\sigma_{\text{mean}}}{\sigma_{\text{UTS}}} = 1 \quad \text{Goodman (England, 1899)} \quad (4.1.2)$$

$$\frac{\sigma_a}{\sigma_e} + \left(\frac{\sigma_{\text{mean}}}{\sigma_{\text{UTS}}}\right)^2 = 1 \quad \text{Gerber (Germany, 1874)} \quad (4.1.3)$$

here  $\sigma_a$  is the alternating stress (stress amplitude),  $\sigma_e$  is the endurance limit,  $\sigma_{\text{mean}}$  is the mean stress,  $\sigma_{\text{yield}}$  is the yield stress and  $\sigma_{\text{UTS}}$  is the ultimate strength of the material. The relations are illustrated in Figure 4-4.

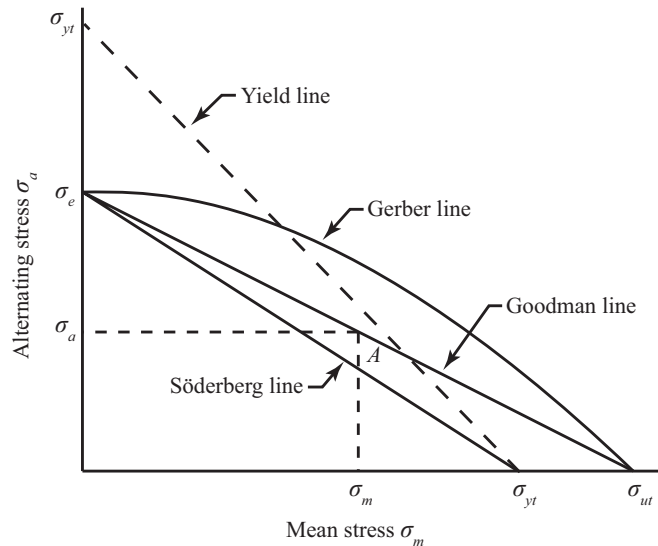


Figure 4-4 Haigh's diagram for stress based fatigue evaluation.

### 4.3 LOW-CYCLE FATIGUE

In contrast to high-cycle fatigue, where the deformation behaviour is nominally linearly elastic, low-cycle fatigue means that plastic deformation is encountered. Low-cycle fatigue testing is performed at low frequencies, from 0.1 to 0.5 Hz when failure is expected after less than  $10^5$  cycles and up to 2 Hz. Failure occurs no further than 50,000 cycles in low-cycle fatigue [58].

*Low-cycle fatigue testing.* When it comes to the low-cycle fatigue testing of a specimen, it is very common to use the Manson-Coffin criterion which is a simple linear relationship between the plastic strain amplitude and the life plotted in log-log scale. Other approaches like the total strain approach, relate the total mechanical strain amplitude to life. If the mean stress has an effect on life, then the Morrow or the Smith-Watson-Topper (SWT) approaches are used while Ostergren's approach accounts for the influence of the cycle frequency in addition to the mean stress influence. These approaches are basically mechanical approaches. That is why; Skelton [59] used a relation between the dissipated energy per cycle and the number of cycles to failure. However, if the damage mechanisms have to be taken into account separately like oxidation and creep, other approaches like Halford and Manson [60] for the strain range partitioning (SRP) method or Neu and Sehitoglu [61] or Lemaitre and Chaboche [62] can be used. Gocmez et al [63] summarized these different approaches as shown in Table 11. Classical approaches can be expressed under a general form of  $\phi(\varepsilon, \varepsilon^p, \sigma, \dots) = f(N_f, \alpha, \beta, \dots)$  where  $N_f$  denotes the number of cycles to failure,  $\alpha$  and  $\beta$  are material constants, and  $\varepsilon$ ,  $\varepsilon^p$  and  $\sigma$  are the response fields during a complete cycle which is generally assumed to be stabilized.

Table 11 Classical life prediction approaches [63]. Parameters are detailed in [63].

Approach	$\phi$	$f$	Parameter range
<b>Manson-Coffin</b>	$\Delta\varepsilon^p$	$\varepsilon'_f N_f^c$	$0.35\varepsilon_f < \varepsilon'_f < \varepsilon_f$
<b>Total strain</b>	$\Delta\varepsilon^{\text{mechanic}}$	$\varepsilon'_f N_f^c + \left(\frac{\sigma'_f}{E}\right) N_f^b$	$-0.7 < c < -0.5$
<b>Morrow</b>	$\Delta\varepsilon^{\text{mechanic}}, \sigma_{\text{mean}}$	$\varepsilon'_f N_f^c + \left(\frac{\sigma'_f - \sigma_{\text{mean}}}{E}\right) N_f^b$	$\sigma'_f \approx 3.5\sigma_{\text{UTS}}$
<b>SWT</b>	$\sigma_{\text{max}}, \Delta\varepsilon^{\text{mechanic}}$	$\sigma'_f \varepsilon'_f E N_f^{b+c} + \sigma_f'^2 N_f^{2b}$	$-0.14 < b < -0.06$
<b>Ostergren</b>	$\sigma_{\text{max}}, \Delta\varepsilon^{\text{mechanic}}$	$AN_b^f v^{\beta(k-1)}$	
<b>Energetic</b>	$\Delta\omega_p = \int_{\text{cycle}} \sigma \, d\varepsilon$	$C N_f^D$	$D \approx b + c$

The mean stress effect has to be taken into account. Most of the time, the S-N curves obtained from tests done in laboratories are generated using a fully-reversed stress cycle in order to avoid mean stress effect. The effect of mean stress on the strain-life curve is shown schematically in Figure 4-5.

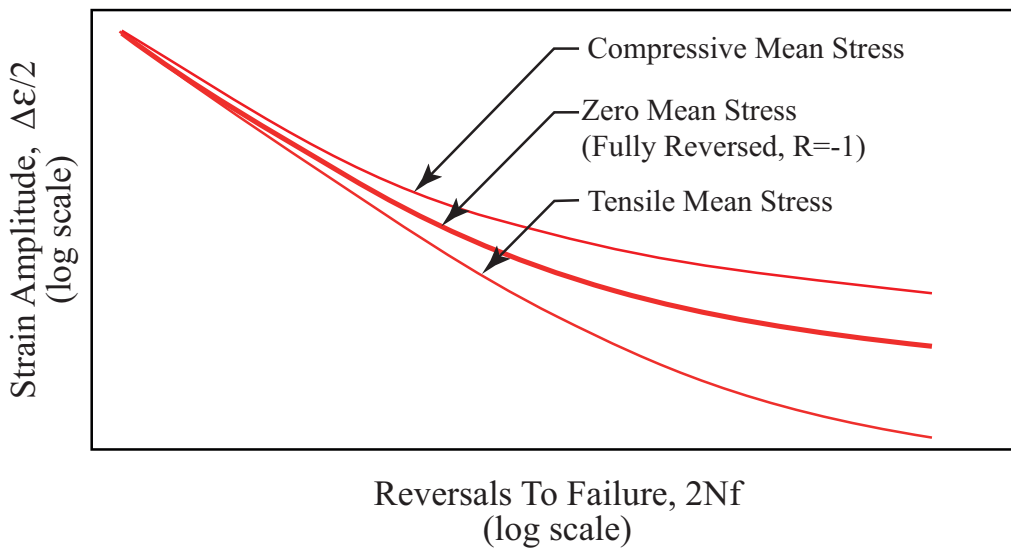


Figure 4-5 Effect of mean stress on strain-life curve [64].

Morrow proposed a model which takes into account the mean stress by altering the fatigue strength coefficient in the elastic component of the stress-strain relationship (4.3.1 where mean stresses can be positive (tensile mean stress,  $\sigma_{\text{mean}} > 0$ ) or negative (compressive mean stress,  $\sigma_{\text{mean}} < 0$ ))

$$\sigma_a = (\sigma'_f - \sigma_{\text{mean}})(2N_f)^b \quad (4.3.1)$$

The Morrow Mean Stress Correction can be expressed in terms of the strain-life relationship by

$$\varepsilon_a = \frac{\Delta\varepsilon}{2} = \frac{\sigma'_f - \sigma_{\text{mean}}}{E} (2N_f)^b + \varepsilon'_f (2N_f)^c \quad (4.3.2)$$

which is also called the modified Morrow equation. Here  $\Delta\varepsilon$  is the total strain amplitude (elastic + plastic),  $\sigma'_f$  is the fatigue strength coefficient,  $E$  is Young's modulus,  $b$  is the fatigue strength exponent and  $c$  is the fatigue ductility exponent. Here  $b$  and  $c$  are material dependent constants.

The effect of a tensile mean stress in modifying the strain-life curve using the equation (4.3.2) is shown in Figure 4-6.

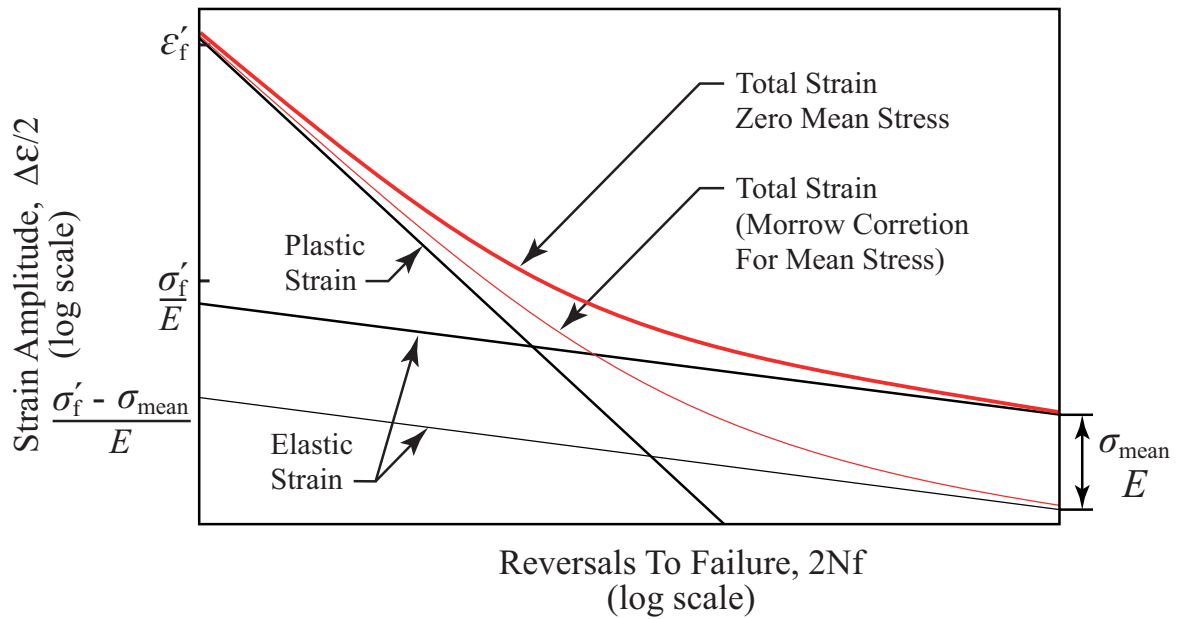


Figure 4-6 Effect of mean stress on strain-life curve (Morrow Correction), adapted from [64].

The Smith, Watson and Topper mean stress correction, see equation (4.3.3), is more conservative than the modified Morrow equation, see equation (4.3.2), and is recommended in cases of predominantly tensile loading because with this approach, no damage occurs if the maximum stress is zero or negative, ie compressive stress.

$$\sigma_{\max} \varepsilon_a = \sigma_{\max} \frac{\Delta \varepsilon}{2} = \frac{(\sigma'_f)^2}{E} (2N_f)^{2b} + \sigma'_f \varepsilon'_f (2N_f)^{b+c} \quad (4.3.3)$$

where  $\sigma_{\max} = \sigma'_f (2N_f)^{2b}$ .

In reality, damage occurs even in compression and the modified Morrow equation is then recommended to use in cases of compressive stresses.

*Fatigue prediction method for cast iron.* In the following, a fatigue prediction method for cast iron [65] is described based on the constant amplitude strain-life method [66] and the PhD thesis by Downing [67] for the model definition. According to [65], there are some similarities between the fatigue prediction method for cast iron and the constant amplitude strain-life method which are

- elastic-plastic behaviour in stress concentrations control fatigue life
- rainflow counting is used to determine damaging events corresponding to closed elastic-plastic hysteresis loops
- mean stresses are tracked according to input loading sequences
- Smith-Watson-Topper parameter accounts for mean stress
- Neuber's rule is used to determine notch root stress and strains.

Due to the presence of graphite and especially its morphology, see section 3.3, the microstructure of a grey iron component is different from other cast iron. Cast iron exhibits more surface cracking and higher compression resistance which means that the monotonic and cyclic stress-strain behaviour is typical for this material and a special model is needed to account for these differences. The stress-strain model, see Figure 4-7, for cast iron under cyclic loading is given by

$$\sigma = A_{\text{eff}}(\sigma_B + \sigma_G) + (1 - A_{\text{eff}})\sigma_{CC} \quad (4.5.1)$$

where the first term,  $A_{\text{eff}}(\sigma_B + \sigma_G)$ , represents the bulk and graphite stresses acting over a fraction of the cross-sectional area unaffected by surface cracking and where the second term,  $(1 - A_{\text{eff}})\sigma_{\text{CC}}$ , is the compressive crack closure stress acting over the remaining area.

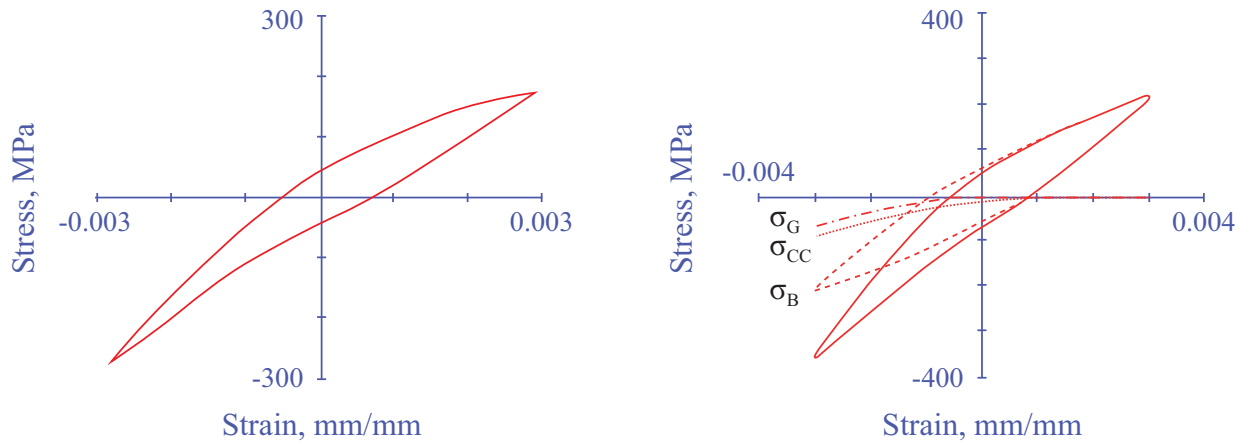


Figure 4-7 Stress-strain curve for grey cast iron (left) and cyclic stress-strain response model (right) [65].

The crack closure stress is given by

$$\sigma_{\text{CC}} = Q(\varepsilon_{\text{max}} - \varepsilon)^q \quad (4.5.2)$$

where  $Q$  and  $q$  are constants which depend on monotonic material properties and the strain limit. It can be noticed that the crack closure stress is nonlinear elastic.

The total strain in equation 4.5.2 is the sum of the secant strain  $\varepsilon_S$  and the remaining plastic strain  $\varepsilon_R$  as given by

$$\varepsilon = \varepsilon_S + \varepsilon_R = \frac{\sigma}{E_0 + m\sigma} + \left(\frac{\sigma}{K}\right)^{\frac{1}{n}} \quad (4.5.3)$$

here  $E_0$ ,  $m_T$ ,  $K_T$ ,  $n_T$ ,  $m_C$ ,  $K_C$  and  $n_C$  are obtained from tensile and compressive stress-strain curves. Equation 4.5.3 assumes an ideal case where material properties in compression and tension have the same value. The bulk behaviour is governed by

$$\varepsilon = \frac{\sigma_b}{E_0 + m_b\sigma_b} + \left(\frac{\sigma_b}{K_b}\right)^{\frac{1}{n_b}} \quad (4.5.4)$$

where  $\sigma_b$  is the bulk stress at a given strain,  $m_b$ ,  $K_b$  and  $n_b$  are material properties (material properties in tension and compression are the same in this case) and  $E_0$  is the slope of the tangent of the monotonic stress-strain curve at the origin as shown in Figure 4-8. It should be observed that equation 4.5.4 is obtained assuming similar characteristics to wrought metal in the elastic and plastic regime.

Some other parameters like the internal graphite behaviour driven by  $\sigma_G$ , see Figure 4-7 (right), and the surface behaviour have to be taken into account in the model but are not described here. Refer to [67] for more information.

In Figure 4-8,  $E_S$  defines the secant modulus which is the slope of a line from the origin to a point on the stress-strain curve. A distinction is made between tension and compression via the subscripts T and C.

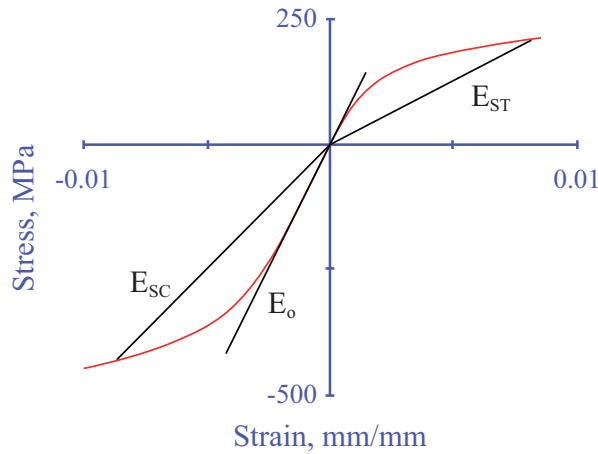


Figure 4-8 Monotonic stress-strain curve for cast iron [65].

The life span can be found using the Smith, Watson, and Tropper (SWT) parameter given by

$$\sigma_{\max} \varepsilon_a = h''(N_f) \tag{4.5.5}$$

where by definition  $\sigma_{\max} = \sigma_m + \sigma_a$ , ( $\sigma_m$  is mean stress and  $\sigma_a$  is amplitude stress) and  $h''(N_f)$  indicates a function of fatigue life. For pearlitic grey iron, it has been found that  $\sigma_{\max} \varepsilon_a = 1.82(N_f)^{-0.25}$  [67].

#### 4.4 THERMOMECHANICAL FATIGUE

Thermomechanical fatigue (TMF) accounts for strain variations induced by the total variations in temperature and/or externally applied loading in combination with external constraints. At high temperatures, creep and other complex phenomena may occur.

Two types of thermomechanical loading patterns can be defined: in-phase and out-of-phase, see Figure 4-9. For in-phase loading the maximum tensile strain is reached when the temperature is maximum. Out-of-phase is the opposite, ie, the maximum tensile strain is reached when the temperature is minimum. Out-of-phase is the dominating loading for brake discs.

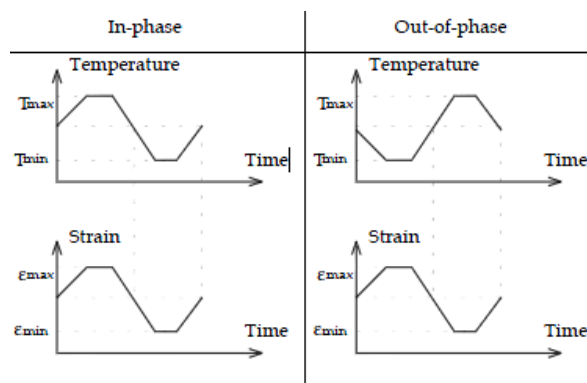


Figure 4-9 In-phase and out-of-phase TMF loading patterns [68].

Spera and Mowbray [69] have proposed a classification for low-cycle fatigue in order to clearly distinguish the different categories or assumptions available for each fatigue mechanism, see Figure 4-10.

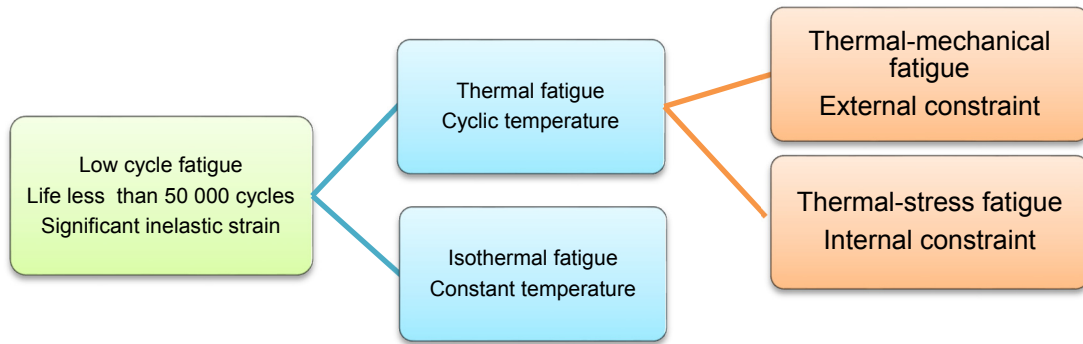


Figure 4-10 Proposed terminology for low-cycle fatigue combined with thermal loading [69].

Under fatigue conditions, different types of damage occur and are shown in Figure 4-11 while the damage mechanisms during an out-of-phase TMF cycle shown in Figure 4-12.

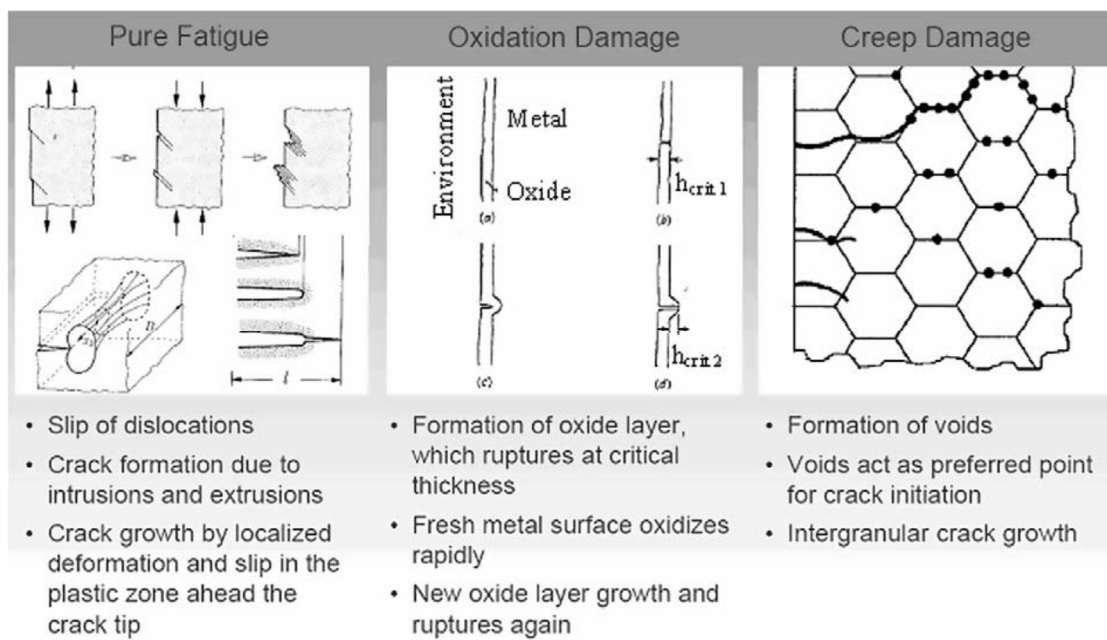


Figure 4-11 Different damage mechanisms that can happen in thermomechanical loading [63].

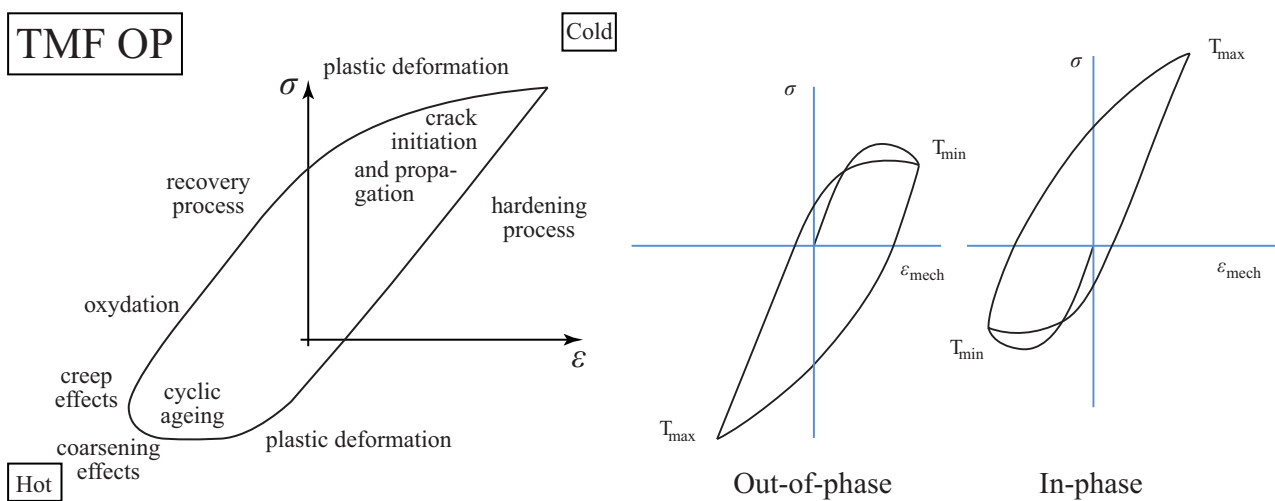


Figure 4-12 Damage mechanisms during an out-of-phase TMF cycle [70] (left) and schematics (right).

Hasbroucq [71] introduced an illustrative problem to study shakedown at thermomechanical loading. It consists of two parallel bars of cross-section  $S$  and  $S/2$  with lengths  $L$  and  $L/2$  as shown in Figure 4-13 (left). The bars

are clamped on one side and are joined to have equal displacements in the horizontal direction. They are subjected to the thermal loading shown in Figure 4-13 (right). In that case, the elastic coefficients are taken as constant except for the Young modulus  $E_1$  and the yield stress  $\sigma_{y1}$  of bar 1 which are linearly decreasing with temperature ( $E_1(\theta) = E_0 - \lambda_1\theta$ ,  $\sigma_{y1}(\theta) = \sigma_{y0} - \lambda_2\theta$ ). The yield stress and Young's modulus of bar 2 are  $\sigma_{y2} = \sigma_{y0}$  and  $E_2 = E_0$  respectively.

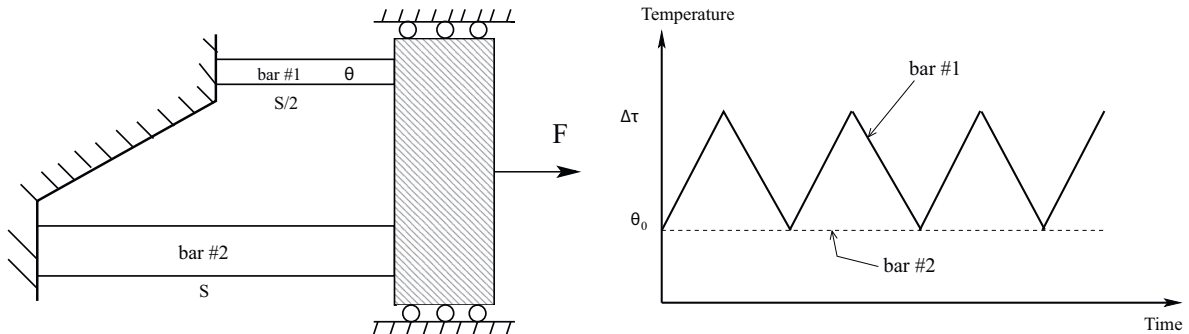


Figure 4-13 The two bars problem (left) and its loading case (right) [71].

Numerical results using an analytical model are presented in Figure 4-14: Different zones are defined depending on the status of bar 1. Four shakedown mode zones (SD1 to SD4), two alternating plastic mode zones (P1 and P2) and a ratcheting zone (R) are defined. In Figure 4-14,  $\sigma_T = E_0\alpha\Delta\tau/2$  is the stress associated to the temperature variation where  $\alpha$  is the coefficient of linear thermal expansion,  $\Delta\tau = \theta - \theta_0$  is the temperature variation while  $\sigma_A = F/S$  where  $F$  is the applied force and  $S$  the cross-section of the bar. In [71]  $\theta_0$  is supposed to be zero for pure simplicity. The plastic shakedown is a steady state which is a closed elastic-plastic loop with no net accumulation of plastic deformation. In a word, the plastic shakedown is the stabilization of the stress-strain diagram of a material after a number of loading and unloading cycles beyond the elastic limit.

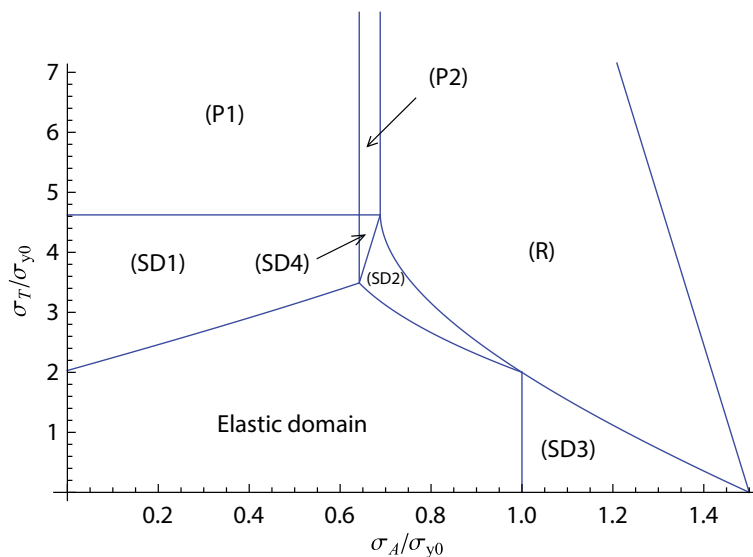


Figure 4-14 Bree diagram of the two-bar system [71].

Many models exist in the literature for material behaviour from a mathematical point of view linked to the thermomechanical fatigue problems. Among these models, six seem to be the most popular and advanced thermomechanical fatigue models: Damage Summation (DS), Frequency Separation (FS), Ductility Exhaustion (DE), Strain-Range Partitioning (SRP), Total Strain Version of SRP (TS-SRP) and Strain Energy Partitioning (SEP), see [68]. These models include damage-based criteria, stress-based criteria, strain-based criteria and energy-based criteria. A complete review of the models can be found in [68]. The damage summation model is described in the following.

There exists three possible damage mechanisms [61] which depend on temperature, strain and phasing: (1) fatigue, (2) environmental (oxidation) and (3) creep. The total damage can, assuming a linear fatigue damage accumulation, be written as

$$D^{\text{tot}} = D^{\text{fatigue}} + D^{\text{oxidation}} + D^{\text{creep}} \quad (4.4.1)$$

Equation 4.4.1 can be rewritten in terms of the number of cycles to  $N_f$  as

$$\frac{1}{N_f} = \frac{1}{N_f^{\text{fatigue}}} + \frac{1}{N_f^{\text{oxidation}}} + \frac{1}{N_f^{\text{creep}}} \quad (4.4.2)$$

Neu and Sehitoglu [72] has defined the fatigue damage as a localized deformation and slip in the cyclic plastic zone of the crack tip. It is commonly assumed that the “fatigue” mechanism is governed by the mechanical strain range  $\Delta\varepsilon^{\text{mechanic}}$ . It is possible to use only the plastic part of the strain range  $\Delta\varepsilon^{\text{mechanic}}$  for different loading conditions but this requires further analyses and does not give better results. The fatigue-life term  $N_f^{\text{fatigue}}$  is estimated from the strain-life relation

$$\frac{\Delta\varepsilon^{\text{mechanic}}}{2} = \frac{\sigma_f'}{E} (N_f^{\text{fatigue}})^b + \varepsilon_f' (N_f^{\text{fatigue}})^c \quad (4.4.3)$$

where  $\sigma_f'$  is the fatigue strength coefficient,  $b$  is the fatigue strength exponent,  $\varepsilon_f'$  is the fatigue ductility coefficient,  $c$  is the fatigue ductility exponent and  $E$  is the elastic modulus.

Oxidation damage mechanisms include (1) crack nucleation in the surface oxides and (2) oxide-induced crack growth. Crack nucleation is basically the rupture of the first oxide layer where the oxide-induced crack growth is described as the repeated formation of an oxide layer at the crack tip and its rupture which expose the component to the surrounding environment [72]. The influence of oxidation damage can be ignored in laboratory if the tests are performed in dry environment or in wet environment with helium atmosphere for a short time. Neu and Sehitoglu [61] has formulated the oxidation problem, in order to take into account this phenomenon in the fatigue equation (4.3.2), as

$$\frac{1}{N_f^{\text{oxidation}}} = \left[ \frac{h_{\text{cr}} \delta_o}{B \Phi^{\text{ox}} K_p^{\text{eff}}} \right]^{-\frac{1}{\beta}} \frac{2(\Delta\varepsilon^{\text{mechanic}})^{(2/\beta)+1}}{\varepsilon^{1-(\alpha/\beta)}}, \quad \Phi^{\text{ox}} = \frac{1}{t_c} \int_0^{t_c} \phi^{\text{ox}} dt \quad \text{with } \phi^{\text{ox}} = e^{\left[ -\frac{1}{2} \left( \frac{\dot{\varepsilon}_{\text{th}} / \dot{\varepsilon}^{\text{mechanic}}}{\zeta^{\text{ox}}} \right)^2 \right]} \quad (4.4.4)$$

with the effective oxidation constant

$$K_p^{\text{eff}} = \frac{1}{t_c} \int_0^{t_c} D_0 e^{\frac{-Q}{RT(t)}} dt \quad (4.4.5)$$

where  $D_0$  is the diffusion coefficient for oxidation,  $Q$  is the activation energy for oxidation,  $R$  is the universal gas constant,  $T(t)$  is the temperature,  $h_{\text{cr}}$  is the critical length for the crack,  $\delta_o$  is a material constant,  $B$  and  $\beta$  are constants,  $t_c = 2\Delta\varepsilon^{\text{mechanic}} / \dot{\varepsilon}$  is the cycle time,  $\dot{\varepsilon}$  is the total strain rate,  $\dot{\varepsilon}^{\text{mechanic}}$  is the mechanical strain rate and  $\dot{\varepsilon}_{\text{th}}$  is the thermal strain rate. The parameter  $\zeta^{\text{ox}}$  is introduced as a measure of the relative amount of damage associated with the different phasings (in-phase or out-of-phase).

Creep damage consists of internal intergranular cracks along pearlite colony boundaries perpendicular to the loading direction [72]. Neu and Sehitoglu [61] have suggested a formula related to creep damage as

$$\frac{1}{N_f^{\text{creep}}} = \int_0^{t_c} A_{\text{cr}} \Phi_{\text{cr}} e^{\left( \frac{-\Delta H^{\text{cr}}}{RT} \right) \left( \frac{\alpha_1 \bar{\sigma} + \alpha_2 \sigma_h}{K} \right)^m} dt, \quad \Phi_{\text{cr}} = \frac{1}{t_c} \int_0^{t_c} \phi_{\text{cr}} dt \quad \text{with } \phi_{\text{cr}} = e^{\left[ -\frac{1}{2} \left( \frac{\dot{\varepsilon}_{\text{th}} / \dot{\varepsilon}^{\text{mech}} - 1}{\zeta^{\text{cr}}} \right)^2 \right]} \quad (4.4.6 a, b)$$



For an un-notched component with a smooth surface, the cracking process can be described as follows, see Figure 4-16,

- ✓ In stage I, the crack is formed and grows in shear (mode II/III) - Cyclic plastic deformation is a prerequisite for fatigue crack initiation
- ✓ In stage II, the crack is longer and grows in mode I
- ✓ Stage III corresponds to final fracture

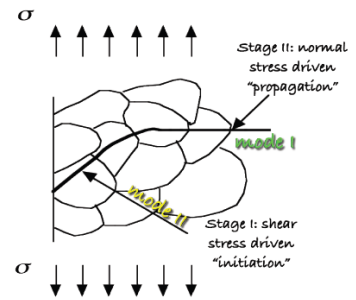


Figure 4-16 Fatigue crack initiation (stage I) & growth (stage II) [75].

According to [57], the fatigue phenomenon is “the progressive, localized, and permanent structural change that occurs in a material subjected to repeated or fluctuating strains at nominal stresses that have maximum values less than (and often much less than) the static yield strength of the material”. Fatigue damage is caused by the simultaneous action of cyclic stress, tensile stress, and plastic strain. If one of these three factors is removed, the fatigue crack will not initiate and propagate. It is stated in [57] that only compressive stresses will never cause fatigue. However, compressive loading may give rise to local tensile stresses that do induce fatigue.

The three modes of loading of a crack are given in Figure 4-17 and an example of loading history is shown in Figure 4-18.

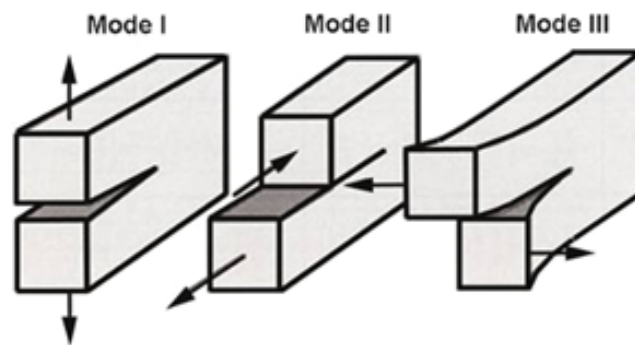


Figure 4-17 Different modes for the crack loading.

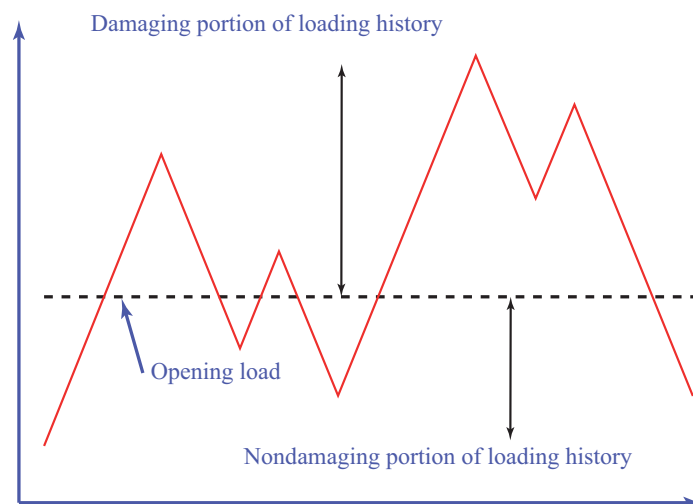


Figure 4-18 Damaging and nondamaging portions of loading history related to crack growth [76].

The range of the stress intensity factor is defined by

$$\Delta K = \Delta\sigma\sqrt{\pi a}F(*) = (\sigma_{\max} - \sigma_{\min})\sqrt{\pi a}F(*) = K_{\max} - K_{\min} \quad (4.4.1)$$

where  $F(*)$  is a geometry factor which depends on the size of the crack and the form of the structure.

A fatigue crack growth threshold value  $\Delta K_{th}$  is defined. For  $\Delta K < \Delta K_{th}$ , crack growth should be negligible (normally below  $10^{-9}$  m/cycle).

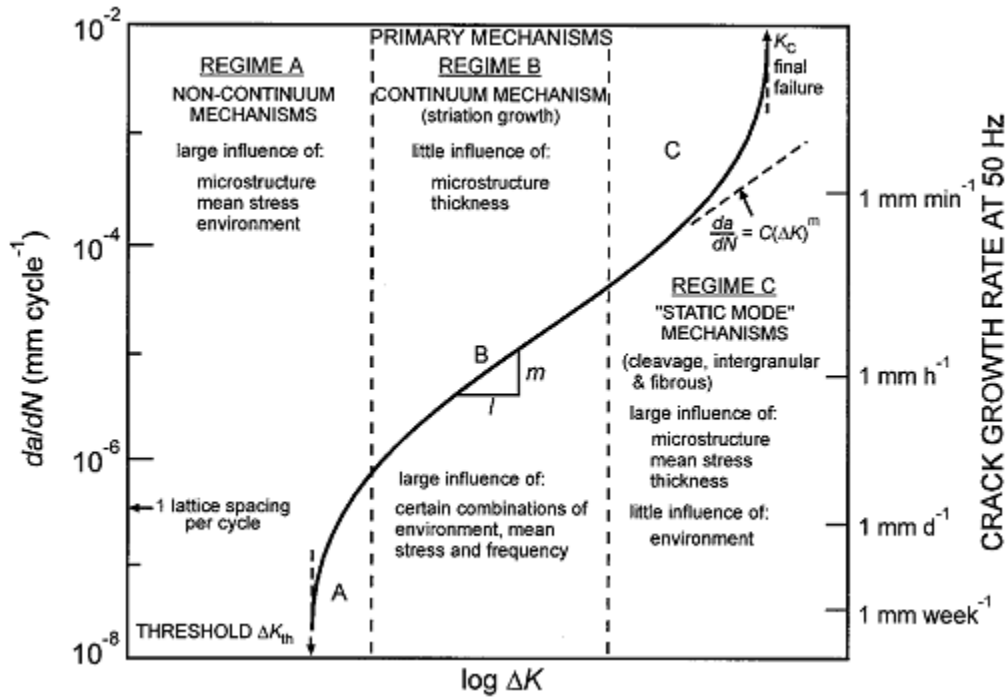


Figure 4-19 Relation between crack propagation rate and stress intensity range [77].

Figure 4-19 shows the relation between the crack propagation rate  $da/dN$  and the stress intensity range  $\Delta K$ , see equation 4.4.1. This curve has the three regimes described below:

- *Regime A:* For low values of  $\Delta K$ , there is a quick decrease of the crack propagation rate up to the threshold value  $\Delta K_{th}$  where the crack propagation rate is zero or negligible. In this regime, the loading case and the environment have a large influence on the crack propagation rate.
- *Regime B:* So-called Paris domain. This regime corresponds to a linear increase in the logarithm of the propagation rate as function of the logarithm of the stress intensity range. This regime follows Paris' law

$$\frac{da}{dN} = C\Delta K^m \quad (4.4.2)$$

- *Regime C:* This regime occurs when  $K_{max}$  becomes close to the value of  $K_C$ . Then, the crack propagation rate increases faster than estimated by Paris' law and final failure occurs. The critical stress intensity factor ( $K_C$  [MPa $\sqrt{m}$ ]) is included to account for unstable crack growth.

The crack growth during a loading cycle will depend not only on its magnitudes, but also on the magnitude of the loading cycles that preceded it [76], see Figure 4-20. Near the crack tip, a monotonic plastic zone is formed during the loading and a cyclic plastic zone is created when the unloading occurs. For each cycle, the crack propagates. The unloading process is referred to as crack closure and is illustrated in Figure 4-20 (b). Residual stresses hold the crack closed until the next loading which will create tensile stress and reopen the crack. Portions of the loading history that induce stresses higher than the so-called opening stress will cause crack growth. The portion of the stress history that is below the opening stress will not cause crack growth as shown in Figure 4-18. Newman's model is used to make an estimate of the opening stress for a loading history.

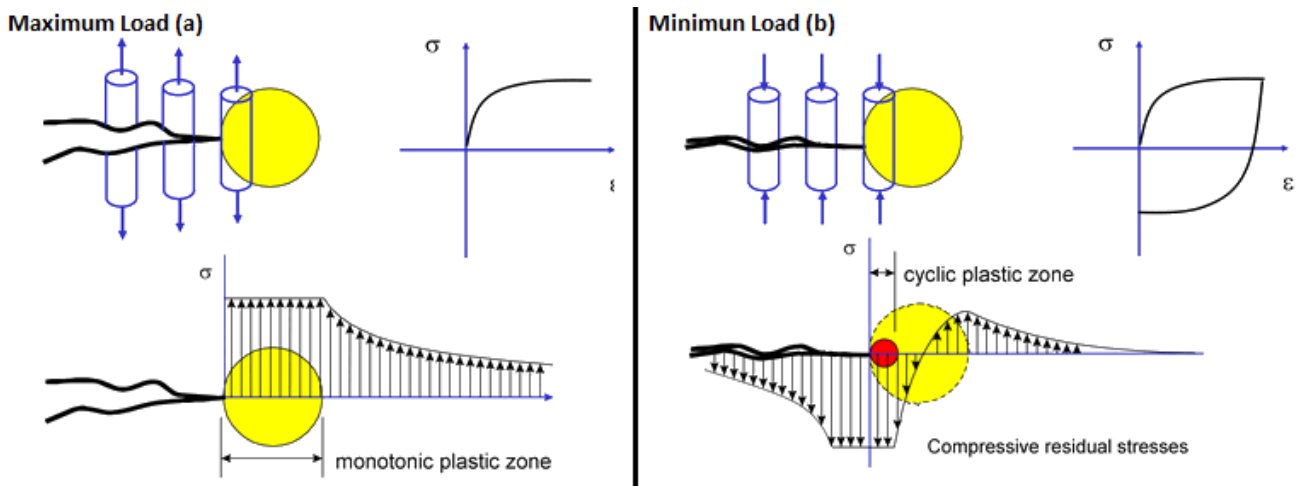


Figure 4-20 (a) Crack and stress fields that surround it at the maximum load in the loading cycle and (b) at minimum load in the loading cycle [76].

In grey cast iron, it is commonly assumed that cracks initiate very quickly due to material imperfections. This is why crack initiation is not studied and all research efforts focus on crack growth, the modelling of which is a major challenge.

Different authors have developed equations for crack propagation rate, see Table 12.

Table 12 Empirical and semi-empirical equations for fatigue crack propagation [78]. Paris' equation has been added to the original table.

Equations	Author	Year
$\frac{da}{dN} = C\Delta K^m$	Paris	1961
$\frac{da}{dN} = \frac{C\Delta K^m}{(1-R)K_c - \Delta K}$	Forman	1967
$\frac{da}{dN} = \frac{C\Delta K^4}{K_c^2 - K_{max}^2}$	Weertman	1966-1969
$\frac{da}{dN} = C(\Delta K^m - \Delta K_{th}^m)$	Klesnil	1972
$\frac{1}{da/dN} = \frac{C_1}{(\Delta K)^{n_1}} + \frac{C_2}{(\Delta K)^{n_2}} + \frac{C_2}{[K_c(1-R)]^{n_2}}$	Saxena	1979
$\frac{da}{dN} = C(\Delta K - \Delta K_{th})^2 \left(1 + \frac{\Delta K}{K_c - K_{max}}\right)$	McEvily	1983
$\frac{da}{dN} = C\Delta K^p K_{max}^q$	Roberts	1965
$\frac{da}{dN} = C(K_{max}^2 - K_{min}^2)^m$	Klesnil	1972
$\frac{da}{dN} = C(K_{max}^2 - K_{min}^2)^m$	Arad	1971
$\frac{da}{dN} = C(\Delta G)^m$	Mostovoy	1975
$\frac{da}{dN} = C(\Delta S)^m$	Badaliance	1980

# 5 WEAR

## 5.1 INTRODUCTION

Wear is a very complex phenomenon with several interacting mechanisms. Archard proposed a wear equation which assumes that the wear is directly proportional to the load applied on the surface times the sliding distance, which means that the volume of the wear debris is proportional to the work done by friction forces. However, such a “simple” relation is almost never true [79], but Archard wear equation is nevertheless implemented in most simulations that account for wear of surfaces in lack of a better alternative. In grey cast iron brake discs, the mechanism of wear is complex due to a variety of causes which are responsible for wear like abrasion by hard particles, adhesion, tribochemical oxidation of wear debris, or surface forming oxides of the kind  $FeO_x$  (where  $0 < x < 1.5$  and normally close to 1.3) [79]. The elevated temperatures at the contacting surfaces in friction brakes make wear phenomena and modelling even more challenging. The situation is further complicated by oxidation and/or corrosion that increases the wear rate and also induces variations in the friction coefficient, so-called friction instability [80].

Figure 5-2 gives an energetic model of friction in brake systems and the principal power flows in frictional systems [81].

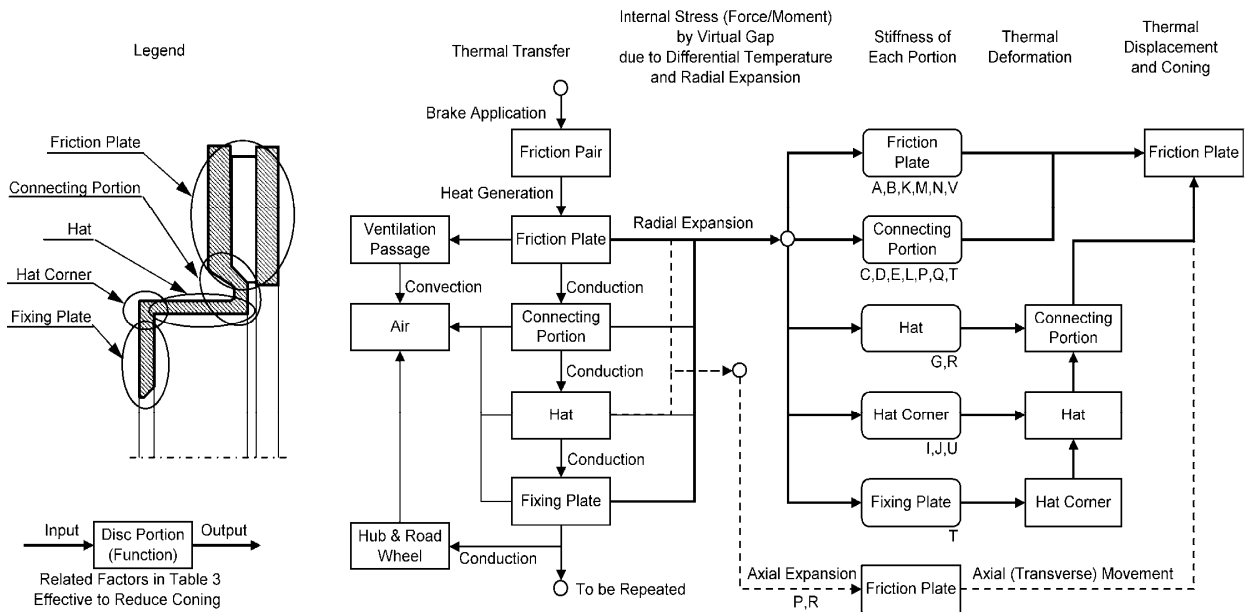


Figure 5-1 Block diagram explaining transfer of heat, internal stress, thermal deformation and displacement [7].

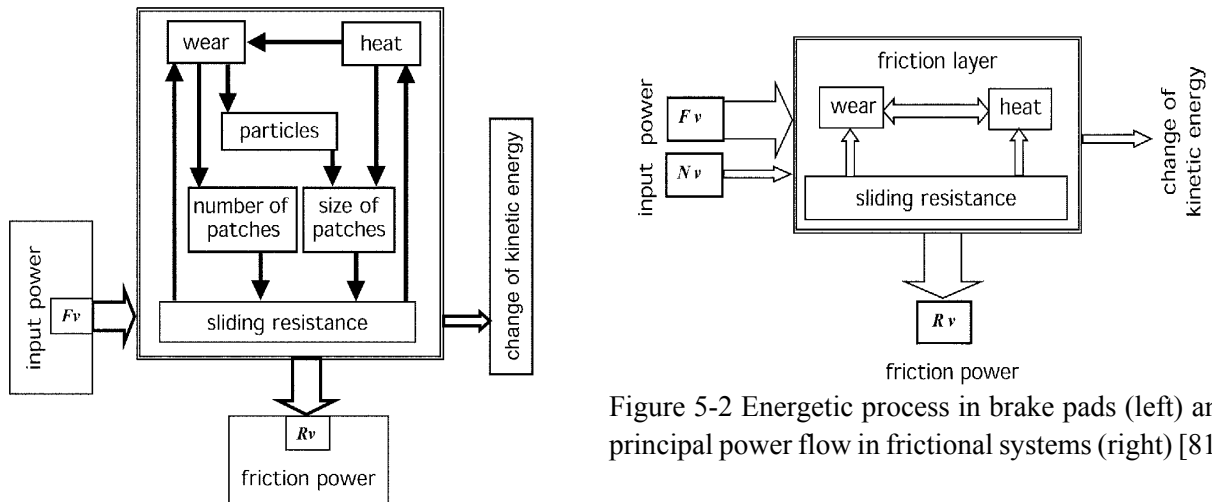


Figure 5-2 Energetic process in brake pads (left) and principal power flow in frictional systems (right) [81].

A close link between wear and friction exists. Coulomb was the first to define a dynamic friction coefficient  $\mu$  for a rigid body in sliding contact condition described as

$$\mu = \frac{R}{N} \quad (5.1.1)$$

where  $R$  is the frictional force and  $N$  is the normal force. Several parameters affect the friction coefficient as shown in Figure 5-3. The variation of the friction coefficient with friction power and temperature will for disc braking introduce substantial challenges when it comes to simulation of wear which is generally assumed to be a function of the friction work.

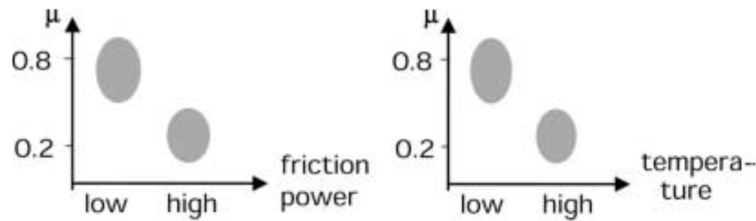


Figure 5-3 Dependence of the dynamic friction coefficient  $\mu$  on friction power (left) and disc temperature (right) [81].

## 5.2 WEAR MODELLING

There are two ways for modelling wear: at the molecular level or at the macro scale, which is of course less detailed. The principle of macro scale modelling is to study particular points on the contact surfaces in order to find a relation between the wear depth at that particular point and the distance the point slides at the interacting surfaces. A wear model can be described by the equation [82]

$$\frac{dh}{dt} = f(\text{load, velocity, temperature, material parameter, ...}) \quad (5.2.1)$$

where  $h$  is the wear depth. The wear rate, at any point on the contact surface is taken as proportional to the local contact pressure  $p$  and the relative sliding velocity  $v$  according to [83], is

$$\frac{dh}{dt} = kvp \quad (5.2.2)$$

where  $k$  is a contact pair dependent wear coefficient.

Mueller et al [84] gave an overview of several mathematical models developed in the past. In 1953, Archard [82] defined the classical model for describing adhesive wear as

$$\Delta W = \frac{KFs}{H} \quad (5.2.3)$$

where  $\Delta W$  is the worn volume given as a function of the normal force  $F$ , the sliding distance  $s$ , the hardness  $H$  of the material exposed to wear and the dimensionless scaling factor  $K$ . In 1965 and 1971, Rabinowicz developed his own formulation based on Archard's formula with regard to abrasive and fretting wear instead of adhesive wear.

When it comes to modelling of wear, the Archard wear model on local form is normally implemented as  $dh/dt = kvp$  [81]. By use of this expression, the wear rate becomes proportional to the local work performed by friction.

The literature provides studies focussed on the variation of wear as a function of several parameters like loading and sliding speed. An example is shown in Figure 5-4 of wear rates for a grey cast iron block sliding on a bearing steel ring. One way to account for varying wear rates caused by different wear mechanisms is the use of so-called wear maps [85]. In a wear map, the wear rate coefficient for a given contact pair is given for combinations of sliding speed and contact pressure, while at the same time the map indicates the dominating wear mechanisms. An example of a wear map for steel sliding on steel is given in Figure 5-5.

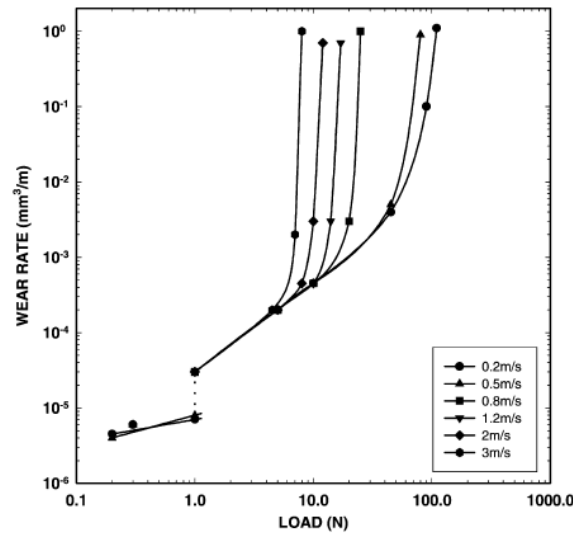


Figure 5-4 Wear rate vs load at various sliding speeds for grey cast iron [86].

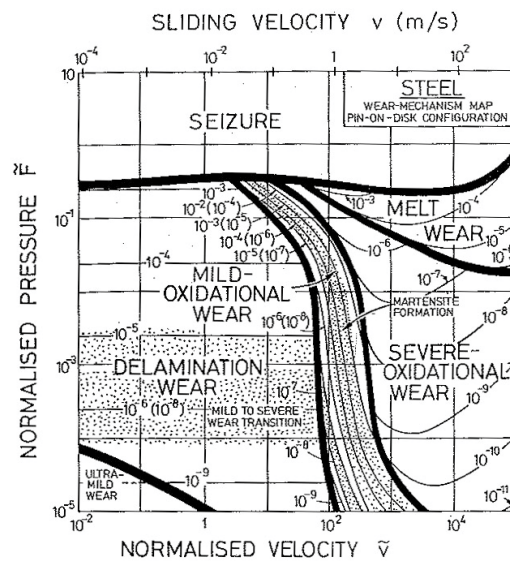


Figure 5-5 Example of a wear map giving normalised wear rates for combinations of normalised pressure and normalised velocity [85].

A field that also should be mentioned and that has attracted much research in recent years, involves the study of the friction layer, or third body, that forms between the two sliding bodies [87]. A new understanding of friction and wear is found by studying the microscopic build-up of the friction material contact surface, which is created from primary plateaus of wear resistant material and secondary plateaus formed by trapped wear debris [88].

When it comes to modelling wear of brake components, the interface temperature will be important [89]. A wear equation that is stated to be “...quite effective in relating brake lining wear data with testing conditions for a broad range of materials, over most of the brake operating temperature range” is

$$V = A + Be^{C/T} \quad (5.2.4)$$

where  $V$  is specific wear rate (wear volume per unit frictional work),  $A$ ,  $B$  and  $C$  are friction material constants and  $T$  is the average interface temperature during braking. It is mentioned that there is a history dependence of the wear from previous cycles, which is not accounted for by this wear equation. For instance if a material has been submitted to severe use, the wear rates at low temperatures will increase. To compensate for this, it is proposed that the material constant  $A$  be modified to include also prior temperature history.

### 5.3 WEAR TESTING

Testing of wear properties can be performed on different scales. One may use small-scale testing machines or component testing using full-scale geometry in a brake dynamometer where controlled tests can be performed. Another choice is in-field testing where all real aspects are considered but the degree of control of influencing parameters is less detailed. All methods have pros and cons, but should, if carefully performed, give results that are in good agreement.

Small-scale testing is often performed in a pin-on-disc test machine, where a small-diameter pin (diameter about 1 cm) is sliding against the flat top surface of a disc (diameter about 10 cm). The pin is loaded using a known weight and the disc is rotating at a constant speed. The output of a test is the friction coefficient and the wear coefficient, where the latter is found by weighing the pin before and after the test. One problem with small-scale testing is that you want to have the same contact temperatures, contact pressure and sliding speed as those prevailing at full scale. However, normally a test cannot fully respect the full-scale testing parameters and hence a trade-off has to be made by use of some scaling rules where choices are made how to best represent the full-scale test [24]. One aspect that cannot be accounted for at small-scale testing is the thermomechanical coupling effects (resulting in eg banding of the contact or hot spotting) that may occur in the full-scale test, since they depend on actual geometrical size and structural stiffness. To account for the influence from such phenomena on the wear rate, full-scale tests should be performed.

An example of a case study of wear testing of four brake disc materials, one CGI (Compact Graphite Iron) and three grey cast irons, is given in [90]. The materials are tested using a pin-on-disc wear testing machine, see Figure 5-6. It is found that for a given load on the pin (made from friction material), the wear was practically identical for the four disc materials used in the rotor. The wear of the CGI material is, for a given (normal) load, found to be substantially higher than that for the grey irons. However, this can be attributed to the higher friction coefficient, resulting in increased friction work and temperatures. For the same order of friction forces, the wear of the CGI is found to be the same or somewhat greater than that of the grey cast irons.

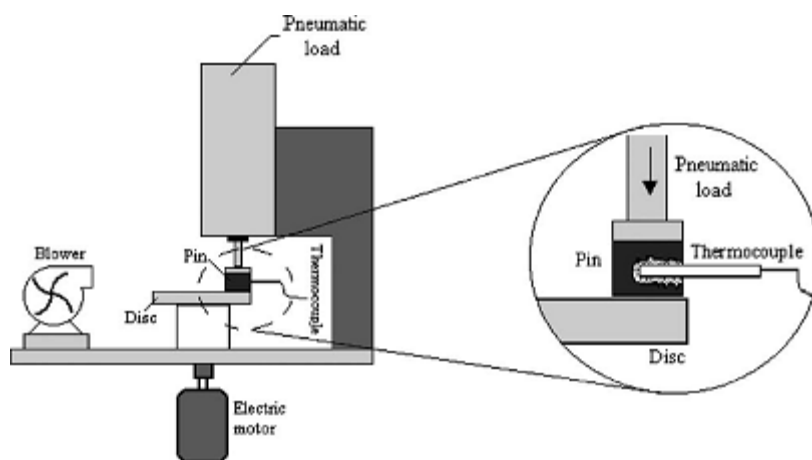


Figure 5-6 Schematics of pin-on-disc test [90].

Results from pin-on-disc testing performed in [90] are shown in Figure 5-7 for different types of compact graphite iron.

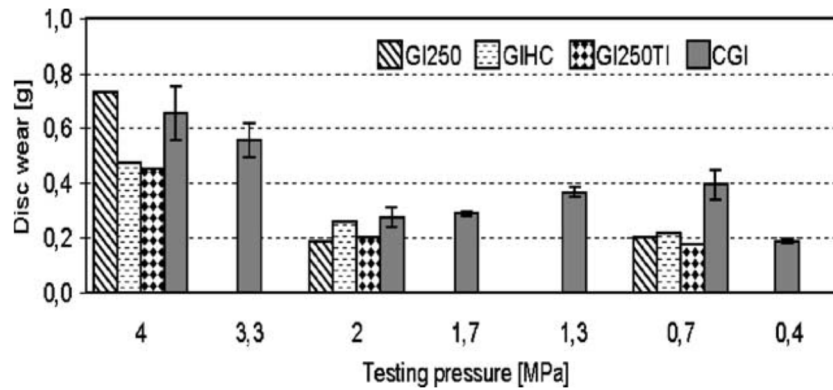


Figure 5-7 Wear of the tested irons CGI as function of applied pressure [90]. Data collected after 300 cycles.

## 6 STRUCTURAL MODELLING AND OPTIMIZATION

### 6.1 INTRODUCTION

Generally when it comes to optimization of a structure, it is essential to account for the appropriate phenomena in the simulation models. Figure 5-1 gives an overview of the mechanisms involved during braking [7].

### 6.2 FE-MODELS

Huang and Chen [91] have established a 3D finite element model with the disc stationary and the pad rotating. This model has been used for analysing the deflection of the disc. A succession of 10 stops from 100 km/h to stop in 6 s is studied by use of sequentially coupled thermal stress analyses. Söderberg and Andersson [83] developed a finite element model for structural analysis of brake discs, see Figure 6-1. The pad-disc pressure distributions are computed and then reused for simulating the wear process of the pad. The pad is modelled by use of finite elements but the disc is modelled as a rigid surface. The modelling method is based on a modular approach which divides the system into components with mating features that are connected by interface models. The geometrical design and the elastic deformation of the calliper that transfers the normal brake force to the brake pads may give rise to different pressure distributions at the two pad-disc interfaces and presumably also different wear patterns.

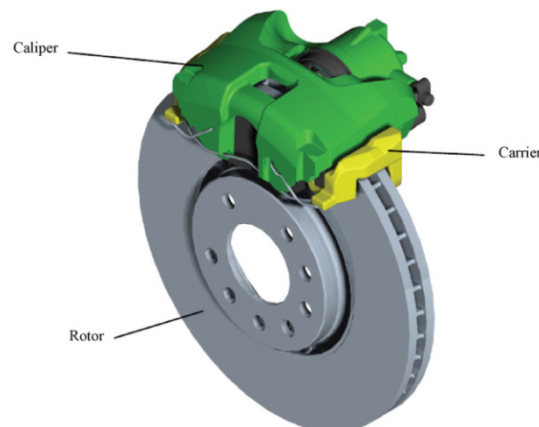


Figure 6-1 Full brake CAD model [83].

Dufrenoy and Weichert [51] modelled the hot spots by a concentrated heat flux on the disc surface using a parabolic shape and assuming that the deceleration is constant, which implies that the heat flux linearly decreases with time after 4 s which corresponds to the duration of the rise in pressure of the pneumatic cylinder,

see Figure 6-2. In [51], a multisurface linear kinematic model has been used instead of a viscoplastic law with a double kinematic and isotropic hardening with memory effect of the plastic strains. Dufrenoy and Weichert [51] explained this choice by the fact that this model quickly leads to elastic or plastic shakedown even if it gives slightly higher stress values and lower plastic strain values. Moreover, the stabilized loop is only obtained after several cycles cyclic softening is not high.

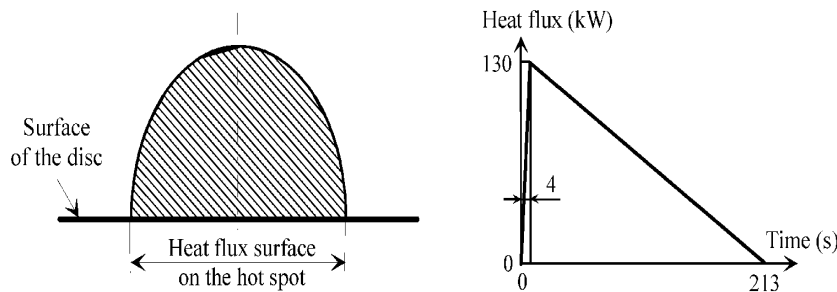


Figure 6-2 (a) Disc surface heat flux distribution on the hot spot (b) heat flux graph of one braking [51].

### 6.3 OPTIMIZATION

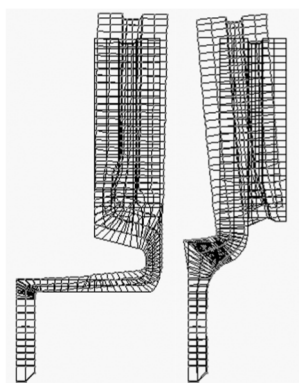


Figure 6-3 Result of thermal deformation analysis [7].

Okamura and Yumoto [7] studied the thermomechanical behaviour for several disc geometries. As explained in the paper, the thermal behaviour of the brake disc is an important issue because heat cracks reduce the life of brake discs, and thermal coning, see Figure 6-6, is responsible for instability, disc thickness variations and noise emission. The model implemented is a sequential thermomechanical model.

The studied geometries in Figure 6-3 represent two kinds of behaviour of the discs

at braking. Scania uses the disc to the right which moves laterally and tilts during braking. The left hand geometry, which is the outcome of an optimization study, expands only in the radial direction at braking. Figure 6-4 shows all geometrical dimensions that have been included in the employed finite element model. Figure 1-1 shows the different geometries used for ventilated brake discs (except for floating discs where some examples can be found in section 1.4).

Before optimizing the geometry, it is important to know which of the parameters that affect the behaviour of a brake disc. One important parameter for cracks is the coning (tilting) behaviour of the disc. Indeed, experiments show that cracks preferably occur on one side of the disc. The exception is for floating discs where both sides have similar crack patterns. Coning plays an important role and experiments show that cracks develop on the hat side for configurations “outer-hat without neck” and “outer hat with neck”, see Figure 1-1, and on the other side for configurations “inner hat without holes” in hat and “inner-hat with holes in hat”. Coning can be experimentally studied using

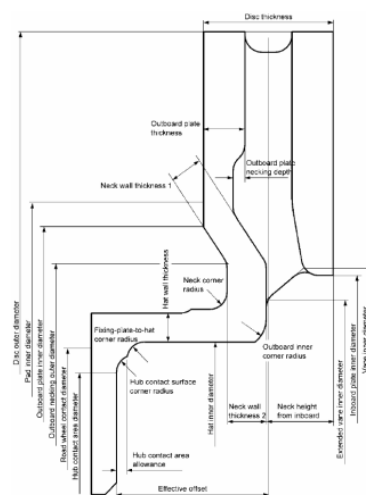


Figure 6-4 Main dimensions of outer-hat brake disc, selected as parameters in a CAE experiment [7].

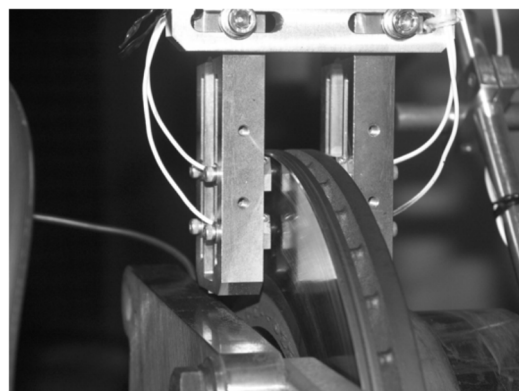


Figure 6-5 Capacitive displacement sensor arrangement on brake dynamometer [7].

a capacitive displacement sensor as shown in Figure 6-5. An interesting conclusion arrived at [7] is that the coning will be reduced if the disc has large holes which reduce the stiffness of the disc. However, these holes behave like notches and initiate cracks. This may explain why some manufacturers have replaced these holes by curved grooves. They allow a higher flexibility of the disc and reduce the stress concentration factor created by the holes. The coning phenomenon is illustrated in Figure 6-6.

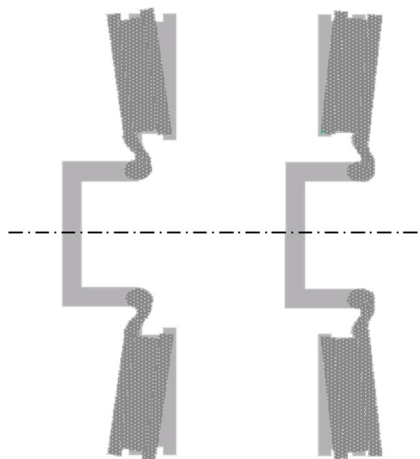


Figure 6-6 Example of coning for a non-floating brake disc [92].

## 7 CASE STUDIES

### 7.1 HIGH SPEED TRAIN TGV

Wicker et al [4] (English version [3] by Degallaix et al) modelled the thermomechanical behaviour of TGV brake discs. Pad materials from four different suppliers were studied and experimental tests and numerical modelling were performed. Discs made from material 26CrMoV5 and pads having different thermal and mechanical properties, geometries and support arrangements were used in the tests. For all pads used, a superficial crack network on the disc surfaces was observed after a short time. This phenomenon is explained by thermal fatigue and is known as crazing [94], see Figure 7-1. The results from the experiments in [3] show that the pad material strongly influences the temperature distribution on the disc surfaces. In the tests, 18 stop brakings were performed from 270 to 0 km/h with braking force 4150 N and energy 11.25 MJ and from 300 to 220 km/h with braking force of 20 000 N and energy 6.42MJ.

During braking, compressive stresses appear in the hot zones of the disc, due to the expansion constraints. As the stress level exceeds the yield stress, plastic flow occurs in compression which leads to tensile residual stresses after cooling. Hot spots which occur during braking are due to a non-uniform distribution of the thermal flux, resulting from the distribution of the pins (cylindric segments) on the pad and the thermal expansion of the pad and disc materials, and from the local physical mechanisms of friction and wear in the disc-pad interface. The hot spot pattern is equally distributed, generally with six spots circumferentially around the disc surface. The pattern is fixed during one brake cycle and is oriented 30° out-of-phase on the two sides of the disc. The pattern is associated to a vibrational wave pattern distortion of the disc. Experimental studies show that the plastic strains and residual stresses in brake discs are higher in the circumferential direction than in the radial direction. However, hot spots observed in railway disc brakes differ from the automotive observations [95].

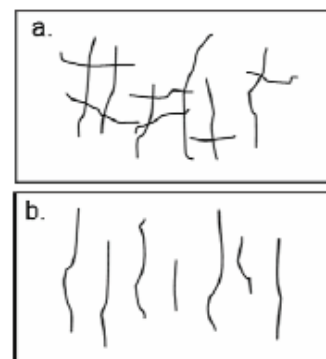


Figure 7-1 Multidirectional network crack crazing (a), unidirectional network crack crazing (b) [93].

Dufrenoy [96] identified 6 different types of hot spot patterns in full-scale disc braking, see Figure 7-2, and introduced a numerical model illustrated in Figure 7-3. Simulations have been performed in order to see which parameters are relevant for modelling hot spots. It has been found in [96] that two parameters are necessary for the modelling. The first parameter contains the thermal localization ( $[t_{400}/t]$ ,  $[Lr_{400}/(R_{ext} - R_{int})]$ ,  $[L_{\theta}/(2\pi \cdot R)]$ ) and the second one contains the thermal intensity and thermal rate ( $[T_{moy\_ang}]$ ,  $[\Delta T/\Delta t]$ ), see Figure 7-4. A complete definition of these parameters is given in the paper.

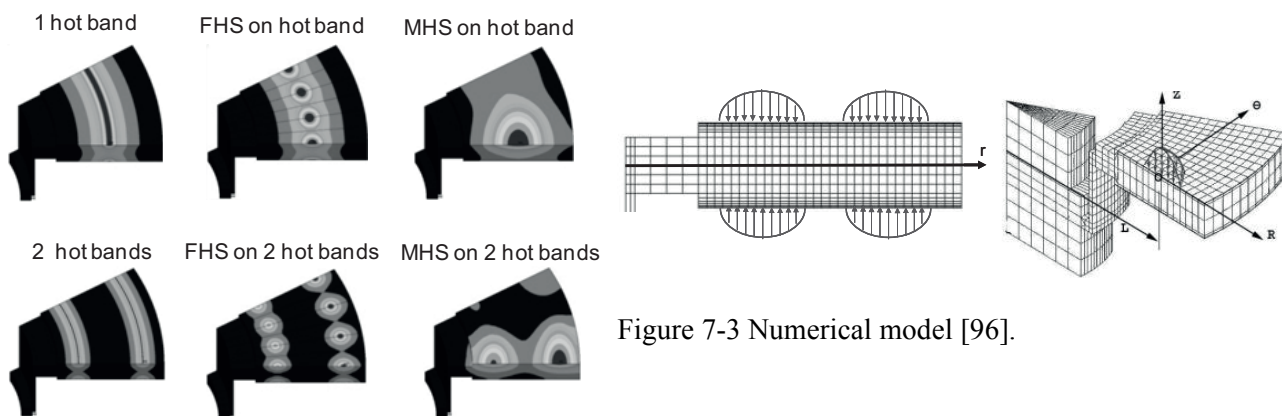


Figure 7-3 Numerical model [96].

Figure 7-2 Idealized thermal gradients used for thermomechanical calculations [96].

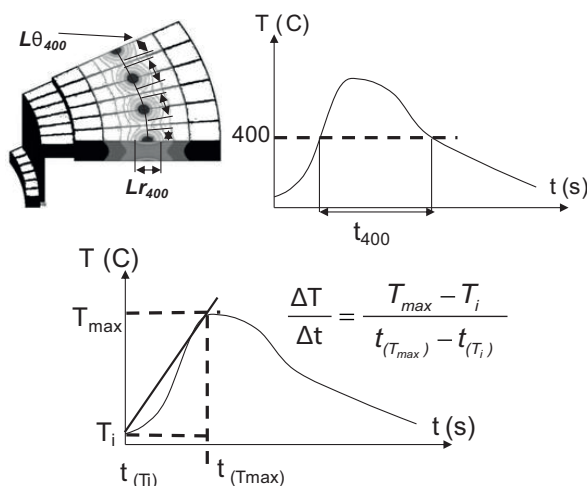


Figure 7-4 Identification of parameters [96].

## 7.2 ALLOYING AND CRACKING OF BRAKE DISCS

Endo et al [97] evaluated new grey cast iron materials for brake discs of trucks. The chemical compositions of each specimen is shown in Table 13.

Table 13 Chemical composition of grey cast iron materials.

	<b>C</b>	<b>Si</b>	<b>Mn</b>	<b>P</b>	<b>S</b>	<b>Cu</b>	<b>Ni</b>	<b>Cr</b>	<b>Sn</b>
<b>A</b>	3.38	2.21	0.78	0.041	0.09	0.05	0.04	0.47	0.071
<b>B</b>	3.72	2.30	0.35	0.022	0.10	1.05	1.56	0.88	0.001
<b>C</b>	4.09	2.50	0.33	0.020	0.10	1.03	1.60	0.72	0.002
<b>D</b>	3.78	2.10	0.36	0.013	0.081	0.95	1.36	0.78	0.026

In [97], laboratory tests on full-scale brake discs have been performed. Each stop braking cycle had starting speed 100 km/h and a deceleration  $2.94 \text{ m/s}^2$ . The aim was to develop a brake disc with a better resistance to heat cracking and wear. As shown in Figure 7-5, the thermal conductivity is not directly linked to the carbon content and moderate addition of tin affects the thermal conductivity. A high amount of carbon, or tin, does not mean that the thermal conductivity is improved. The disc D, for instance, has the third highest value for the carbon content but the best thermal conductivity. This can be explained by a higher content of tin present in disc D which has been found to reduce the wear.

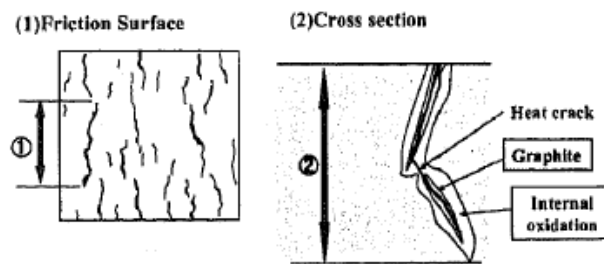
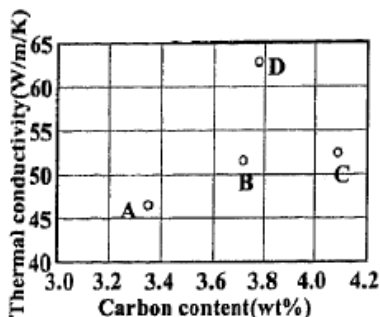


Figure 7-5 Relationship between carbon content and thermal conductivity [97]. Figure 7-6 Evaluation of heat crack length [97].

Figure 7-6 explains how the crack length is measured on the friction surface and in the cross section of the brake disc. The best disc is D which has the highest content of tin. Aspects not mentioned in [97] are that the graphite flake morphology is important for the crack growth and also for the thermal conductivity because the study focused mainly on few chemical elements which are used for brake discs. However, it is concluded in [97] that a high amount of carbon is not good since it increases the oxidation in the graphite flake structure.

Yamabe [42, 98] developed a new alloyed grey cast iron material in order to reduce heat crack propagation in brake discs. The thermal fatigue strength of a disc can be improved if the propagation of heat cracks is properly controlled. This can be accomplished by reducing the amount of thermal stress and/or improving the resistance of the material against crack propagation. One common way to increase the resistance to heat cracks is to add high-cost materials like nickel, chromium and molybdenum. It was found that the amounts of these expensive materials could be reduced by inoculating with cerium.

One should note that for the specimens No 1 to 4 used in [42, 98] the amounts of nickel and cerium, which produce the greatest effect on thermal fatigue strength, were varied in consideration of squeal noise, wear resistance and other required characteristics. There were no significant changes of the other alloying elements compared to the “current material” defined in [42]. Considering the thermal conductivity, the highest value was obtained for material No 2 while the lowest value was obtained with the current material. Additions of nickel and cerium reduce the thermal conductivity. At room temperature, the difference in the thermal conductivity between FC250 (which is a standard brake disc material according to [42]) and the current material is about 15%. There is no significant difference in the coefficient of thermal expansion and Young’s modulus between FC250 and the current material.

Figure 7-7 shows the relationship between the graphite number (number of graphite grains per  $\text{mm}^2$ ) and the crack propagation rate. The conclusion is that the crack propagation rate is strongly dependent on the graphite number. Graphite with fine grains promotes a low crack propagation rate. Addition of nickel and cerium makes the graphite being distributed in refined grains. It was also found that an addition of cerium allows a decrease of nickel while keeping the crack propagation rate at the same level (see Figure 7-7). In the experiments, a special “high speed testing” was employed to reduce the testing time.  $\sigma \lambda^\circ$

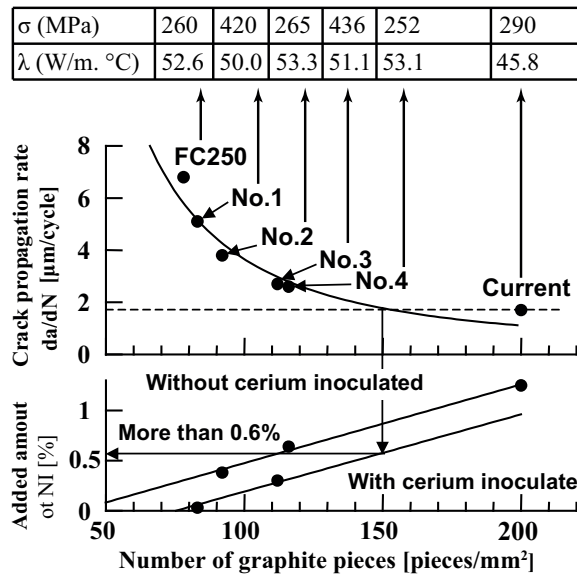


Figure 7-7 Crack propagation rate  $da/dN$  related to graphite number and added amount of nickel with tensile strength and thermal conductivity at room temperature, from [42]. The test rig was a pin-on-disc type wear test machine modified for high speed braking with the contact pad-disc maintained at a constant pressure.

The number of cycles to crack initiation does not give a big contribution to the total thermal fatigue life for a grey cast iron material, contrary to the crack propagation which follows the crack initiation. The crack propagation rate is therefore used for determining the thermal fatigue life of a material. The crack propagation rate is lower when a large amount of graphite is distributed in refined grains. But no clear correlation exists between the crack growth rate and the values of the tensile strength and the thermal conductivity. It leads to the question: do the tensile strength and thermal conductivity have a significant effect on crack propagation in, or life of, brake discs?

## 8 CONCLUDING REMARKS

This state-of-the-art survey shows that the high thermomechanical loading due to braking creates thermal stress, wear and crack growth which lead to a reduction of the life of brake discs. In order to maintain a required braking performance – friction coefficient, thermal “resistance”, etc, different aspects of mechanics have been studied and synthesized as a “reference” for a better understanding of the phenomena that occur at braking. This state-of-the-art survey also reveals some contradictions in the literature and indicates that the problems are more complex than some authors seem to indicate. The three main parameters stated in several papers (related to thermal properties of the material) will not be the only parameters that should be taken into consideration and optimized. Moreover, the thermal diffusivity is not directly linked to the carbon equivalent as stated in some papers. For example, saying that the thermal diffusivity and thermal conductivity are two of the main parameters for designing brake discs with good crack resistance is far from true. Also parameters like chemical elements or casting processes have to be taken in account. Due to the multitude of parameters involved during braking and the complex phenomena (friction wear, hot spots), it is difficult to find a general model for optimization of brake discs.

Geometrical parameters of a brake disc affect its coning behaviour which, in some cases increases the crack growth by increasing the thermomechanical effect. The casting process creates local residual stresses which differ from one brake disc to another.

The opinion of the author is that a trans-disciplinary approach is required for improving the performance of brake discs. Knowledge in FEM, CFD, material modelling and TEI will be very useful. A “global” approach and a multicriterion optimization will eventually be required.

## 9 REFERENCES

1. **Mackin, T.J., Noe, S.C., Ball, K.J., et al.** Thermal cracking in disc brakes. *Engineering Failure Analysis*, 2002, **9**(1), pp 63-76
2. **Talati, F. and Jalalifar, S.** Analysis of heat conduction in a disk brake system. *Heat and Mass Transfer*, 2009, **45**(8), pp 1047-1059
3. **Degallaix, G., Dufrenoy, P., Wong, J., et al.** Failure mechanisms of TGV brake discs. *Key Engineering Materials*, 2007, **345-346**, pp 697-700
4. **Wicker, P., Wong, J., Degallaix, G., et al.** Analyse et simulation thermomécanique de l'endommagement des disques de frein du TGV. *La Revue Métallurgie*, 2009, pp 311-316
5. **Voller, G., Tirović, M., Morris, R., et al.** Analysis of automotive disc brake cooling characteristics. *Proceedings of the Institution of Mechanical Engineers, Part D: Journal of Automobile Engineering*, 2003, **217**(8), pp 657-666
6. **Vernersson, T.** Control of railway block braking - Thermomechanical performance of wheels: a literature survey, Research report 2002:6, *Chalmers University of Technology, Department of Applied Mechanics / CHARMEC*, Göteborg, Sweden, 2002, 71 pp (Research report)
7. **Okamura, T. and Yumoto, H.** Fundamental study on thermal behavior of brake discs, *Proceedings 24th Annual Brake Colloquium and Exhibition*, Grapevine, Texas, USA, 2006, 16 pp
8. **AP Racing** Floating Disc Mounting, 2007, [http://www.apracing.com/info/info.asp?section=Floating+Disc+Mounting\\_93](http://www.apracing.com/info/info.asp?section=Floating+Disc+Mounting_93), Accessed: May 2011
9. **Palmer, E., Mishra, R. and Fieldhouse, J.** An optimization study of a multiple-row pin-vented brake disc to promote brake cooling using computational fluid dynamics. *Proceedings of the Institution of Mechanical Engineers, Part D: Journal of Automobile Engineering*, 2009, **223**(7), pp 865-875
10. **Chatterley, T.C. and Macnaughtan, M.P.** Cast iron brake discs - Current position, performance and future trends in Europe, *Proceedings SAE International Congress and Exposition*, Detroit, Michigan, USA, 1999, 10 pp
11. **Tirović, M. and Voller, G.P.** Heat dissipation from high speed train brakes - the efficiency compromise, *Proceedings TILT 2003 conference*, Lille, France, 2003, 8 pp
12. **Palmer, E., Mishra, R. and Fieldhouse, J.** A computational fluid dynamic analysis on the effect of front row pin geometry on the aerothermodynamic properties of a pin-vented brake disc. *Proceedings of the Institution of Mechanical Engineers, Part D: Journal of Automobile Engineering*, 2008, **222**(7), pp 1231-1245
13. **Tirović, M.** Energy thrift and improved performance achieved through novel railway brake discs. *Applied Energy*, 2009, **86**, pp 317-324
14. **Mazidi, H., Alalifar, S., Jalalifar, S., et al.** Mathematical Modeling of Heat Conduction in a Disk Brake System During Braking. *Asian Journal of Applied Sciences*, 2011, **4**, pp 119-136
15. **Selin, M., Holmgren, D. and Svensson, I.L.** Effect of alloying elements on graphite morphology in CGI, *Proceedings Materials Science Forum*, Miskolc-Lillafured, 2010, pp 171-176
16. *Heat-resistant materials* ASM Specialty Handbook, ed. J.R. Davis, ASM International, 1997, 591 pp
17. **Toshikazu, O. and Masanori, I.** Increasing thermal strength of brake discs by improving material homogeneity, *Proceedings 27th Annual Brake Colloquium and Exhibition*, Tampa, Florida, USA, 2009, 7 pp
18. **Dufrenoy, P. and Weichert, D.** Prediction of Railway Disc Brake Temperatures Taking the Bearing Surface Variations into Account. *Proc Instn Mech Engrs, Part F: Journal of Rail and Rapid Transit*, 1995, **209**, pp 67-76
19. **Vernersson, T.** Tread Braking of Railway Wheels – Noise-related Tread Roughness and Dimensioning Wheel Temperatures - Field Tests, Rig Measurements and Numerical simulations, Doctoral Dissertation, *Department of Applied Mechanics, Chalmers University of Technology*, Gothenburg, Sweden, 2006, 136 pp
20. **Johansson, L. and Klarbring, A.** Thermoelastic frictional contact problems: Modelling, finite element approximation and numerical realization. *Computer Methods in Applied Mechanics and Engineering*, 1993, **105**(2), pp 181-210
21. **Talati, F. and Jalalifar, S.** Investigation of heat transfer phenomena in a ventilated disk brake rotor with straight radial rounded vanes. *Journal of Applied Sciences*, 2008, **8**(20), pp 3583-3592

22. **Eisengräber, R., Grochowicz, J., Schuster, M., et al.** Comparison of different methods for the determination of the friction temperature of disc brakes, *Proceedings International Congress and Exposition*, Detroit, Michigan, 1999, pp 498-504
23. **Siroux, M., Cristol-Bulthé, A.-L., Desplanques, Y., et al.** Thermal analysis of periodic sliding contact on a braking tribometer. *Applied Thermal Engineering*, 2008, **28**(17-18), pp 2194-2202
24. **Roussette, O., Desplanques, Y. and Degallaix, G.** Représentativité thermique d'essais tribologiques à échelle réduite (Thermal representativity of tribological reduced-scale testing). *Comptes Rendus Mecanique*, 2003, **331**(5), pp 343-349
25. **Rukadikar, M.C. and Reddy, G.P.** Thermal fatigue resistance of alloyed, pearlitic flake, graphite irons. *International Journal of Fatigue*, 1987, **9**(1), pp 25-34
26. **Bhadeshia, H.K.D.H.** *Handbook of Residual Stress and Deformation of Steel: Material Factors*. Handbook of Residual Stress and Deformation of Steel, ed. G. Totten, M. Howes and T. Inoue, ASM International, Materials Park, Ohio, USA, 2002, 499 pp
27. **Withers, P.J. and Bhadeshia, H.K.D.H.** Residual stress part 1 - Measurement techniques. *Materials Science and Technology*, 2001, **17**(4), pp 355-365
28. **TWI Ltd** Residual stresses, 2005, <http://www.twi.co.uk/content/ksrhl001.html>, Accessed: Mars 2011
29. **Barber, J.R., Beamon, T.W., Waring, J.R., et al.** Implications of thermoelastic instability for the design of brakes. *Journal of Tribology*, 1985, **107**(2), pp 206-210
30. **Choi, J.-H. and Lee, I.** Finite element analysis of transient thermoelastic behaviors in disk brakes. *Wear*, 2004, **257**(1-2), pp 47-58
31. **Rémy, L.** Thermal-mechanical fatigue (including thermal shock), in *Comprehensive structural integrity, vol 5*, I. Milne, R.O. Ritchie and B. Karihaloo, Editors, 2003, Elsevier. pp 113-199
32. **Janssens, K.G.F., Niffenegger, M. and Reichlin, K.** A computational fatigue analysis of cyclic thermal shock in notched specimens. *Nuclear Engineering and Design*, 2009, **239**(1), pp 36-44
33. **Siliconfareast**, Thermal Shock Test (TST), 2004, <http://www.siliconfareast.com/TST.htm2010>
34. **Siliconfareast**, Temperature Cycle Test (TCT), 2004, <http://www.siliconfareast.com/TCT.htm2010>
35. **Properties and Selection: Irons, Steels, and High-Performance Alloys** ASM Handbook, Vol. 1, ASM International, 1990, 1063 pp
36. **David C. Woodruff**, Why compacted graphite iron?, <http://www.competitiveproduction.com/articles/why-compacted-graphite-iron/2011>
37. **Maluf, O., Angeloni, M., Castro, D.B.V., et al.** Effect of Alloying Elements on Thermal Diffusivity of Gray Cast Iron Used in Automotive Brake Disks. *Journal of Materials Engineering and Performance*, 2009, **18**(7), pp 980-984
38. **Atlas Foundry Company, Inc.** Gray iron casting and other foundry tips and facts, 2010, <http://www.atlasfdry.com/tips.htm>, Accessed: June 2011
39. **Stefanescu, D.** *Physical Properties of Cast Iron*. Iron Castings Engineering Handbook, ed. G.M. Goodrich, American Foundry Society, 2003, 420 pp
40. **George M. Goodrich and American Foundry Society** Introduction to Cast Irons, in *Castings, ASM Handbook*, G.M. Goodrich, (editor). 2008, ASM International. pp 785–811
41. **Diószegi, A. and Holmgren, D.** Elevated temperature properties of cast iron, *Jönköping University, Departement of Mechanical Engineering*, Jönköping, 2004, 42 pp (Literature survey)
42. **Yamabe, J., Takagi, M. and Matsui, T.** Development of disc brake rotor for heavy and medium duty trucks with high thermal fatigue strenght. *Technical Review*, 2003(13), pp 42-51
43. **Suprihanto, A., Harsokoesoemo, D. and Suratman, R.** The effect of Cr & Cu on the fatigue strength of grey cast irons. *Key Engineering Materials*, 2006, **306-308 II**, pp 953-958
44. **Hecht, R.L., Dinwiddie, R.B. and Wang, H.** The effect of graphite flake morphology on the thermal diffusivity of gray cast irons used for automotive brake discs. *Journal of Materials Science*, 1999, **34**(19), pp 4775-4781
45. **Holmgren, D., Diószegi, A. and Svensson, I.L.** Effects of carbon content and solidification rate on the thermal conductivity of grey cast iron. *Tsinghua Science and Technology*, 2008, **13**(2), pp 170-176a
46. **Elkem AS**, Graphite Structures in Cast Iron, 2004, <http://www.elkem.no/dav/ef8eb3f187.pdf2010>
47. **Holmgren, D., Källbom, R. and Svensson, I.L.** Influences of the graphite growth direction on the thermal conductivity of cast iron. *Metallurgical and Materials Transactions A*, 2007, **38**(A), pp 268-275
48. **Bodner, S.R., Partom, I. and Partom, Y.** Uniaxial cyclic loadind of elastic-viscoplastic materials. *Journal of Applied Mechanics, Transactions ASME*, 1979, **46**(4), pp 805-810

49. **eFatigue LLC** Thermal Mechanical Technical Background, 2011, <https://www.efatigue.com/hightemp/background/tmf.html>, Accessed: February 2011
50. **Samrout, H., Abdi, R.E. and Chaboche, J.L.** Model for 28CrMoV5-8 steel undergoing thermomechanical cyclic loadings. *International Journal of Solids and Structures*, 1997, **34**(35-36), pp 4547-4556
51. **Dufrénoy, P. and Weichert, D.** A thermomechanical model for the analysis of disc brake fracture mechanisms. *Journal of Thermal Stresses*, 2003, **26**(8), pp 815-828
52. **Kim, D.-J., Seok, C.-S., Koo, J.-M., et al.** Fatigue life assessment for brake disc of railway vehicle. *Fatigue & Fracture of Engineering Materials & Structures*, 2010, **33**(1), pp 37-42
53. **Gorash, Y.** Development of a creep-damage model for non-isothermal long-term strength analysis of high-temperature components operating in a wide stress range, *Zentrum für Ingenieurwissenschaften*, Martin-Luther-Universität Halle-Wittenberg, Halle, Germany, 2008
54. **NDT**, Elastic/Plastic Deformation, <http://www.ndt-ed.org/EducationResources/CommunityCollege/Materials/Structure/deformation.htm2010>
55. **Dowling, N.E.** *Mechanical behavior of materials : engineering methods for deformation, fracture and fatigue*, Pearson Prentice Hall, Upper Saddle River, New Jersey, USA, 2007, 912 pp
56. **Starns, G.K.** Strain Life Analysis, 2004, <http://www.public.iastate.edu/~gkstarns/ME417/me417.htm>, Accessed: April 2011
57. *Fatigue and Fracture* Vol. 19, ASM International, 1996, 1057 pp
58. *Manual on Low-Cycle Fatigue Testing*. ASTM special technical publication 465, American Society for Testing and Materials, 1969, 193 pp
59. **Skelton, R.P.** Energy criterion for high temperature low cycle fatigue failure. *Materials Science and Technology*, 1991, **7**(5), pp 427-439
60. **Halford, G. and Manson, S.S.** Life prediction of thermal–mechanical fatigue using strain range partitioning, in *Thermal Fatigue of Materials and Components*, D.A. Spera and D.F. Mowbray, Editors, 1976, ASTM STP. 270 pp
61. **Neu, R.W. and Sehitoglu, H.** Thermomechanical fatigue, oxidation, and Creep: Part II. Life prediction. *Metallurgical Transactions A*, 1989, **20**(9), pp 1769-1783
62. **Lemaitre, J. and Chaboche, J.** *Mechanics of solid materials*, Cambridge University Press, 1990
63. **Gomez, T., Awarke, A. and Pischinger, S.** A new low cycle fatigue criterion for isothermal and out-of-phase thermomechanical loading. *International Journal of Fatigue*, 2010, **32**(4), pp 769-779
64. **Engrasp Inc.**, Strain-life fatigue analysis, 2008, [http://www.fea-optimization.com/ETBX/strainlife\\_help.html](http://www.fea-optimization.com/ETBX/strainlife_help.html), Accessed: 07-07-2011 2011
65. **eFatigue LLC** Cast iron technical background: fatigue prediction method for cast irons, 2011, <https://www.efatigue.com/castiron/background/castiron.html>, Accessed: July 2011
66. **eFatigue LLC** Constant amplitude strain-life technical background, 2011, <https://www.efatigue.com/constantamplitude/background/strainlife.html>, Accessed: July 2011
67. **Downing, S.D.** Modeling cyclic deformation and fatigue behavior of cast iron under uniaxial loading, *Department of Mechanical and Industrial Engineering, UIUC, College of Engineering. University of Illinois*, Urbana-Champaign, USA, 1984, 114 pp
68. **Zhuang, W.Z. and Swansson, N.S.** Thermo-mechanical fatigue life prediction: A critical review, *Australian Government - Department of Defence, Airframes and Engines Division*, 1998, 25 pp (Technical Report)
69. **Spera, D.A. and Mowbray, D.F.** *Thermal fatigue of materials and components*, ASTM International, Philadelphia, USA, 1976, 262 pp
70. **Eichlseder, W., Winter, G. and Köberl, H.** Material and fatigue life models for thermo-mechanical loaded components. *Materialwissenschaft und Werkstofftechnik*, 2008, **39**(10), pp 777-782
71. **Hasbroucq, S., Oueslati, A. and de Saxcé, G.** Inelastic responses of a two-bar system with temperature-dependent elastic modulus under cyclic thermomechanical loadings. *International Journal of Solids and Structures*, 2010, **47**(14-15), pp 1924-1932
72. **Neu, R.W. and Sehitoglu, H.** Thermomechanical fatigue, oxidation, and creep: Part I. Damage mechanisms. *Metallurgical Transactions A*, 1989, **20**(9), pp 1755-1767
73. **Sabour, M.H. and Bhat, R.B.** Lifetime prediction in creep-fatigue environment. *Materials Science-Poland*, 2008, **26**(3), pp 563-584

74. **Charkaluk, E. and Constantinescu, A.** Plastic work in thermal fatigue design, *Proceedings 6th European Conference on Braking JEF 2010*, Lille, France, 2010, 7 pp
75. **Ekberg, A.** Continuum analysis of fatigue strength and influence of some key factors, *Department of Applied Mechanics, Chalmers University of Technology*, Gothenburg, Sweden, 2010 (Course)
76. **eFatigue LLC** Variable amplitude crack growth: technical background, 2011, <https://www.efatigue.com/variable/background/crackgrowth.html>, Accessed: February 2011
77. **Ritchie, R.O.** Mechanisms of fatigue-crack propagation in ductile and brittle solids. *International Journal of Fracture*, 1999, **100**(1), pp 55-83
78. **Tanaka, K.** *Mechanics and micromechanics of fatigue crack propagation*. Fracture mechanics: perspectives and directions (twentieth symposium), ASTM 1020, Philadelphia, USA, 1989, pp 151-183
79. **Dante, R.C. and Navire, C.** A basic overview on brake disc wear, *Proceedings International Body Engineering Conference and Automotive & Transportation Technology Conference*, Paris, France, 2002, 8 pp
80. **Shin, M., Cho, K., Kim, S., et al.** Friction instability induced by corrosion of gray iron brake discs. *Tribology Letters*, 2010, **37**(2), pp 149-157
81. **Ostermeyer, G.P.** Friction and wear of brake systems. *Forschung im Ingenieurwesen*, 2001, **66**(6), pp 267-272
82. **Archard, J.F.** Contact and rubbing of flat surfaces. *Journal of Applied Physics*, 1953, **24**(8), pp 981-988
83. **Söderberg, A. and Andersson, S.** Simulation of wear and contact pressure distribution at the pad-to-rotor interface in a disc brake using general purpose finite element analysis software. *Wear*, 2009, **267**(12), pp 2243-2251
84. **Mueller, M., Ostermeyer, G.-P. and Graf, M.** Towards an explicit computation of wear in brake materials, *Proceedings 27th Annual Brake Colloquium and Exhibition*, Tampa, Florida, USA, 2009, 15 pp
85. **Lim, S.C. and Ashby, M.F.** Overview no. 55 wear-mechanism maps. *Acta Metallurgica*, 1987, **35**(1), pp 1-24
86. **Riahi, A.R. and Alpas, A.T.** Wear map for grey cast iron. *Wear*, **255**(1-6), pp 401-409
87. **Godet, M.** The third-body approach: a mechanical view of wear. *Wear*, 1984, **100**(1-3), pp 437-452
88. **Eriksson, M., Bergman, F. and Jacobson, S.** On the nature of tribological contact in automotive brakes. *Wear*, 2002, **252**(1-2), pp 26-36
89. *Friction, lubrication, and wear technology*, ASM Handbook, ed. P.J. Blau. Vol. 18, 1992, 1210 pp. ASM International
90. **Cueva, G., Sinatora, A., Guesser, W.L., et al.** Wear resistance of cast irons used in brake disc rotors. *Wear*, 2003, **255**(7-12), pp 1256-1260
91. **Huang, Y.M. and Chen, S.-H.** Thermal effect of design parameters on the deflection of a disk brake. *21st Biennial Conference on Mechanical Vibration and Noise, Parts A, B, and C*, 2008, **1**, pp 1005-1012
92. **Nguyen-Tajan, T.M.-L.** Modélisation thermomécanique des disques de frein par une approche eulérienne, Doctoral Dissertation, *Department of Mécanique des Solides, École Polytechnique*, Lille, France, 2002, 204 pp
93. **Wong, J.** Analyse de l'endommagement par fatigue thermique et modélisation du comportement thermomécanique de couples disques-garnitures de type TGV, Doctoral Dissertation, *Department of Mécanique, École centrale de Lille*, Lille, 2008, 163 pp
94. **Dufrénoy, P., Bodovillé, G. and Degallaix, G.** Damage mechanisms and thermomechanical loading of brake discs, in *European Structural Integrity Society*, L. Rémy and J. Petit, Editors, 2002, Elsevier. pp 167-176
95. **Hernik, S.** Modeling FGM brake disk against global thermoelastic instability (hot-spot). *Z. Angew. Math. Mech.*, 2009, **89**(2), pp 88-106
96. **Dufrénoy, P., Kasem, H., Wicker, P., et al.** Quantitative identification of braking disc cracking parameters: hot spots, pad type, disc material, *Proceedings 6th European Conference on Braking, JEF 2010*, Lille, France, 2010, 8 pp
97. **Endo, S., Takahashi, J.I. and Hara, I.** Development of disc brake rotor material for heavy duty trucks. Influence of carbon and tin on heat crack resistance and wear resistance of gray cast iron. *Transactions of Society of Automotive Engineers of Japan*, 2002, **33**(1), pp 105-109
98. **Yamabe, J., Takagi, M., Matsui, T., et al.** Development of disc brake rotors for trucks with high thermal fatigue strength. *JSAE Review*, 2002, **23**(1), pp 105-112

## TABLE OF CONTENTS

---

Abstract .....	1
1 Introduction .....	1
1.1 Background.....	1
1.2 Aim of study .....	2
1.3 Overview of disc braking .....	3
1.4 Disc geometries .....	3
1.5 Vane geometries .....	5
2 Temperatures and stresses .....	8
2.1 Introduction .....	8
2.2 Heat generation.....	8
2.3 Heat transfer .....	11
2.4 Thermal stresses .....	14
2.5 Plastification and residual stresses .....	14
2.6 Thermoelastic instabilities and hot spots.....	14
2.7 Thermal shock .....	16
3 Material properties.....	17
3.1 Introduction .....	17
3.2 Thermal and mechanical properties.....	17
3.3 Alloying elements.....	20
3.4 Material modelling .....	24
3.5 Material testing.....	25
4 Fatigue and cracks .....	27
4.1 General .....	27
4.2 High cycle fatigue.....	28
4.3 Low cycle fatigue .....	29
4.4 Thermomechanical fatigue .....	33
4.5 Fracture mechanics and crack growth .....	37
5 Wear .....	41
5.1 Introduction .....	41
5.2 Wear modelling .....	42
5.3 Wear testing.....	44
6 Structural modelling and optimization .....	45
6.1 Introduction .....	45
6.2 FE-models.....	45
6.3 Optimization .....	46
7 Case studies .....	47
7.1 High speed train TGV.....	47
7.2 alloying and cracking of brake discs .....	48
8 Concluding remarks.....	50
9 References .....	51



# **Paper B**

**Disc brakes for heavy vehicles – An experimental study of temperatures and cracks**



This paper has been removed from the  
present online thesis for copyright  
reasons due to international publication



# **Paper C**

## **Modelling of grey cast iron for application to brake discs for heavy vehicles**



This paper has been removed from the  
present online thesis for copyright  
reasons due to international publication



# **Paper D**

**Improvement of brake disc design for heavy vehicles  
by parametric evaluation**



This paper has been removed from the  
present online thesis for copyright  
reasons due to international publication



# **Paper E**

**Thermomechanical fatigue of grey cast iron brake discs for heavy vehicles**



This paper has been removed from the  
present online thesis for copyright  
reasons due to international publication

